

AFIT/DS/ENY/96-5

AN INVESTIGATION OF THE CHARACTERISTICS
OF REGENERATIVE HEAT EXCHANGERS

DISSERTATION

Timothy J. Murphy, Captain, USAF

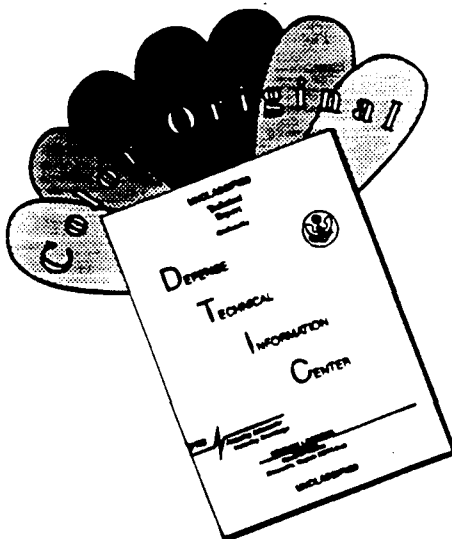
AFIT/DS/ENY/96-5

19960718 114

Approved for public release; distribution unlimited

DTIC QUALITY INDEXED 3

DISCLAIMER NOTICE



**THIS DOCUMENT IS BEST
QUALITY AVAILABLE. THE COPY
FURNISHED TO DTIC CONTAINED
A SIGNIFICANT NUMBER OF
COLOR PAGES WHICH DO NOT
REPRODUCE LEGIBLY ON BLACK
AND WHITE MICROFICHE.**

The views expressed in this dissertation are those of the author and do not reflect the official policy or position of the Department of Defense or the U.S. Government.

AFIT/DS/ENY/96-5

AN INVESTIGATION OF THE CHARACTERISTICS
OF REGENERATIVE HEAT EXCHANGERS

DISSERTATION

Presented to the Faculty of the Graduate School of
Engineering of the Air Force Institute of Technology
Air University
in Partial Fulfillment of the
Requirements for the Degree of
Doctor of Philosophy

Timothy J. Murphy, B.S.M.E.,M.S.S.M.,M.S.A.E.
Captain, USAF

June 1996

Approved for public release; distribution unlimited

AN INVESTIGATION OF THE CHARACTERISTICS
OF REGENERATIVE HEAT EXCHANGERS

Timothy J. Murphy, B.S.M.E.,M.S.S.M.,M.S.A.E.
Captain, USAF

Approved:

W. Jerry Bowman
Lt Col W. Jerry Bowman

17 May 1996

Paul I. King
Paul I. King

17 May 1996

Maj Glen P. Perram
Maj Glen P. Perram

17 May 1996

Rodney D. W. Bowersox
Rodney D.W. Bowersox

17 May 1996

Accepted:

Robert A. Calico
Robert A. Calico
Dean, Graduate School of Engineering

Acknowledgments

While bringing this project to a successful end, I received help from many people. First and foremost, I must thank my dissertation advisor, Lt Col Jerry Bowman, for always being willing to help me. Jerry's enthusiasm and patience with a grouchy old man will always be remembered. I leave AFIT with a keen interest in helping people to see "the big picture" due to Jerry's influence.

I would also like to thank Dr. King, Maj Perram, and Dr. Bowersox for being on my committee. They took the time to talk to me when I needed help. Their many thoughtful comments are greatly appreciated. I have gained enormous respect for those who do experimental research.

I am grateful to the laboratory technicians who were so helpful. In particular, Andy Pitts was very generous with his technical knowledge and time, and made the long hours of work more enjoyable. Tim Hancock from the AFIT shops was also a big help and made the tedious job of fabricating the screen units tolerable.

Thanks also go to the space power and thermal management directorate at Phillips Lab, and in particular to Capt Jeff Wiese, for their sponsorship.

Finally, let me say with great love that I could not have accomplished this project without the care, encouragement, and companionship of my wonderful wife, Maria, and my smiling daughter, Nora Elizabeth. I dedicate this work to them and thank them with all my heart.

Timothy J. Murphy

Table of Contents

	Page
Acknowledgments	iii
List of Figures	vi
List of Tables	viii
List of Notations	ix
Abstract	xii
I. Introduction	1
Objective	1
Motivation	2
Approach	3
Important Terms	4
II. Background and Justification	5
Background	5
The Stirling Cycle	6
Performance Factors	13
Regenerator Effectiveness	13
Pressure Drop	15
The Dead Volume	16
Justification	19
III. Methodology	26
Theory	26
Step-Change Transient Technique	26
Problems with the Step-Change Transient Technique	30
Improvements to the Step-Change Transient Technique	35
Numerical Model	43
Numerical Model of the Transient	43
Calculations	48
Stability	49
Validation of the Numerical Model	50
Determining the Heat Transfer Coefficient	53
Zeroin Subroutine	53
The <i>main</i> Program	55
The Three Criteria	55
Other Results	58
IV. Experimental Apparatus and Procedure	61
Apparatus	61
Experimental Procedure	70

Data Reduction Technique	71
V. Results and Discussion	75
Preliminary Results	75
Comparisons to Published Data	80
Repeatability	82
Heat Transfer Coefficient	84
Friction Factor	86
Compactness Factor	89
Criteria Comparisons	93
Effectiveness	100
Special SU	103
Reynolds Analogy	104
Discussion	105
Uncertainties	105
Effects of Uncertainties	106
Summary	108
VI. Conclusions and Recommendations	110
Appendix A: Test Procedures	114
Appendix B: MATLAB m.files	117
Appendix C: FORTRAN Codes - <i>tsie</i> and <i>main</i>	122
Appendix D: Calibrations	149
Temperature Calibration	149
Pressure Drop	150
Mass Flow Rate	151
Appendix E: Test Data	152
Bibliography	154
VITA	159

List of Figures

Figure	Page
1. Simple Two-Cylinder Stirling Refrigerator	8
2. Ideal Stirling Thermodynamic Cycle	9
3. COP vs Compression Ratio and Effectiveness	14
4. Effect of Dead Volume on COP	18
5. NS30A Performance and Pressed Screen Results	21
6. Temperature Gap for Empty Tube	33
7. Temperature of the Tube	36
8. Regenerator Sponge Effect Delay Time	39
9. Comparison of Trace for Tube and No Tube	42
10. Control Volume for Energy Equation	45
11. Verification of Numerical Approach for Large NMAX	52
12. Model Verification Using Lumped Thermal Mass . . .	54
13. Root-Mean-Squared-Difference as a Function of the Heat Transfer Coefficient	57
14. Diagram of Experimental Apparatus	61
15. Instrumentation Holders	65
16. Photo of Screen Unit (S/U)	66
17. Specific Surface Area vs Reduction Factor	78
18. Typical Experimental Temperature Trace	79
19. Friction and Nusselt Number Comparisons	82
20. Repeatability of the Data	83
21. Heat Transfer Results for All SUs	84

Figure		Page
22.	Reduced Nusselt Number as a Function of Reduction Factor	86
23.	Friction Factor Results for All SUs	87
24.	Reduced Friction Factor vs Reduction Factor . . .	88
25.	Reduced Friction Factor vs Reduction Factor for RF > 0.7	89
26	Compactness Factors for All SUs	91
27.	Compactness Factors for Each Screen Size	92
28.	Global Compactness Factor vs Reduction Factor . .	93
29.	Reduced Compactness Factor vs Reduction Factor . .	94
30.	Outlet Temperature Traces for All Three Criteria .	95
31.	Comparison of Delay Time and Root-Mean-Squared Difference Methods	96
32.	Comparison Between Delay time and Analytical Maximum Slope Results	98
33.	Comparison Between Delay Time and Experimental Maximum Slope Results	99
34.	Comparison Between Analytical and Experimental Maximum Slope Results	100
35.	Effectiveness vs Reduction Factor	101
36.	Reduced Effectiveness vs Reduction Factor	102
37.	Reynolds Analogy Revisited	105

List of Tables

Table	Page
1. Instrumentation List for Fig. 10	62
2. List of Screen Units	67
3. Test Run Matrix	81
4. Comparison of S/U #13 to the Unrolled Case	103
5. Uncertainties in Measurements	106

List of Notations

A	cross-sectional area of the tube ($\pi D^2/4$) - m^2
A^*/A^{**}	constants used in Eq (8) and (9)
A/B	constants used in a Nusselt number correlation, p. 82
A_1/B_1	constants used in reduced CF correlation, p. 89
A_2/B_2	constants used in SPEFF correlation, p. 98
A_{ext}	cross-sectional area of the tube wall - m^2
A_f	area for flow in the matrix (ΦA) - m^2
A_i	constants used in Eq (30), App. D
A_r	specific area per unit unrolled volume of matrix - m^{-1}
A_{sur}	total surface area for a matrix, p. 50 - m^2
A_s	surface area in one space increment ($A_r A \Delta x$) - m^2
$A_{s'}$	surface area per unit volume for an unrolled matrix, used in Eq (29) - m^{-1}
A_{ST}	surface area of the tube in a space increment ($\pi D \Delta x$) - m^2
B	constant used in Eq (10)
C_M	specific heat for the matrix material - $J/kg/\text{ }^\circ C$
C_p	specific heat at constant pressure for the gas - $J/kg/\text{ }^\circ C$
C_v	specific heat at constant volume for the gas - $J/kg/\text{ }^\circ C$
C	Courant number ($\Delta x/\Delta t$) - m/s
CF	Compactness Factor
COP	coefficient of performance
COP_i	coefficient of performance for an ideal cycle
d_h	hydraulic diameter - m
d_w	wire diameter - m
D	diameter of the tube holding the regenerator matrix - m
DAS	data acquisition system
EL	length of the screen unit - m
EL_0	length of the unrolled screen - m
$ELOC$	time step of the maximum outlet temperature slope - s
f	friction factor, Eq (23)
f_1	correlation for unrolled friction factors, p. 86
h_{conv}	heat transfer coefficient - $W/m^2/\text{ }^\circ C$
h_{min}	guess at minimum heat transfer coefficient - $W/m^2/\text{ }^\circ C$
h_{max}	guess at maximum heat transfer coefficient - $W/m^2/\text{ }^\circ C$
I	time increment index
j_H	Colburn Factor ($St Pr^{.333}$)
k	thermal conductivity of the gas - $W/m/\text{ }^\circ C$
k_s	thermal conductivity of the matrix material - $W/m/\text{ }^\circ C$
$K_A, K_B, K_C, K_D, K_E, K_F, K_H, K_J$	constants used in Eqs (19), (20), and (21)
l	distance between wire strands ($1/MESH - d_w$) - m
L	characteristic length - m
L_A	Armour and Cannon dimension, Eq (28) - m
\dot{m}	mass flow rate - kg/sec
$MESH$	number of strands of wire per inch - in^{-1}
N	space increment index
Nu	Nusselt number ($h_{conv} L_A/k$)
N_{tu}	number of thermal units ($h_{conv} A_s / \dot{m} / c_p$)

P	pressure - Pa
P_1	pressure at the inlet to the regenerator - Pa
PIT	pitch ($1/MESH$ or $1+d_w$) - m
Pr	Prandtl number ($c_p \mu/k$)
PS	pore size $((1/MESH)^2 (2 d_w RF))^{.333}$ - m
Q	tortuosity factor
Q_e	heat transferred from the refrigerated volume - J/kg
Q_{ei}	heat transferred from the refrigerated volume in an ideal cycle - J/kg
Q_R	heat transferred to the regenerator - J/kg
r_c	compression ratio
R	perfect gas constant - J/kg/K
Re	Reynolds number based on Armour's dimension ($\rho U_g L_A/\mu$)
Re_{dh}	Reynolds number based on hydraulic diameter
Re_{dw}	Reynolds number based on wire diameter
Re_{ps}	Reynolds number based on pore size
RF	Reduction Factor (EL/EL_0)
R_T	electrical resistance of thermistor material - ohms
SEDT	sponge effect delay time - s
SPEFF	matrix effectiveness
St	Stanton number ($Nu/Re/Pr$)
SU	screen unit
t	time - sec
t_s	screen thickness - m
t_t	tube wall thickness - m
T_c	temperature in the compression space - °C
T_e	temperature in the expansion space - °C
$T_{g1/2}$	temperature of the gas at the inlet/outlet - °C
T_r	temperature of the regenerator matrix - °C
T_{tube}	temperature of the tube - °C
TG_N^I	gas temperature in the finite difference equation - °C
U_g	gas mass velocity - m/s
V	volume - m³
w_{ind}	indicated engine power - kw
W_{SU}	mass of the SU - kg
x	axial distance - m

Greek Symbols

$\alpha_{t/m}$	thermal diffusivity of the tube/matrix - m²/s
γ	ratio of specific heats of the gas (c_p/c_v)
Δx	space increment - m
Δt	time increment - s
ΔP	pressure drop - Pa
ϵ	effectiveness of the regenerator
η_{ind}	indicated engine efficiency - %
Θ	dimensionless temperature $(T_g - T_{g0}) / (T_{gf} - T_{g0})$
μ	dynamic viscosity - Ns/m²
ν	kinematic viscosity - m²/s
ρ	gas density - kg/m³

ρ_m matrix material density - kg/m³
 τ dimensionless time or time constant ($\rho c / h_{CONV} / A_s$) - s
 τ_m time constant for the matrix - s
 τ_r time constant for a length of matrix - s
 τ_t time constant for a length of tube - s
 τ_2 time when the outlet gas temperature begins to rise - s
 τ_0 time when transient begins - s
 τ_f time when transient ends - s
 Φ porosity (volume of gas in matrix/total matrix volume)

Abstract

The objective of the current research was to investigate the effects of reducing screen thickness on the volume and compactness factor (j_H/f) of stacked, wire-screen regenerators. An improved transient step-change method was devised which integrated experimental data with a numerical model of the flow to determine the heat transfer coefficient and friction factor. The improvements to the approach are: 1) the measured inlet temperature trace is used, 2) the heat transfer coefficient is based on a parameter called the sponge effect delay time, and 3) the important effect of the tube surrounding the matrix is included in the numerical model. The data show that the heat transfer is the same for reduced thickness screens as it is for unrolled screens once the decrease in surface area caused by rolling the screens is taken into account. However, the friction factor increases, particularly for a 50% reduction in screen thickness. Consequently, the ratio of Colburn factor to friction factor, the compactness factor, decreases as the thickness of the screens decrease. The effectiveness of the regenerators is also adversely affected by the rolling.

AN INVESTIGATION OF THE CHARACTERISTICS
OF REGENERATIVE HEAT EXCHANGERS

I. Introduction

As the chapter title states, this is an introduction to the research described in this dissertation. A concise statement of the problem, motivation, and approach for the research is given here, as well as two definitions which require clarification in advance. Background information on stacked-screen regenerators and justification for the research are given in Chapter II. Chapter III describes the theory behind determining a heat transfer coefficient for a porous medium, and describes the improved approach used for the current research. The experimental apparatus and procedure are described in Chapter IV. The results are presented in Chapter V, while some concluding remarks and recommendations appear in Chapter VI. Other important information which includes MATLAB m.files, FORTRAN codes, test procedures, calibration techniques, and experimental data are given in the appendices.

Objective

The hypothesis central to this research may be stated as follows:

The reduced thickness of pressed, round wire screens decreases the volume of a stacked, wire-screen regenerator, and reduces its compactness factor (j_H/f).

The definition of pressed is any process which reduces the thickness of the screens without removing material. The specific objective is to determine the heat transfer coefficient, friction factor, and other flow and geometrical properties of a porous medium regenerator made from rolled screens, and to compare these results to those for unrolled screens. To accomplish this objective, an integrated experimental-numerical method which produces dependable data was developed.

Motivation

Improving the performance of regenerative refrigeration cycles is important to the Air Force. A better understanding of the processes in porous medium regenerators which are an integral part of regenerative refrigeration cycles will lead to improvements in performance. One specific improvement is to reduce the dead volume of the regenerator. But this should only be done if the method for reducing the dead volume does not decrease the heat transfer coefficient or increase the pressure drop characteristics of the regenerator significantly, since good performance also depends on good

heat transfer and small pressure drops. Hence, a comprehensive study of the effects of reducing the screen thickness on the compactness factor, which is the ratio of the Colburn factor to the friction factor (Radebaugh and Louie, 1986:180), was conducted.

Approach

A three-step approach to this research was used. First, an experimental apparatus was designed and built to measure temperatures, pressures, and other properties of reduced-thickness, wire-screen regenerators for a range of flow and geometrical conditions. Second, a data reduction technique and numerical model of the flow that determine the heat transfer coefficient based on criteria from the experimental data, and that calculate friction factors for each case, was developed. And third, the results were analyzed and conclusions about the effect on the compactness factor of reducing the volume by rolling the screens were drawn. A by-product of this approach was a better understanding of how the heat transfer coefficient can be more accurately determined by accounting for non-idealizations and omissions present in the experimental and analytical techniques used by other researchers of regenerative heat exchanger characteristics.

Important Terms

Two terms should be clarified in advance. First, the matrix is the porous medium, i.e. the stack of wire-mesh screens. The regenerator is a collection of parts which includes the matrix, tube, spacers, connectors, etc. Second, SU is the designation for screen unit. Thirteen screen units, SUs, were fabricated for the current research, each with a different combination of mesh size and screen thickness reduction factor. More definitions of terms are made in Chapter II, Background and Justification.

II. Background and Justification

The current research is being done to contribute to the knowledge of heat and momentum transfer in a porous medium, and to demonstrate a better way to study these phenomena. The how part will be addressed in Chapter III, Methodology. This chapter describes the rationale for the hypothesis stated in Chapter I. The Background section relates the importance of cryocooler technology to the Air Force, defines terms, and explains how regenerators are essential to the operation of cryocoolers. In the Justification section, the literature search and available data are described, and the hypothesis is formulated.

Background

The particular application which motivates the current research is regenerative refrigeration. Regenerative refrigeration technology is important for a wide range of space-based applications (Chan et al, 1990; Thieme and Swec, 1992; Ledford, 1994). The Air Force currently oversees a large research and development program in this area (Thomas, 1992; Ross, 1992; Wyche and Bruning, 1990). Regenerative refrigeration cycles are especially suited to space applications because they are low-maintenance, low-vibration devices with demonstrated long-endurance capabilities (Walker, 1983: Chapter 4). At the low temperatures commonly found in

outer space (less than 120 K), these refrigerators are referred to as cryocoolers (Radebaugh, 1989). The most important application for cryocoolers is in thermal management of electronic components. In particular, satellite imaging systems are equipped with semi-conductor, photon-collecting components that are kept as cold as possible for maximum resolution (Chan et al, 1990).

The stringent requirements placed on space-based, energy conversion equipment exist for one simple reason: Routine maintenance and refueling are impractical for space-based assets due to a lack of access. Consequently, even small improvements in energy conversion efficiency are important for extending space asset lifetimes. Much of the current research on cryocoolers pursues this goal (Thieme and Swec, 1992).

There are various types of regenerative refrigeration cycles used in cryocoolers, but the free-piston Stirling cycle has received the most attention since it is very reliable and holds promise for high-efficiency space utilization (Chan et al, 1990: 1244; Ledford, 1994). As the name regenerative refrigeration cycle implies, a regenerator is an integral part of the system. In order to demonstrate the purpose and importance of the regenerator, a Stirling refrigeration cycle will be examined.

The Stirling Cycle. This section describes the basic elements of a Stirling refrigerator and the associated ideal

thermodynamic cycle. The aim of this section is to explain what a cryocooler is and how it goes about performing its task.

Fig. 1 shows the basic elements of a simple, two-cylinder Stirling cycle refrigerator. The working fluid is typically a low boiling-point, monatomic gas such as helium. Heat is transferred from the refrigerated volume at T_e into the expansion space; heat is rejected to a sink at T_c from the compression space. A regenerator is placed between these two spaces. The gas is under high pressure, typically around 25 atmospheres, and oscillates between the compression space and the expansion space through the regenerator. A regenerator is a heat exchanger which receives energy from the gas during one part of the cycle (the hot blow), holds the energy, and returns it to the gas on the reverse passage through the regenerator (the cold blow). The regenerator may be thought of as a thermal sponge, alternately absorbing and releasing heat energy (Walker, 1983:45).

The thermodynamic processes of an ideal Stirling cycle are shown in the P-V and T-S diagrams in Fig. 2. The cycle begins with all of the gas in the compression space. A constant-temperature compression occurs between state 1 and state 2 during which heat is transferred out of the gas at T_c . Next, a constant-volume heat transfer takes place during which heat is transferred from the gas to the regenerator. From state 3 to state 4, a constant-temperature expansion occurs

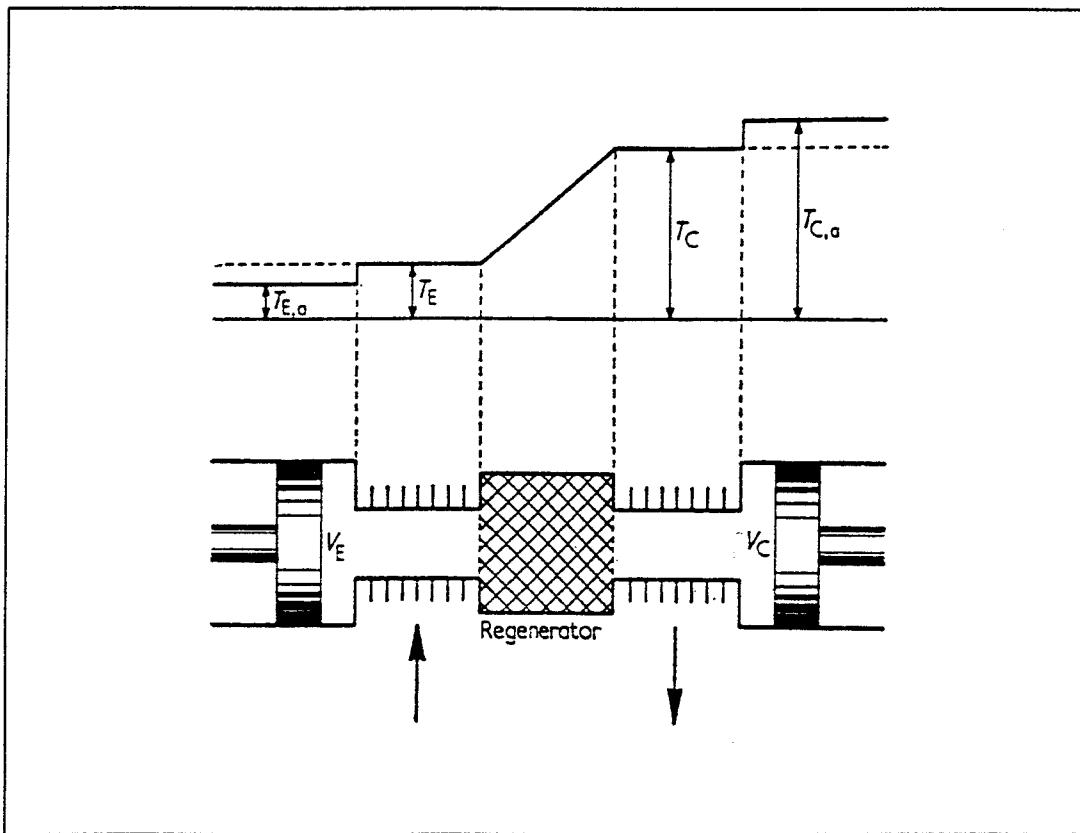


Figure 1. Simple Two-Cylinder Stirling Refrigerator
 (Haselden, 1971: 46)

during which heat is transferred into the gas from the refrigerated volume at T_e . Finally, the energy stored in the regenerator during the hot blow is returned to the gas by a constant-volume process which returns it to state 1. Differences exist between real and ideal Stirling cycles, but the above description is sufficient for illustrative purposes.

The dominant energy transfer process in a Stirling cycle is the exchange of heat between the working gas and the regenerator. The heat transferred to the regenerator during each half-cycle is typically ten to fifty times larger than the heat removed from the refrigerated volume (Atrey et al.,

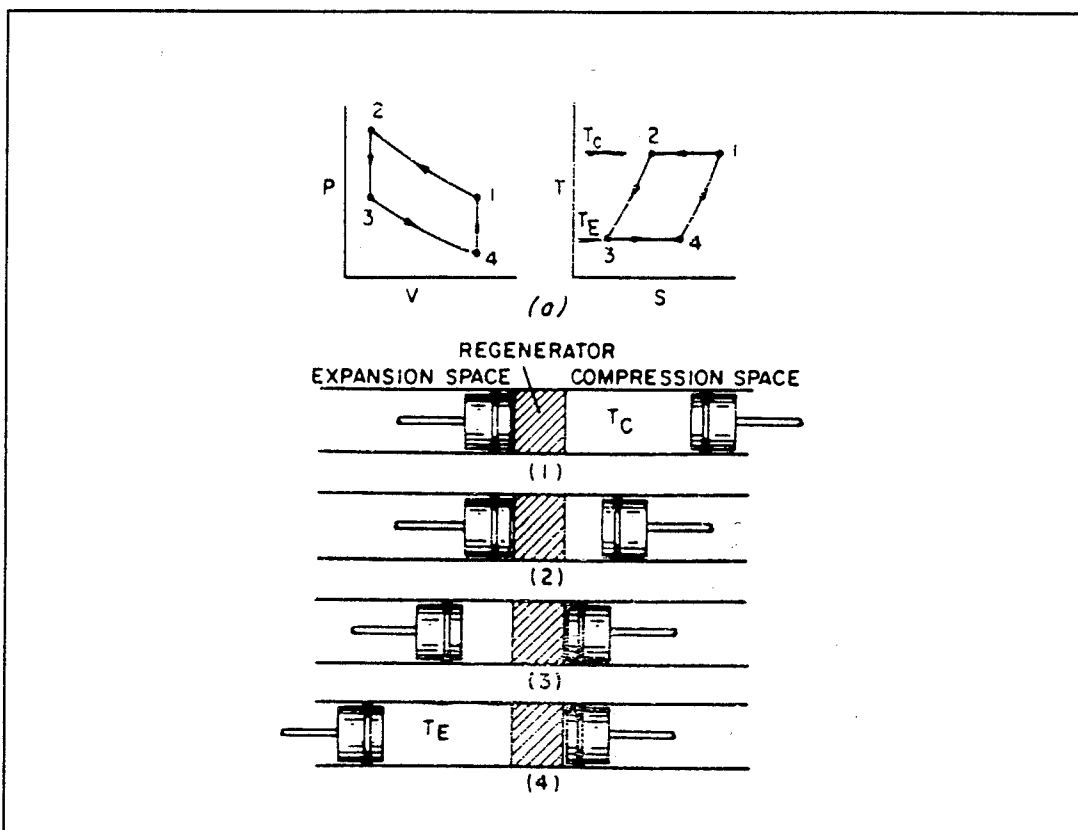


Figure 2. Ideal Stirling Thermodynamic Cycle
(Walker, 1983:45)

1990:236). The heat transferred to the regenerator during each half-cycle is usually even larger than the work input from the compressor. Consequently, the ability of the regenerator to effectively transfer and store energy is very important to the performance of a cryocooler.

Cryocooler performance can be measured in various ways. A common figure of merit for a refrigeration cycle is the coefficient of performance (COP). For a refrigeration cycle, work is put into the compression space and heat is removed from the refrigerated volume. The COP for a cycle is defined as the ratio of the heat removed from the refrigerated volume

to the net work input to the compression space (Walker, 1983:42). Consequently, a high *COP* is desirable.

The *COP* is a system-level figure-of-merit for a cryocooler. For the regenerator component of the cryocooler, the compactness factor is used as the figure-of-merit. It is a ratio of the heat transfer to pressure drop in the regenerator. The heat transfer is characterized by the Colburn factor, j_h , while the pressure drop is characterized by the friction factor, f (Kays and London, 1984:7).

A relationship between the *COP* and the compactness factor can be written for a given set of operating conditions and geometrical parameters of a cryocooler. For example, for an ideal Stirling cycle operating between T_c and T_e , with a volume compression ratio, r_c , and using a perfect gas with gas constant R , the heat removed from the refrigerated volume is written (Huang, 1976:304-305)

$$Q_{ei} = R T_e \ln(r_c) \quad (1)$$

The net work input to the ideal cycle is written

$$W_{net} = R (T_c - T_e) \ln(r_c) \quad (2)$$

Consequently, the ideal *COP* is written

$$COP_i = \frac{T_e}{T_c - T_e} \quad (3)$$

To account for the imperfection in the regenerator, the shortfall in heat transfer during one blow through the regenerator must be deducted from the ideal heat transfer from the refrigerated space,

$$Q_e = Q_{ei} - (1 - \epsilon) Q_R \quad (4)$$

where ϵ is the effectiveness, i.e. the ratio between the heat transfer to the regenerator, Q_R , and the ideal heat transfer to the regenerator under the same conditions. Q_R is written

$$Q_R = C_V (T_c - T_e) \quad (5)$$

Hence, the *COP* for the non-ideal cycle is

$$COP = COP_i - (1 - \epsilon) (T_c - T_e) \frac{C_V}{R (T_c - T_e) \ln(r_c)} \quad (6)$$

But, a simplified analysis shows (Urielli and Berchowitz, 1984:118)

$$\epsilon = \frac{N_{tu}}{N_{tu} + 1} \quad (7)$$

where N_{tu} is the number of thermal units. Consequently, the *COP* is written

$$COP = COP_i - A^* \frac{(T_c - T_e)}{(N_{tu} + 1)} \quad (8)$$

where $A^* = c_v / (T_c - T_e) / \ln(r_c) / R$. But, for a perfect gas, $(T_c - T_e) = \Delta p / \rho / R$, therefore

$$COP = COP_i - A^{**} \frac{1}{\frac{N_{tu}}{\Delta p} + \frac{1}{\Delta p}} \quad (9)$$

where $A^{**} = A^* / \rho / R$

From the definition of the compactness factor, $CF = j_h / f$, the ratio $N_{tu}/\Delta p$ can be written

$$\frac{N_{tu}}{\Delta p} = B^* CF \quad (10)$$

where $B^* = A_{sur}/A/Pr^{2/3}/(0.5\rho U_g^2)$
 A_{sur} = surface area of the matrix - m^2
 A = cross sectional area of the matrix - m^2
 Pr = Prandtl number ($c_p \mu / k$)
and U_g = gas velocity

Hence, the COP is written

$$COP = COP_i - \frac{A^{**}}{B^* CF + \frac{1}{\Delta p}} \quad (11)$$

This equation shows that the best efficiency (Carnot) can be approached for large values of CF and small Δp , although the term involving CF is usually much larger than the inverse of

the pressure drop. The importance of the heat transfer and pressure drop characteristics of a regenerative heat exchanger is explained more fully in the next section.

Performance Factors. There are three factors which significantly affect the *COP* of a regenerative refrigeration cycle: 1) regenerator effectiveness, 2) pressure drop, and 3) dead volume. All three factors are influenced by the design of the regenerator.

Regenerator Effectiveness. Below, a definition for regenerator effectiveness is given, as well as the importance of effectiveness for a good *COP*. The most common design approach for maximizing effectiveness is described and a typical range of effectiveness values is included to facilitate comprehension of current capabilities.

The regenerator effectiveness is defined as the ratio of the energy transferred during a blow through the regenerator, to the energy that would have been transferred in an ideal regenerator operating between the same two temperatures, T_e and T_c . During the cold blow, for example, the regenerator ideally receives gas at T_e and gives it up at T_c , meaning an ideal energy transfer per unit mass of $c_p(T_e - T_c)$, where c_p is the specific heat of the gas at constant pressure. However, real regenerators have finite heat capacities, and inducing heat transfer between the gas and the regenerator matrix requires a temperature difference. Consequently, the cold blow gas leaves the regenerator at a temperature lower than T_c .

and the hot blow gas leaves the regenerator at a temperature higher than T_e . For high-efficiency, space-based cryocoolers, a typical regenerator effectiveness exceeds 0.95.

The COP of a Stirling cycle is strongly dependent on the regenerator effectiveness. In Fig. 3, the results of a study by Tailor and Narayankhedkar (1988) show the COP plotted versus the volume compression ratio, r_c , which is defined as the ratio of the volume of the gas before compression, to the volume of gas after compression. For a range of compression ratios common to cryocoolers, a COP reduction of nearly 20% occurs for just a 1% reduction in effectiveness. Clearly, it is important to have as high a regenerator effectiveness as possible.

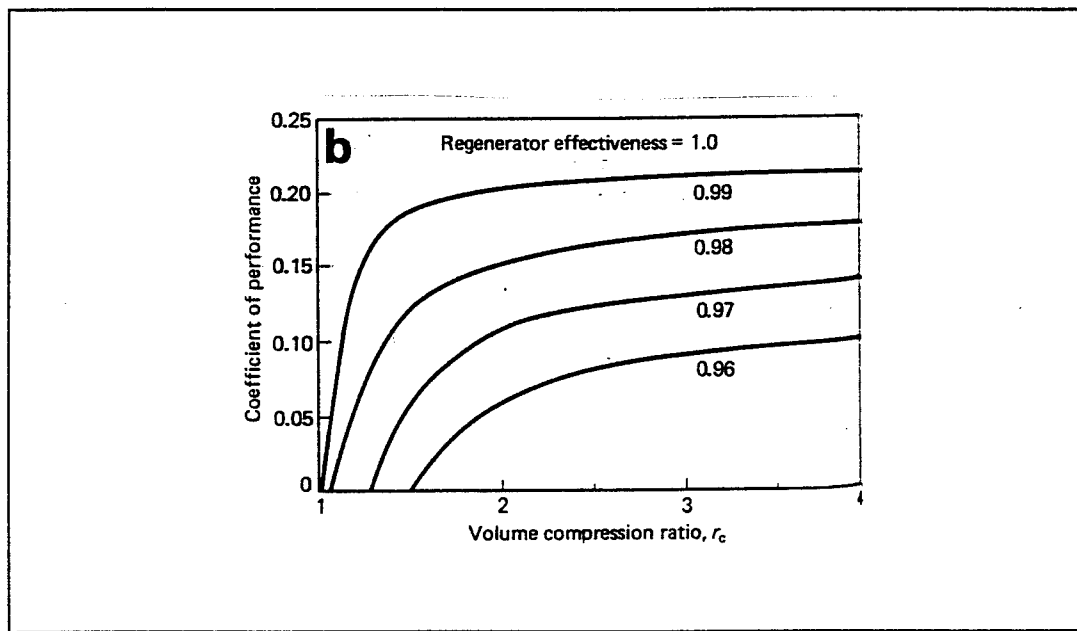


Figure 3. COP vs Compression Ratio and Effectiveness
(Tailor and Narayankhedkar, 1988:40)

High regenerator effectiveness is achieved in the following way. Small-diameter wire (0.02 - 0.20 mm), closely-packed (100-400 mesh), stainless steel or phosphor-bronze screens are used. The screens are punched into disks the diameter of the conduit between the expansion and compression spaces. A number of randomly-oriented disks are then stacked together to form the regenerator. The tortuous path the gas must travel through the tightly-spaced, randomly-oriented wire screens causes the gas to have extensive contact with the regenerator material in short axial distances, i.e. the regenerator has a large surface-area-to-volume ratio. The turbulent flow has a large heat transfer coefficient, usually greater than $5000 \text{ W/m}^2/\text{°C}$. A linear temperature profile exists in the regenerator (Yuan et al, 1992; Tanaka et al, 1990). Consequently, as the gas weaves its way through the regenerator, it effectively exchanges energy with the wire screens which are made from a material with a relatively high thermal capacity. The combination of large surface-area-to-volume ratio, large heat transfer coefficient, and large thermal capacity causes the regenerator to have a large effectiveness. Regenerator configurations other than stacked wire screens are used (Radebaugh and Louie, 1986:180; Venkatarathnam, 1990), but wire screens are the most common.

Pressure Drop. A negative consequence of the tightly-packed porous material in the regenerator is a large pressure drop, compared to flow through an open pipe for

example. Both inertial effects (numerous accelerations due to change in direction and pore size) and surface shear stresses, contribute to this pressure drop (Organ, 1984; Krazinski, 1986; Kays and London, 1984; Armour and Cannon, 1968). The larger the pressure drop in the cryocooler, the larger the net work input becomes. This reduces the *COP*. Consequently, the cryocooler designer tries to minimize the losses associated with pressure drops in the regenerator.

However, minimizing the pressure drop poses a dilemma. The steps one would take to reduce the pressure drop in the regenerator, e.g., making the pore size large and straightening the gas flow channels, would also reduce its effectiveness. As stated above, the effectiveness of the regenerator is the dominant factor for determining cryocooler performance (Martini, 1980:57; Urieli and Berchowitz, 1984:99; Tanaka et al, 1990:177). Hence, the regenerator designer chooses the wire screen geometry that produces the effectiveness needed to fulfill the *COP* requirement of the system, and the pressure drop plays a secondary role. But there is one other factor to consider.

The Dead Volume. The third factor which significantly affects the performance of a cryocooler and which is directly influenced by regenerator design is the dead volume. The dead volume is any gas-filled space in the cryocooler which is not part of the expansion or compression spaces, for example conduits, heater tubes, and pore space in

the regenerator. Martini (1980), Jones (1986), Radebaugh and Daney (1984), Tailor and Narayankhedkar (1988), and Romm and Smith (1993) have shown the performance of the cryocooler is degraded by excessive dead volume. Fig. 4 shows *COP* plotted versus volume compression ratio, r_c , defined above. For a typical r_c of around 3.0, and a dead volume ratio of 1.0 (here defined as the ratio of the dead volume to the swept volume in the expansion space), the *COP* is 0.21. If the dead volume is reduced by a factor of 25%, the *COP* can be increased to 0.218, which is an increase of 4% in *COP*. This represents a significant improvement in the performance of a cryocooler since by the time the compressor and solar panel efficiencies are included in the overall energy savings, considerable weight and solar panel area have been saved.

The porosity of the regenerator matrix determines its dead volume. Porosity is defined as the ratio of the volume of the dead space to the total volume of the regenerator. The value of the porosity for most regenerators ranges from 0.5 to 0.8. But these porosities also indicate over half of the space occupied by the regenerator is dead volume. If a way could be found for achieving the effectiveness needed for system *COP* requirements without increasing the pressure drop while also decreasing the dead volume in the regenerator, overall cryocooler performance would be improved.

Rolling the wire screens would reduce their thickness. Stacking thinner screens together reduces regenerator volume

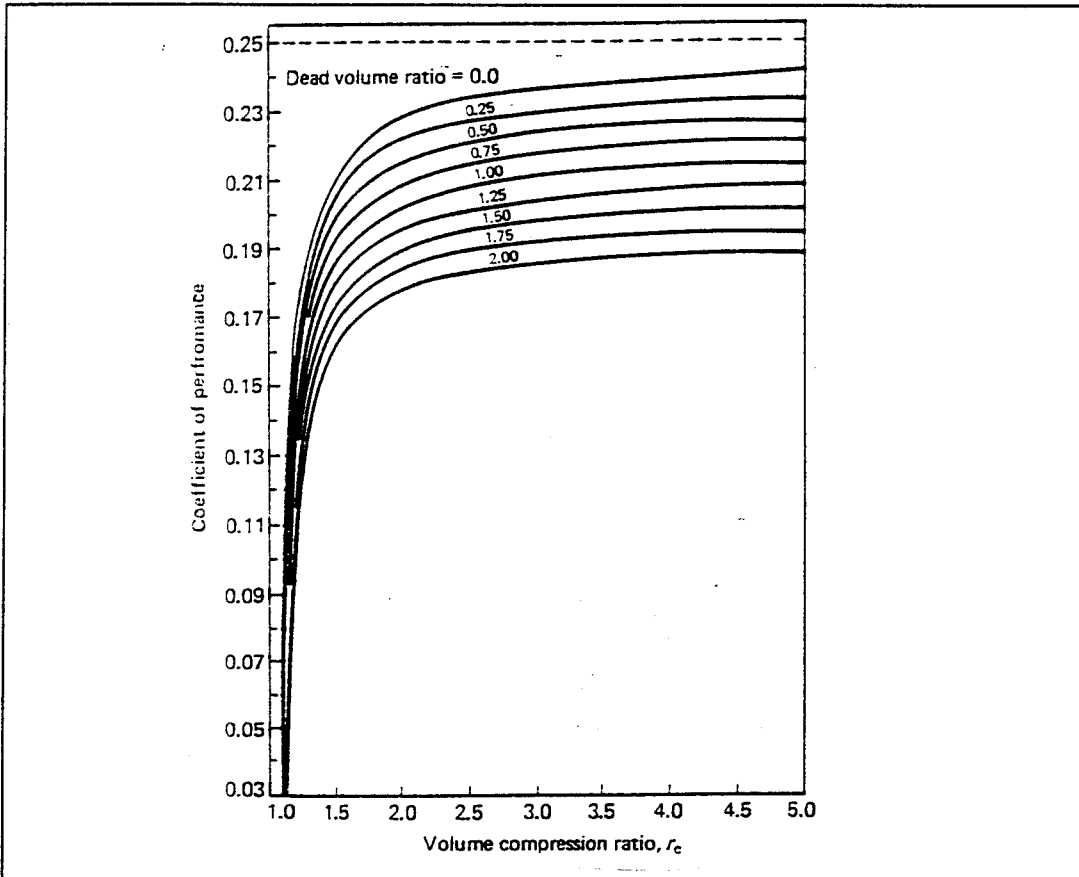


Figure 4. Effect of Dead Volume on COP
 (Tailor and Narayankhedkar, 1988:41)

without reducing the volume of wire. Hence, pore sizes in the reduced-thickness regenerator are smaller, and the amount of dead volume is decreased. The objective of this research is to investigate the effect of rolled screens on the heat transfer and pressure drop characteristics of stacked wire-screen regenerators and to determine if the reduction in thickness causes a decrease in the compactness factor.

Justification

It is impossible to predict how the heat transfer and friction characteristics would change if the geometry of the screen wires were flattened. The flow of gas through a wire-screen regenerator is very complicated. A number of small-scale phenomena, such as increased apparent conductivity, channelling (non-uniform flow through the porous medium), and secondary vortices, influence the effectiveness and pressure drop of the regenerator (Hutchinson and Ross, 1987; West, 1986). These phenomena are not well understood nor quantified (Organ, 1992). If they were, the precise geometry and orientation of the regenerator matrix could be determined in advance. And yet, there is no reason to believe that screens made from perfectly round wire give the best results. They are certainly the easiest to manufacture, but flattening the screens by 15 or 30 percent, may have only a minor effect on important flow characteristics in the regenerator, like pressure drop and heat transfer coefficient. All the while, the benefit of a reduction in dead volume would be realized.

Evidence exists that supports the contention flattening the screens improves system-level performance. The first piece of evidence is shown in the top part of Fig. 5. Cycle efficiency and indicated power for a newly-developed engine are plotted as a function of engine speed (Nagawa, et al, 1987). These results are for a power generation cycle, as opposed to a refrigerator, but the conclusions can be directly

applied. The indicated efficiency, which is the ratio of the indicated power output to the net rate of energy input, is reportedly improved by as much as 5% using a regenerator which is made of alternately-stacked, rolled (assumed the same as pressed) and round wire screens.

Other data given in Fig. 5 indicate the pressure drop characteristics of a regenerator change if the geometry of the screens changes. The bottom part of Fig. 5 shows the pressure drop for rolled wire screens is significantly higher than the pressure drop for normal round wire screens. Also shown in the bottom part of Fig. 5 is that alternately rolled and round wire screens stacked randomly curiously results in a lower pressure drop. These data indicate for the operating conditions in the test, a combination of rolled and round wire screens reduced pressure drop through the regenerator, while using rolled wire screens alone increased it. However, a range in pressure drops might be achieved by rolling the wire screens by various amounts. An optimal condition for overall cycle performance should exist.

Although the issue of regenerator effectiveness is not directly addressed in the Nagawa article, the following can be concluded. If the effectiveness had been degraded excessively by the arrangement of rolled and round wire screens, the cycle efficiency would not have been improved as shown. In fact, the authors reported their regenerator not only achieved a reduction of flow friction loss, but also achieved effective

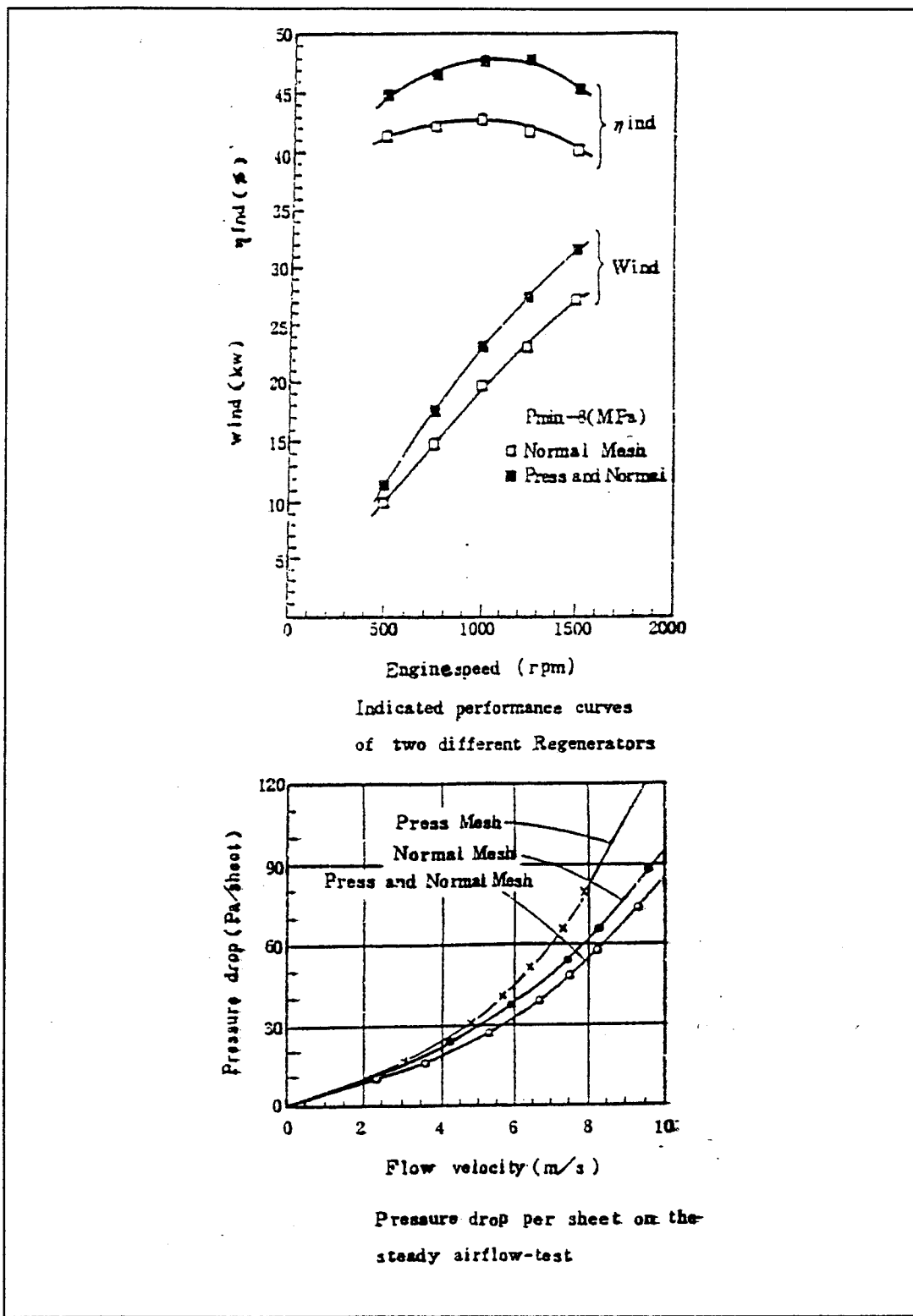


Figure 5. NS30A Performance and Pressed Screen Results
(Nagawa et al., 1987:1799)

heat transfer (Nagawa et al., 1987:1799). Hence, although it is not clear which if any of the three performance factors discussed earlier caused the improvement in the engine performance, using a mixture of rolled and unrolled wire screens in the regenerator altered the performance significantly. For the NS30A engine, the performance was improved, but this might not always be the case.

The evidence given above cannot be considered complete. Details about the amount and type of rolling, the arrangement of the screens, definition of terms, and the experimental procedure are not available for scrutiny. It is not obvious staggering rolled and unrolled wire screens would cause an improvement in pressure drop. Perhaps a quirk in the definition of terms or testing procedure caused the reported results. Yet, some rationale may exist to explain these improvements in efficiency and pressure drop. Hence, although the evidence given above seems to contradict the hypothesis given in Chapter I, it is for only one case, and the documentation is not complete. In any case, direct correlation between the improvement in system-level performance and the characteristics of the regenerator as measured by the compactness factor have not been made. Since a higher compactness factor correlates with higher engine efficiency (shown earlier), the improvement in engine efficiency due to a reduction in dead volume caused by manufacturing the regenerator with pressed screens may

outweigh the decrease in compactness factor due to the pressed screens shown in this study. The focus of the current research is on a component-level characteristic, i.e., the effect of rolled screens on the compactness factor, and not on the system-level performance.

Other evidence exists which directly addresses the hypothesis. An experimental result by Wiese (1993) using a single-blow, transient procedure, showed that the screens could be reduced in thickness by as much as 30% without significantly increasing the pressure drop. The heat transfer results from Wiese's study are not as conclusive. His research indicated that at very low Reynolds number (based on hydraulic diameter, $Re_{dh} = U_g d_H / v$), the heat transfer coefficient is significantly reduced, while at higher Re_{dh} , the effect on heat transfer coefficient is less pronounced. These results indicate that some Reynolds number range may exist where both the pressure drop and heat transfer characteristics of the rolled screen regenerator are only changed slightly, e.g., the compactness factor is not changed, while the reduction in dead volume is significant. Wiese's testing range was for $Re_{dh} \leq 100$. This range is low compared to typical cryocooler operating conditions which is $50 \leq Re_{dh} \leq 800$ (Organ, 1992: App. VI; Seume and Simon, 1986: 533-538; Walker, 1983:127).

The evidence given above seems to contradict the contention that using rolled screens in the regenerator

decreases the compactness factor. Detailed studies which cover a range of operating conditions and regenerator configurations are scarce. A literature search which encompassed the last 40 years, 170 documents (books, papers, contractor reports), and research on three continents (North America, Asia, and Europe) revealed only the Wiese and Nagawa citations mentioned above. Wiese described his recent discussions with cryocooler experts who attended the 8th International Cryocooler Conference in June of 1994 , and who had attempted to improve regenerative refrigeration cycles with rolled screens, revealed mixed results. One researcher noted a significant improvement in COP using rolled wire screens (as much as 30%), while another reported no improvement at all (Wiese, 1994). A more comprehensive study is needed. The study should include varying the amount of rolling (reduction factor), different mesh sizes and porosities, and a range of Re applicable to cryocoolers. A better understanding of the effects of screen thickness reduction on the compactness factor over a wide range of operating conditions would allow regenerator designers to perform trade off studies between the benefits of lower dead volume and the detriments of lower compactness factor.

In summary, regenerative refrigeration cycles are an important technology. The performance of these cycles is improved by reducing the dead volume in the system. Rolling the screens which are used to make the regenerator in these

systems would reduce the dead volume. Currently, the effects of this screen thickness reduction on the heat transfer and friction characteristics of the regenerator, or their ratio, the compactness factor, are neither quantified nor well understood. Hence, the hypothesis given in Chapter I which motivates the current research was formulated.

III. Methodology

This chapter describes the method for proving the hypothesis stated in Chapter I. The theory of the classical approach for finding the heat transfer coefficient in a porous medium is given, and how this approach was modified for the current research is explained. Next, the numerical model and procedure for determining the heat transfer coefficient and other important results are described. The experimental apparatus and data reduction technique are described in Chapter IV.

Theory

This section of the dissertation addresses three topics. First, a description is given of the step-change transient technique which has been used to determine heat transfer coefficient for porous material heat exchangers for nearly thirty years. Second, an explanation of the shortcomings of the technique is presented. Third, improvements to this approach are offered along with the rationale behind the modifications.

Step-Change Transient Technique. This technique was originally described by Pucci, et al. (1967). As an overview, the heat transfer coefficient is determined with the step-change transient technique by comparing an experimental measurement of the maximum slope of the outlet temperature

trace for a gas flowing through a porous medium subjected to an impulsive change in inlet temperature, with an analytical solution for the maximum slope. Directly measuring the area, energy flow, and temperature difference which define the heat transfer coefficient cannot be done since instrumenting the tiny porous structure in a regenerator causes changes in the local flow conditions. Even if a local heat transfer coefficient could be determined, it would not be representative of the entire porous medium since the velocity of the fluid and the surface area of the porous medium change significantly from one location to another. Hence, certain assumptions are made in a simplified model of the flow, e.g. that the heat transfer coefficient, h_{conv} , is constant, and the magnitude of the heat transfer coefficient is determined by comparing the results of an easily measured quantity like the outlet temperature, to the analytical result.

Predicting the magnitude and direction for flow of a gas through a porous medium regenerator is complicated by the numerous accelerations and changes in direction experienced by the gas as it winds its way through the randomly oriented pore structure. To make the task manageable, certain assumptions are made about the flow. The pore sizes are assumed uniform and the flow is assumed to be one-dimensional. The average velocity at any location in the regenerator is presumed to be in the direction of the regenerator axis with a magnitude

equal to the total mass flow rate divided by an average density, divided by the average cross-sectional area for flow. If the Mach number is kept below 0.2, compressibility effects can be ignored (Walker, 1983:Part I, Section 5.3) and the mass velocity, U_g , is constant. If it is further assumed that temperature and pressure differences throughout the regenerator are kept small (say $< 20^\circ \text{C}$ and 50 kPa), then gas properties are constant. Further, if convective heat transfer between the gas and the regenerator is the only energy exchange mechanism considered, the energy equations for the gas and matrix are written as follows:

Gas:

$$-\dot{m} c_p \frac{\partial T_g}{\partial x} \Delta x + h_{conv} A_s (T_r - T_g) = \rho c_v A \Phi \Delta x \frac{\partial T_g}{\partial t} \quad (12)$$

Matrix:

$$h_{conv} A_s (T_g - T_r) = \rho_m c_m A \Delta x (1 - \Phi) \frac{\partial T_r}{\partial t} \quad (13)$$

where	\dot{m}	is the mass flow rate (kg/sec)
	c_p, c_v	is the specific heat of the gas at constant pressure and volume, respectively (J/kg/°C)
	c_m	is the specific heat of the matrix (J/kg/°C)
	T_g, T_r	are gas and matrix temperature, respectively (°C)
	Δx	is a linear increment (m)
	h_{conv}	is the heat transfer coefficient (W/m ² /°C)

ρ/ρ_M are the gas and matrix densities (kg/m^3)
 A is the tube cross sectional area (m^2)
 A_s is matrix surface area (m^2)
 x, t are the axial location and time
and Φ is the porosity defined as the volume of the gas divided by the total volume of the regenerator.

Pucci, et al. (1967:30) showed that with the introduction of the appropriate dimensionless variables, along with an adiabatic boundary condition and the impulsive step-change initial condition, this equation could be solved for the temperature of the gas as a function of time and axial location. The solution is an infinite series of Bessel functions which depends on a previous knowledge of the heat transfer coefficient. However, Locke (1950) showed that the maximum slope of the dimensionless temperature at the outlet is solely a function of the heat transfer coefficient:

$$\frac{\partial \Theta}{\partial \tau} \Big|_{\max} = \frac{Ntu^2}{\sqrt{Ntu \tau}} [-i J_1(2 i \sqrt{Ntu \tau})] \exp^{-(Ntu + \tau)} \quad (14)$$

where Θ is a dimensionless temperature
 τ is a dimensionless time
and N_{tu} is the number of thermal units =
 $(h_{conv} A_s / \dot{m} C_p)$

This solution to the governing equations of the step-change transient approach offered an elegant method for determining the heat transfer coefficient. First, introduce an impulsive

step-change in inlet temperature to the flow of gas through a porous medium regenerator. Next, measure the maximum slope of the outlet temperature trace. Finally, from the maximum gradient of the dimensionless outlet temperature Θ with respect to the dimensionless time, a value for Ntu can be calculated. From this Ntu , the h_{conv} can be calculated. This method for determining the heat transfer coefficient will be referred to as the analytical method due to Pucci, et al., in the remainder of this text.

Other researchers take a slightly different approach. Liang and Yang (1975) used outlet temperature data at four or five points to calculate a minimum root-mean-squared difference between an experimental outlet temperature and one determined by an analytical solution. In fact, since its introduction, several modifications and improvements have been made to the step-change transient technique (Stang and Bush, 1974; Yagi, 1991), but the basic approach remains the same.

Problems with the Step-Change Transient Technique. There are three major problems with the technique described in the last section. First, obtaining an adequate approximation to an exact step-change in the laboratory is impractical. Second, if one chooses to use the maximum slope approach, it is very difficult to obtain an accurate slope from experimental data. Third, the model ignores some important physics. In this section, the cause of these discrepancies

between the theory and experimental results is reported as well as the effect on the determination of the heat transfer coefficient.

With regard to the first problem, any attempt at producing a step-change in temperature in the laboratory will have some time delay. Consequently, whether using a maximum slope, or a root-mean-squared difference, the calculated heat transfer coefficient will be smaller than it should be, because the output temperature trace will be less steep than it should be if the input temperature trace is less steep than ideal.

The second major problem is associated with using the maximum slope. Digitally acquired experimental data inherently lack smoothness. Digital data are not continuous, a mathematical requirement for the existence of the slope. Data are collected at sampling rate intervals which are small, but are not continuous, even in the limit. Second, experimental data have some scatter. Gradients can shift wildly from one set of sampling points to the next, particularly if one uses a very high sampling rate and the time step between data points is small. One could use filtering techniques or Fourier transforms to improve the appearance of the data, but these techniques have a deleterious effect on the final value for the slope. For example, large order filters smooth out any discontinuities in

the data, but this can significantly change the value of the slope. Other researchers have noted these problems also (Shoup, 1977: 220).

The third major problem with the step-change technique is that heat transfer to the tube wall is ignored. The importance of the wall became apparent during check-out of the experimental set-up. During some preliminary transients, an unexpected outlet temperature behavior was observed. In Fig. 6, a temperature transient for an empty tube is shown. The inlet and outlet temperatures at the start of the test run were at the same steady-state value. When the transient began, the inlet temperature, T_{g1} , abruptly fell, and soon began to relax towards another steady-state value. Similarly, the outlet temperature trace, T_{g2} , fell sharply, and relaxed toward a new steady-state value. But the later time T_{g2} is approximately 1-2° C above that of the later time T_{g1} . This indicated a discrepancy in the energy exchange terms included in Pucci's model in Eqs (12) and (13). T_{g1} and T_{g2} should relax toward the same late-time temperature since only interaction between the gas and the matrix is relevant.

Before taking any heat transfer coefficient data, the discrepancy had to be explained. After repeated careful calibrations of the thermistors which measure T_{g1} and T_{g2} , and modifications to the instrumentation, the temperature gap at late time remained. Apparently, the tube and its connections

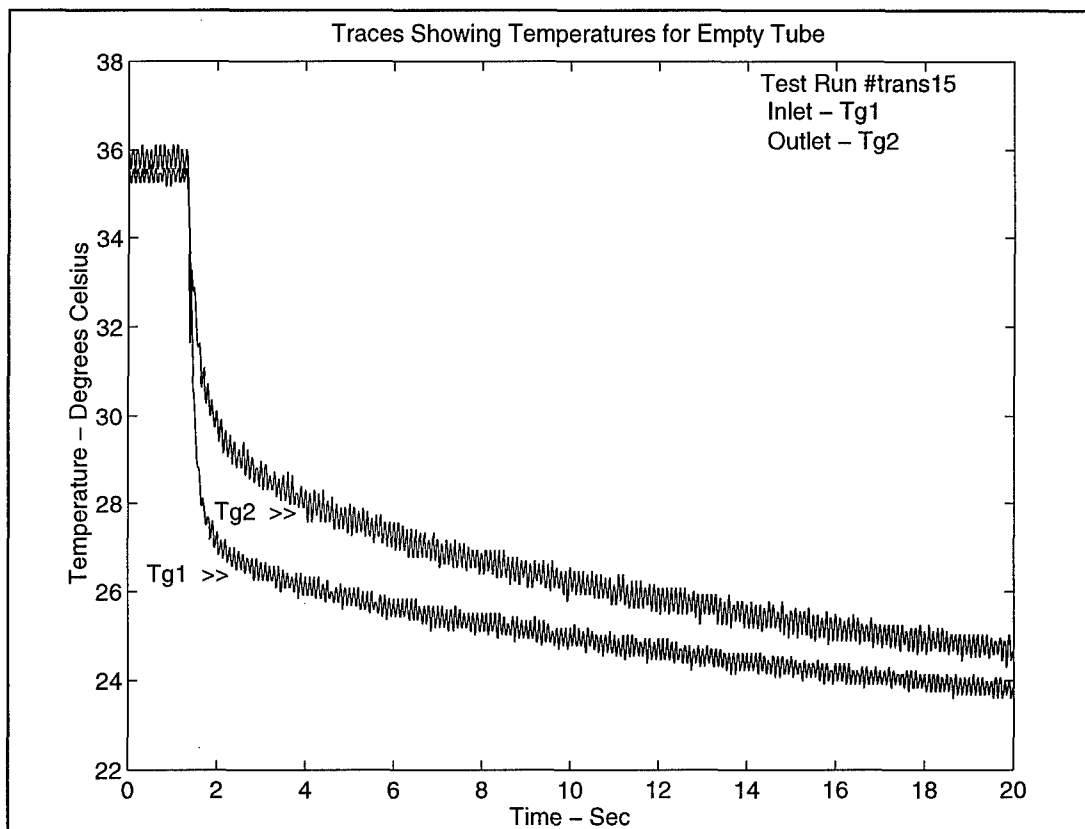


Figure 6. Temperature Gap for Empty Tube

were supplying enough energy to measurably influence the temperature of the gas for a significant time after the transient was completed. A simple calculation shows the thermal inertia of the tube and environment is much larger than the thermal inertia of the matrix. If the tube and matrix are treated in a lumped-parameter sense, and if the heat transfer coefficient between the gas and the tube is considered the same as between the gas and the matrix, the ratio of time constants for heat transfer for a length of tube to that for a length of matrix is written:

$$\frac{\tau_t}{\tau_r} = A_r \frac{t_t}{(1 - \Phi)} \quad (15)$$

where τ_t is the time constant for a length of tube (sec)
 τ_r is the time constant for a length of regenerator matrix (sec)
 t_t is the tube thickness (m)
 Φ is the porosity
and A_r is the specific surface area for heat transfer per unit volume of the matrix (m^{-1})

For the twelve SUs used in the current research, this ratio ranged from 16.4 for SU #1 (100 mesh, Reduction Factor = 1.0), to 47.2 for SU #12 (250 mesh, RF=0.5). Consequently, the heat transfer in the matrix occurred at a higher rate than that for the tube. Thus, the early-time heat transfer should be studied to get the best estimate of the heat transfer coefficient for the matrix. However, the step-change transient technique concentrates on relatively late time events. Hence, both the maximum slope and the minimum root-mean-squared difference approach to the classical step-change transient technique result in erroneous, low values for the heat transfer coefficient.

In summary, the step-change transient technique is a simple approach for determining the heat transfer coefficient for a complicated phenomena, flow through a porous media. However, it focuses on properties of the outlet temperature trace to calculate the heat transfer coefficient. If these

properties are altered by the inability to accurately produce a step-change in temperature, or by the measurement of the maximum slope, or by heat transfer between the gas and the tube wall, then an erroneous value for the heat transfer coefficient will be calculated. An improved approach is offered next, based on the same fundamentals of the step-change technique, but which mitigates the problems discussed above.

Improvements to the Step-Change Transient Technique.

Three major modifications to the classical method described above are made in the current research. The first is to eliminate the assumption that an exact step-change in temperature occurs at the inlet. This is accomplished by measuring the inlet temperature trace and using it in a numerical model. Current data acquisition systems and computers make this task manageable.

The second major improvement is the inclusion of the tube which surrounds the matrix in the model. Before deciding on just how to do this, further investigation on the effects of the tube was done. SU #1 was instrumented with a small thermocouple on the outside surface of the tube midway between the ends. The temperature of the tube was monitored during a transient. The results are shown in Fig. 7. The tube temperature stayed constant at its original value until midway through the transient, then it rose rapidly and relaxed to a

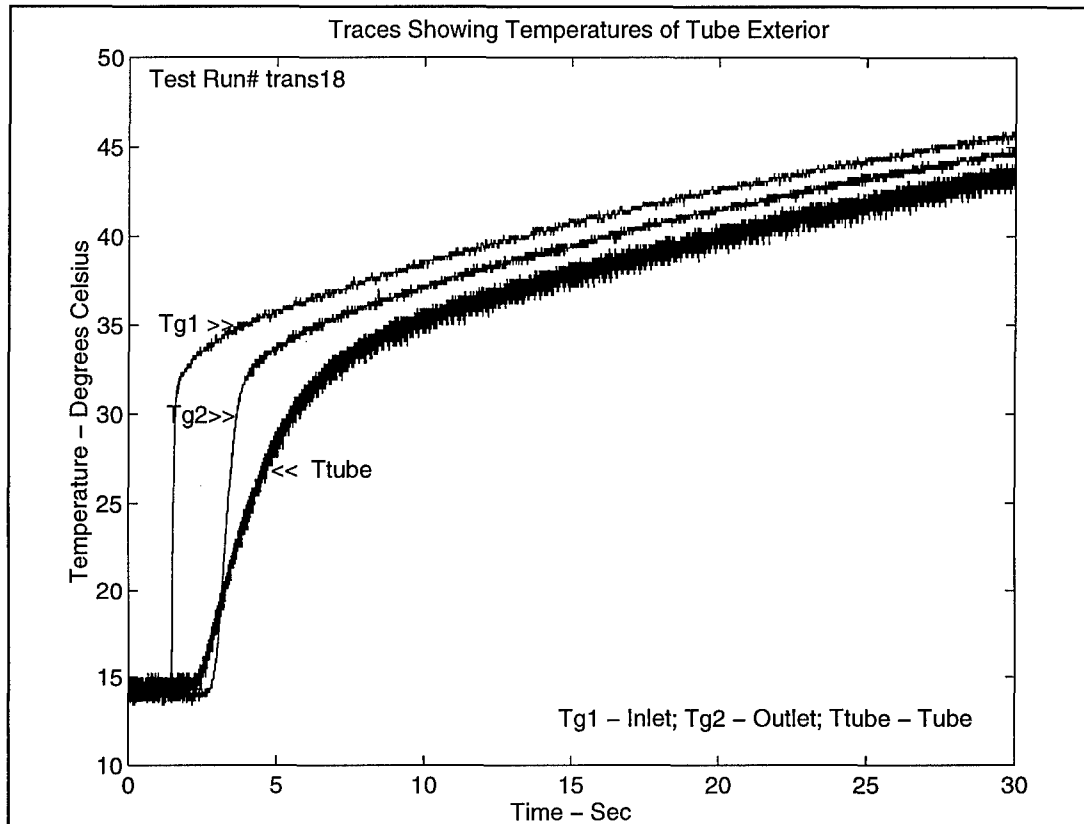


Figure 7. Temperature of the Tube

steady state value below that of either the inlet or outlet gas.

Three comments about transient heat transfer to the tube are important. First, the data show, when a regenerator is in the flow, a temperature wave travels down the tube and matrix, i.e. rather than a smooth transition between the initial and final step-change in temperature, the transition is abrupt, and the location of this abrupt transition moves down the axis of the regenerator with time. Second, because of this traveling temperature wave, whether the tube is a thin-walled

conductor or an insulator, the boundary condition for the tube changes with time. No simple analytic boundary condition, e.g. adiabatic or isothermal, could replace the effect of the tube. Third, a comparison between the time constant for a unit length of tube to that for a unit length of matrix was shown earlier. This comparison showed that the tube by itself has a much longer relaxation time than the matrix. The tube is connected on either end to copper tubing. The effect of the adjoining web of highly conductive copper tubing is to increase the relaxation time of the tube temperature by conducting heat through the sealed connections at each end. This effect of conduction through the ends of the tube would require additional instrumentation and modelling. In view of the above considerations, a simple lumped-parameter approach was assumed for inclusion of the tube, i.e. the heat transfer coefficient between the gas and the tube is assumed to be the same as between the gas and the matrix, and the tube wall temperature is assumed constant in the radial and azimuthal directions at each axial location of the tube. Since the choice of heat transfer coefficient depends on early time criteria (see below), and the time constant for the matrix is at least 16-40 times faster than the time constant for the tube and surroundings, the results obtained by treating the tube as a lumped thermal mass are acceptable. The merits of this approach are discussed below and in Chapter IV.

The third major improvement deals with the criteria for selecting the heat transfer coefficient. A characteristic of porous media is that it acts like a thermal sponge. The rest of this section describes this characteristic in more detail, defines a parameter of each SU called the sponge effect delay time, SEDT, and explains how this parameter can be used to calculate the heat transfer coefficient.

The sponge effect of a regenerator can be demonstrated from results shown in Fig. 6 and Fig. 8. For the empty tube in Fig. 6, the outlet temperature trace changes almost immediately, in tandem with the inlet temperature trace. The difference between the two traces is attributed to some heat transfer between the tube and the gas. However, when a regenerator is present as in Fig. 8, the gas at the outlet stays at nearly the initial steady state temperature for some time before it begins to change. As discussed in Chapter II, porous medium regenerators are effective in capturing a large amount of energy from the incoming stream of gas. This effectiveness of the regenerator matrix causes the observed delay time between the beginning of the transient and when the outlet temperature begins to fall.

The definition of the sponge effect delay time is as follows: It is the time it takes for the outlet gas temperature to change a measurable amount. For the current research, the definition of a measurable temperature change is

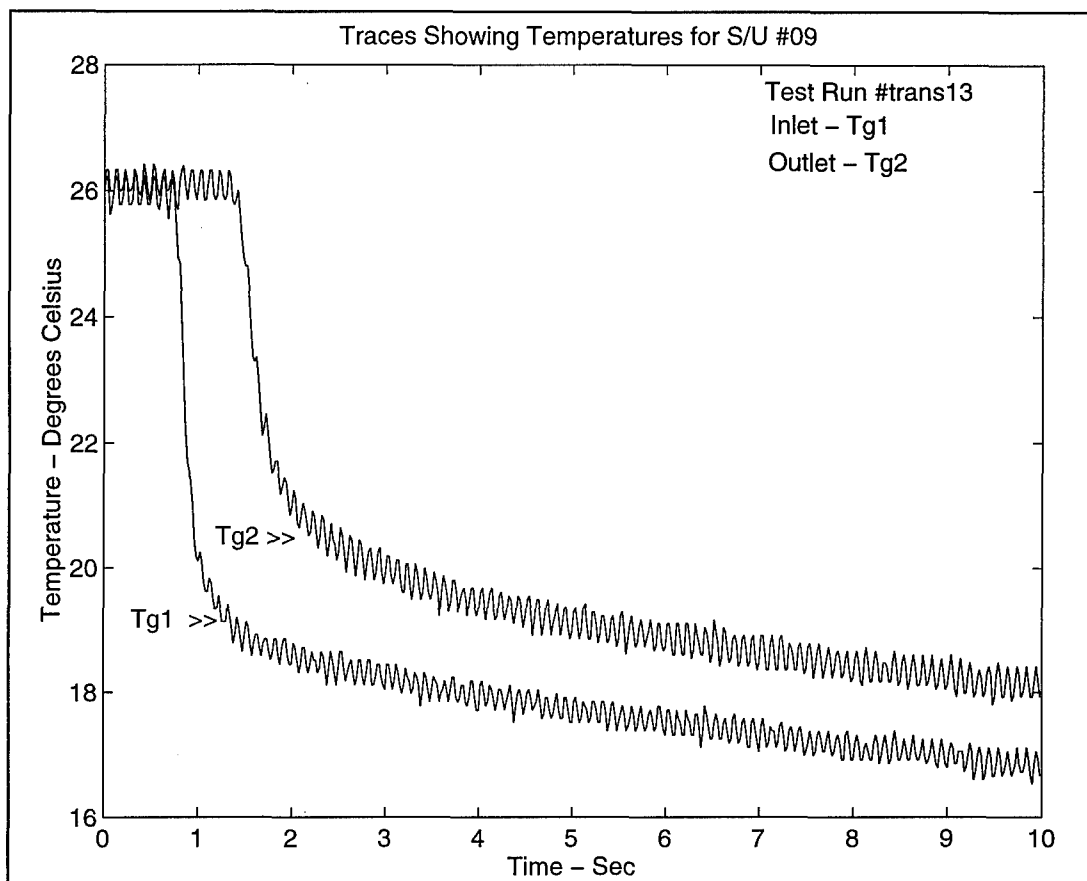


Figure 8. Regenerator Sponge Effect Delay Time

that the value of the outlet temperature deviates from its running average by more than twice the accuracy of the temperature measuring device, or about 0.4° C for the current research.

Using the sponge effect delay time in conjunction with the step-change transient technique gives a better value for the heat transfer coefficient than either the maximum slope or the minimum root-mean-squared difference approach described

above. Three arguments can be made to substantiate this claim.

First, the best value for the heat transfer coefficient will be found during that time when heat transfer between the gas and the matrix dominates. Early in the transient, the interaction between the tube and the gas is less important than energy exchange between the gas and matrix because the surface area per unit length of the porous medium ranges from 40.5 times larger (100 mesh) to 101 times larger (250 mesh) than the surface area of the tube (Miyabe, et al., 1982:1840) while the temperature gradient is approximately the same. The analysis of time constants for a length of tube given above showed that the tube and its environment are sixteen to forty seven times slower to respond to the transient than the regenerator. Hence, during the sponge effect delay time, heat transfer between the gas and the matrix dominates energy exchange. The assumptions made in the numerical model more nearly match the physics of the flow during this early time, and a better result for the heat transfer coefficient is obtained.

The second part of the argument that a heat transfer coefficient based on the sponge-effect delay time would be better than one based on either the maximum slope or a minimum root-mean-squared difference is that the delay time is a characteristic of the regenerator while the outlet temperature

trace is not. Fig. 9 shows calculated outlet temperature traces from the numerical model described below for an artificial step-change in inlet temperature. One of the traces includes the effects of the tube, the other shows the result without tube effects. Clearly, one can obtain a wide range of slopes for the same regenerator since the temperature trace with no tube effect is much steeper than the trace including the tube effect. The minimum root-mean-squared difference approach is no better since the heat transfer coefficient chosen with this approach gives the best match between the experimental outlet temperatures and those calculated by a selected analytical model, whether the analytical model includes all the important physics of the flow or not. Hence, an approach which includes choosing the heat transfer coefficient based on the outlet temperature trace has inherent difficulties which are better addressed by using the sponge effect delay time.

The third part of the argument for the improvement offered by the current method can also be seen from Fig. 9. Whereas a wide range of outlet temperature traces can be manufactured depending on how much the tube and other factors affect the flow, the delay time is nearly insensitive to these extraneous factors. For the example in Fig. 9, the maximum slopes differ for the two cases by approximately 150%, whereas the delay times are only different by about 5% which can be

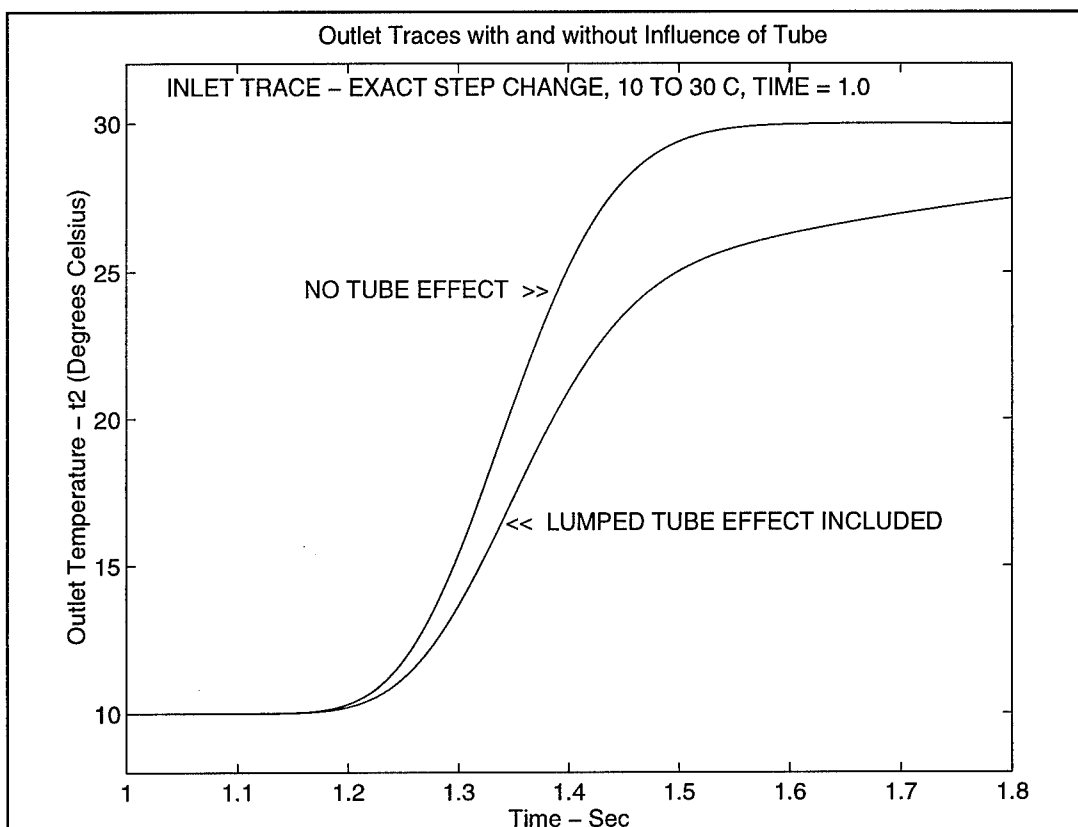


Figure 9. Comparison of Trace for Tube and No Tube

seen by comparing the time it takes for the two traces to change by 0.4°C from the initial temperature. Hence, the sponge effect delay time is an easily measured parameter of a SU which gives better results for the heat transfer coefficient than other parameters described above.

To summarize, one of the objectives of this research is to measure the heat transfer coefficient and friction factors for flow through regenerators made of stacked screens of varying reduction factors. The heat transfer coefficient cannot be measured directly, so an experimental set-up was

built to measure the inlet and outlet gas temperature during a quasi-step-change transient, along with other important measurements like pressure and mass flow rate. This data was put into a form suitable for use with a numerical model of the flow. This model generates an outlet temperature trace from which a characteristic parameter of the flow, the sponge effect delay time, can be determined. The criteria for choosing the heat transfer coefficient was the best match between the sponge effect delay time measured from experimental T_{g2} data and the one calculated by the numerical model. Details about the experimental set-up and data reduction technique are given in Chapter IV. A description of the numerical model and computational process is next.

Numerical Model

In this section, the numerical model for flow through a regenerator is described, and the process for choosing the best heat transfer coefficient is given. The discussion is in two parts. First, the governing equations, assumptions, boundary and initial conditions, and definitions for the FORTRAN program called *tsie* (for temperature solution, incompressible, explicit) are given. Second, the way that *tsie* was used within a larger FORTRAN program called *main* to determine the heat transfer coefficient is described.

Numerical Model of the Transient. The FORTRAN program named *tsie* is an explicit, finite difference numerical model

of an quasi-step-change transient. Its model is the same as the one used in the analytical approach of Pucci, et al., described above for the step-change transient solution except for two things: 1) the inlet temperature trace is used rather than an assumed step-change, and 2) the influence of the tube is included in the model. A lumped parameter approach to the gas/tube interaction is used and the heat transfer coefficient between the tube and the gas is assumed to be the same as the heat transfer coefficient between the gas and the regenerator matrix. Other assumptions in the model include no axial conduction (Wiese, 1993:2-7), no conduction between the tube and the matrix (they are locally at nearly the same temperature), perfect gas relations, constant properties, low Mach numbers, one-dimensional, incompressible flow, and a constant heat transfer coefficient. With these assumptions, the momentum equation shows the mass flow rate, and consequently, the mass velocity, is a constant. The important terms for the energy equation are shown in Fig. 10. There is internal energy flowing with the gas, convective heat transfer between the gas and the matrix, convective heat transfer between the tube and the matrix, conduction in the tube, and change in internal energy of the tube, matrix, and gas in the control volume. The outside surface and ends of the tube were considered adiabatic. With these interactions and assumptions in mind, three governing

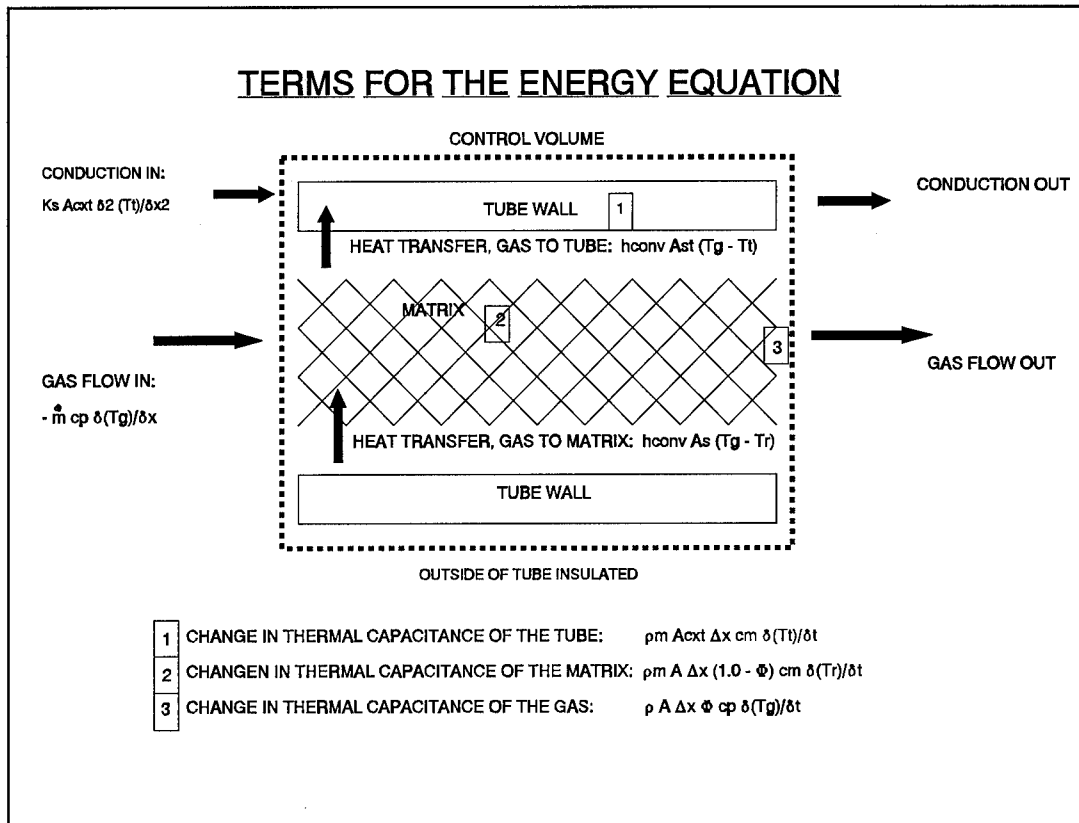


Figure 10. Control Volume for Energy Equation

equations can be written as follows:

Gas:

$$-\dot{m} C_p \frac{\partial T_g}{\partial x} \Delta x + h_{conv} A_s (T_r - T_g) + h_{conv} A_{st} (T_t - T_g) = \rho c_v A \Phi \Delta x \frac{\partial T_g}{\partial t} \quad (16)$$

Regenerator:

$$-h_{conv} A_s (T_r - T_g) = \rho_M c_M A (1 - \Phi) \Delta x \frac{\partial T_r}{\partial t} \quad (17)$$

Tube:

$$k_s A_{cx} \frac{\partial^2 T_t}{\partial x^2} - h_{conv} A_{st} (T_t - T_g) = \rho_m C_m A_{cx} \Delta x \frac{\partial T_t}{\partial t} \quad (18)$$

where \dot{m} is the mass flow rate (kg/sec)
 c_p, c_v are the specific heat of the gas at constant pressure/volume, respectively (J/kg/°C)
 h_{conv} is the heat transfer coefficient (W/m²/°C)
 A_s is the regenerator surface area (m²)
 A_{st} is the tube surface area (m²)
 A_{cxt} is the cross-sectional area associated with the tube wall thickness (m²)
 T_g, T_r, T_t are the gas, regenerator, and tube temperatures, respectively (°C)
 ρ is the gas density (kg/m³)
 A is the cross-sectional area of the inner diameter of the tube (m²)
 Φ is the porosity
 ρ_m is the density of the steel (kg/m³)
 C_m is the specific heat of steel (J/kg/°C)
and $\Delta x, \Delta t$ are the axial location and time increments, respectively (m, sec)

By grouping geometrical and physical properties together, using a first-order accurate forward difference in time, and a second-order accurate central difference in space, the equations can be recast as follows:

Gas:

$$TG_N^I = \left(-TG_{N+1}^{I-1} + TG_{N-1}^{I-1} + K_A TR_N^{I-1} + K_J TT_N^{I-1} + K_D TG_N^{I-1} \right) / K_B \quad (19)$$

Regenerator:

$$TR_N^I = K_C \ TG_N^{I-1} + (1.0 - K_C) \ TR_N^{I-1} \quad (20)$$

Tube:

$$TT_N^I = K_E (TT_{N+1}^{I-1} + TT_{N-1}^{I-1}) + K_F \ TG_N^{I-1} + K_H \ TT_N^{I-1} \quad (21)$$

where

I, N is the time, space index

$K_A = 2.0 \text{ St } (A_S/A_f)$

$K_B = (2.0/\gamma) (C/U_g)$

$K_C = \Delta t/\tau_m$

$K_J = 2.0 \text{ St } (A_{ST}/A_f)$

$K_D = K_B - K_A - K_J$

$K_E = \alpha_m \Delta t$

$K_F = \Delta t/\tau_t$

$K_H = 1.0 - (2.0 K_E) - K_F$

$A_f = \Phi A \quad (\text{flow area})$

$\text{St} = \text{Nu}/\text{Re}/\text{Pr} \quad (\text{Stanton number})$

$C = \text{Courant Number}, \Delta x/\Delta t$

$\alpha_t = \text{thermal diffusivity of the tube}$

$\gamma = c_p/c_v$

τ_m, τ_t are thermal time constants for the
matrix and tube

and U_g is gas mass velocity

With the finite difference form of the governing equations given, the next step was to define the initial and boundary conditions. The initial condition is the same for each of the three equations above. The gas, regenerator, and tube are all at the same initial, steady-state temperature. This temperature was determined by an averaging of the experimental gas temperatures for the one hundred time steps before the transient begins. The program begins calculations at $t=\tau_0$ and continues calculating until $t=\tau_f$, the end of the

transient. There are two boundary conditions: 1) the inlet gas temperature equals the experimentally measured value of T_{g1} , and 2) there is no conduction from the ends of the tube, i.e. an adiabatic boundary condition.

Calculations. A printout of the computer code is given in Appendix C. A summary of the way *tsie* calculates the outlet temperature trace, T_{g2} , is given here.

Step #1: Certain variables are input to the model, i.e. the starting guess for the heat transfer coefficient, h_{conv} , the maximum number of space increments, NMAX, and the value of the time increment, Δt .

Step #2: The geometrical, parametrical, and experimental data for a given test run are read into the program from the data file for that test run.

Step #3: The initial temperature, T_0 , is calculated. The gas, tube, and regenerator are set equal to T_0 at the initial time step, τ_0 .

Step #4: The values of the coefficients of the finite difference equation are calculated.

Step #5: The temperatures for the current time step at each spacial location of N are calculated with the finite difference equations, Eqs (19), (20), and (21). This is done using temperature values at the current (I) and one previous time step ($I-1$), and at locations one space increment before ($N-1$) and one beyond ($N+1$) the current space increment.

Step #6: The outlet temperatures, T_{NMAX}^I , are saved to a file.

Step #7: The current time step temperatures are renamed as previous time step temperatures.

Step #8: The process is repeated until the end of the transient, τ_f .

Stability. The FORTRAN program *tsie* becomes unstable at certain combinations of Δx and Δt . This is common for explicit finite difference models. Because three interacting equations are involved in the model, determining the stable time step involves finding the eigenvalues for a matrix of coefficients and setting the largest eigenvalue less than 1.0 for stability. This matrix would be large (*NMAX* by *IMAX*), sparse, and different for each value of the heat transfer coefficient used. After reviewing the requirements for *main* (that a high and low guess for the heat transfer coefficient be input, see below), a less complicated method was sought to fulfill the stability requirement. A conservative approach is merely to ensure the coefficients in the governing equations are all positive (Kreith, 1973:186; Patankar, 1980:37). For a given value of the ratio between the time and the space increment, or the Courant number, *C*, the maximum heat transfer coefficient for stability is

$$h_{max} = \frac{C \cdot C_p \cdot \rho \cdot A_F}{(A_S + A_{ST}) \cdot \gamma} \quad (22)$$

where c_p is the specific heat of the gas at constant pressure ($J/kg/\text{ }^\circ\text{C}$)
 C is the Courant number, $\Delta x/\Delta t$
 ρ is the gas density (kg/m^3)
 A_F is the flow area in the matrix, ΦA (m^2)
 A_s is the surface area of the matrix
 A_{st} is the surface area of the tube (m^2)
and γ is the ratio c_p/c_v for the gas.

This stability requirement gives a rough estimate for the maximum heat transfer coefficient allowed for a certain Δx and Δt . With this criteria, any value for h_{conv} could have been used, and no stability problems were encountered.

Validation of the Numerical Model. The model was validated in two ways. Both involve a comparison between a known analytical solution for the temperature, and one calculated by the current numerical model (with some modifications explained below).

In the Theory section of this chapter, the exact analytical solution to the classical step-change transient method is presented. The current finite difference model should give the same solution as the analytical one when two modifications are made. First, an artificial, impulsive step-change in temperature was fabricated numerically to use as the input trace, T_{g1} . Second, the area of the tube surface, A_{st} , was set equal to zero. This effectively disengages the interaction between the tube and the flowing gas. Hence, all the details of the model by Pucci, et al., (1967) match the current modified model. The results for the maximum slope of

the outlet trace, T_{g2} , should be the same for both. The smooth, artificially fabricated inlet data produced a smooth output for which the slope was determined by a second-order accurate, five point, finite difference definition (Anderson, et al., 1984:45). This procedure was followed for a test case with an arbitrarily chosen heat transfer coefficient, an artificial, impulsive step-change from 10 to 30° C, and the properties of SU #09. To determine the influence of Δt and Δx on accuracy, the time increment, Δt , was varied from 10^{-4} to 10^{-7} seconds, and the number of space increments was varied from twenty one to one hundred twenty one. By fitting the difference in maximum slope between the analytical and numerical solutions for the outlet temperature to a curve, and taking a limit as NMAX became very large, the error in maximum slope approached 0.01%. These results are shown in Fig. 11. For the current research, NMAX of 101 was deemed the best balance between accuracy (1.8%), and the length of time it took to run the numerical program.

The second test for validating the numerical model also involved using the artificial, impulsive, twenty degree step-change in inlet temperature. In this case, the temperature trace of the matrix at the second spacial increment was observed. Since the wire diameter of the mesh, d_w , is so small, and the thermal conductivity of the 304 stainless steel, k_s , is so large, treating the matrix as a lumped

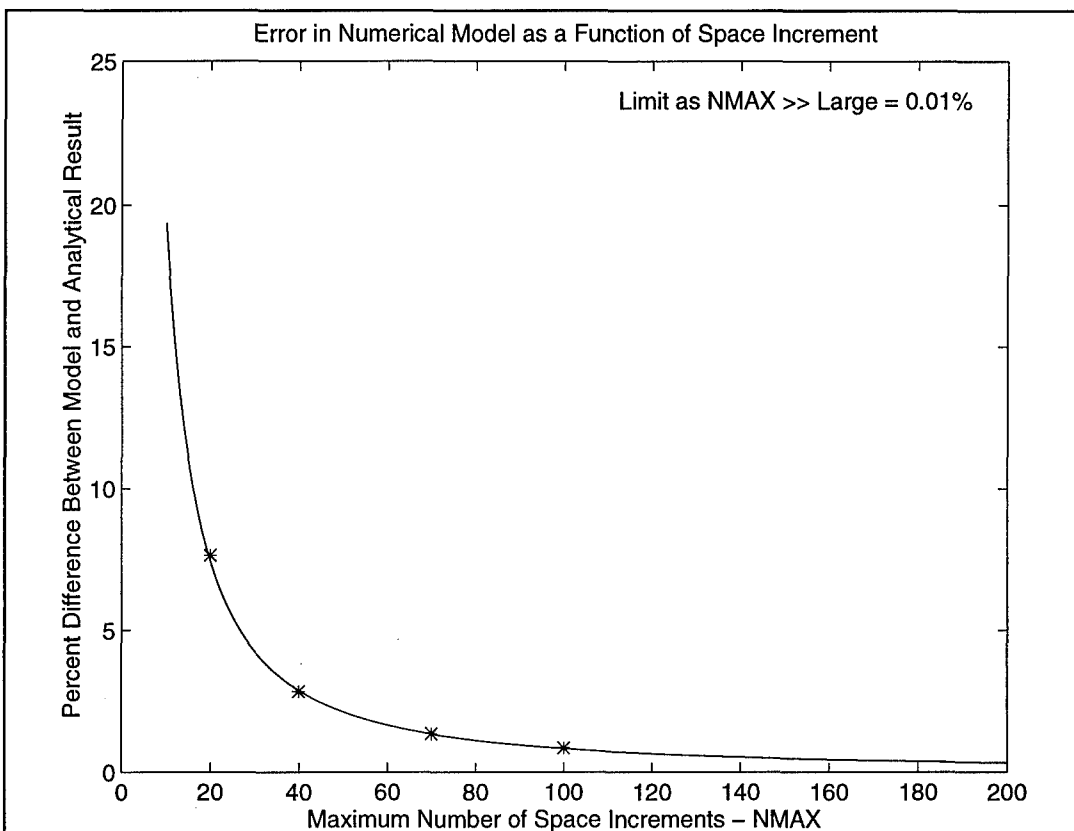


Figure 11. Verification of Numerical Approach for Large NMAX

thermal mass is permissible. The average Biot Number ($h_{conv} d_w/k_s$) for the thirteen SUs equals 0.048 which meets the requirement that it be less than 0.1 (Incropera and Dewitt, 1985:179). Consequently, the calculated trace for the second spacial cell should match an exponential temperature rise with a thermal time constant defined by $\tau = \rho c_M V/h_{conv}/A_{sur}$, where ρ is the density, c_M is the thermal capacity of the steel, V is the volume of steel, h_{conv} is the heat transfer coefficient, and A_{sur} is the surface area of the matrix (Ibid:176). A test

case was performed for a time increment $\Delta t = 10^{-5}$ seconds, and twenty one space increments. The comparison is shown in Fig. 12. The calculated trace for T_{g2} matched the theoretical trace with a mean difference of $3.1 \times 10^{-5}^\circ C$ over the 0.2 seconds of the transient. Again, the comparison is very good. Hence, these two validation tests give confidence the numerical model is working as intended.

Determining the Heat Transfer Coefficient. With $tsie$ available, the outlet temperature trace can be obtained for any combination of geometric and flow conditions, and a value for the heat transfer coefficient. The actual heat transfer coefficient can be determined by requiring that a characteristic of the calculated outlet temperature trace match the same characteristic of the experimental temperature trace.

ZeroIn Subroutine. What is needed then is a way to find the best heat transfer coefficient. This particular problem has attracted attention for centuries; it is called a root-solving problem. In a root-solving problem, one seeks the value of the independent variable for which a function of the variable equals zero, in the current research $fn(h_{CONV})=0$. Fortunately, all this attention has resulted in an algorithm by Dekker (1969), improved by Brent (1973) as reported in Forsythe (1977: Section 7.2). The authors claim that this algorithm, called ZeroIn, should always converge, and needs

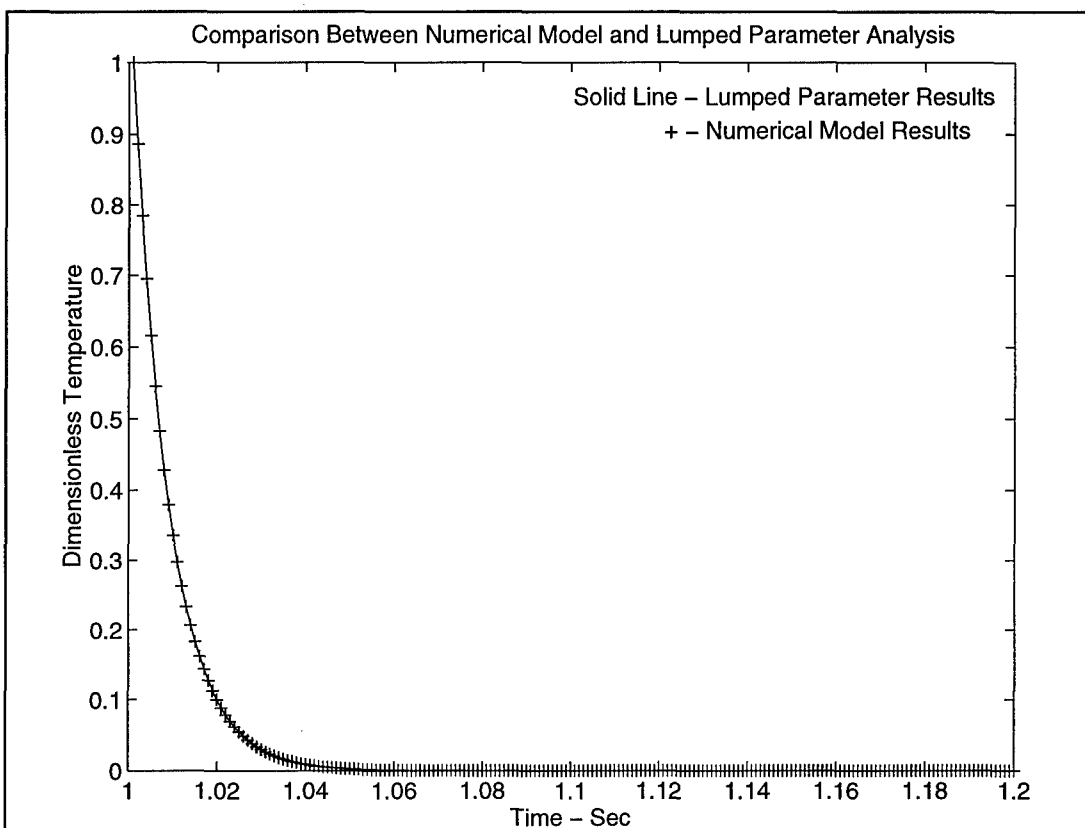


Figure 12. Model Verification Using Lumped Thermal Mass

less than eleven iterations to converge for smooth functions (Brent, 1973). A requirement of Zeroin is that some initial bounding guesses for h_{conv} are input to the algorithm such that $fn(h_{min})$ and $fn(h_{max})$ have different signs, i.e. one is greater than zero and the other is less than zero. The algorithm starts by evaluating $fn(h_{conv})$ for the initial bounds and corrects this value until the best heat transfer coefficient is chosen. This is determined when the difference between h_{conv} from one iteration to the next is smaller than a chosen tolerance. For the current research, this tolerance was

chosen to be $\Delta h_{conv} < 100 \text{ W/m}^2/\text{°C}$, which is two per cent of the average value for the heat transfer coefficient measured in the thirty test runs. This error matches the error in the numerical model (1.8 %) given above for NMAX = 100.

The main Program. A FORTRAN program called *main* controls the calculation of the heat transfer coefficient by employing *tsie* and *Zeroin* as subroutines. After the inputs to *main* are made, *Zeroin* is called, which in turn calls *tsie* to calculate T_{g2} , and the best heat transfer coefficient is chosen as described above. *Main* also calculates the friction factor, the effectiveness of the regenerator, and the theoretical heat transfer coefficient based on the approach of Pucci et al. (1967) described in the Theory section. These other results are discussed below.

The Three Criteria. Many criteria could be chosen from which the heat transfer coefficient is determined. The maximum slope of the output temperature trace and the minimum root-mean-squared difference between the experimentally measured rising temperature trace and an analytical solution were mentioned above. In the current research, these two criteria, maximum slope and minimum root-mean-squared difference, are considered, as well as requiring the sponge effect delay time, *SEDT*, to be the same for both experimental and calculated results. The maximum slope and delay time cases are straightforward. But finding the heat transfer

coefficient which minimizes the root-mean-squared difference between calculated and experimental temperature traces required some ingenuity.

There are two difficulties defining a criterion for the minimum root-mean-squared difference approach. First, a root-mean-squared difference is always greater than zero. As mentioned above, the Zeroin algorithm requires two initial guesses for h_{conv} which bound its value and for which $fn(h_{conv})$ has a different sign. In the root-mean-squared difference case, $fn(h_{conv})$ is always greater than zero. To get around this difficulty, a related property of the root-mean-squared difference is used. Fig. 13 shows the anticipated appearance of the root-mean-squared difference versus h_{conv} curve. The minimum value of the root-mean-squared difference is where the slope is zero. The slope before and after the minimum is of different signs. Since the function should be smooth, the value of the slope at any h_{conv} can be approximated by a simple forward difference, i.e. the value of the root-mean-squared difference is calculated at a particular value of h_{conv} , and also at a value some small amount larger, say $h_{conv} + 100$. The difference in these two, divided by the difference in h_{conv} (or 100), gives the local value of the slope. Using this approach, Zeroin and tsie can be used to solve $fn(h_{conv}) = 0$ where the function is the slope of the root-mean-squared difference versus h_{conv} line. When the slope is near zero,

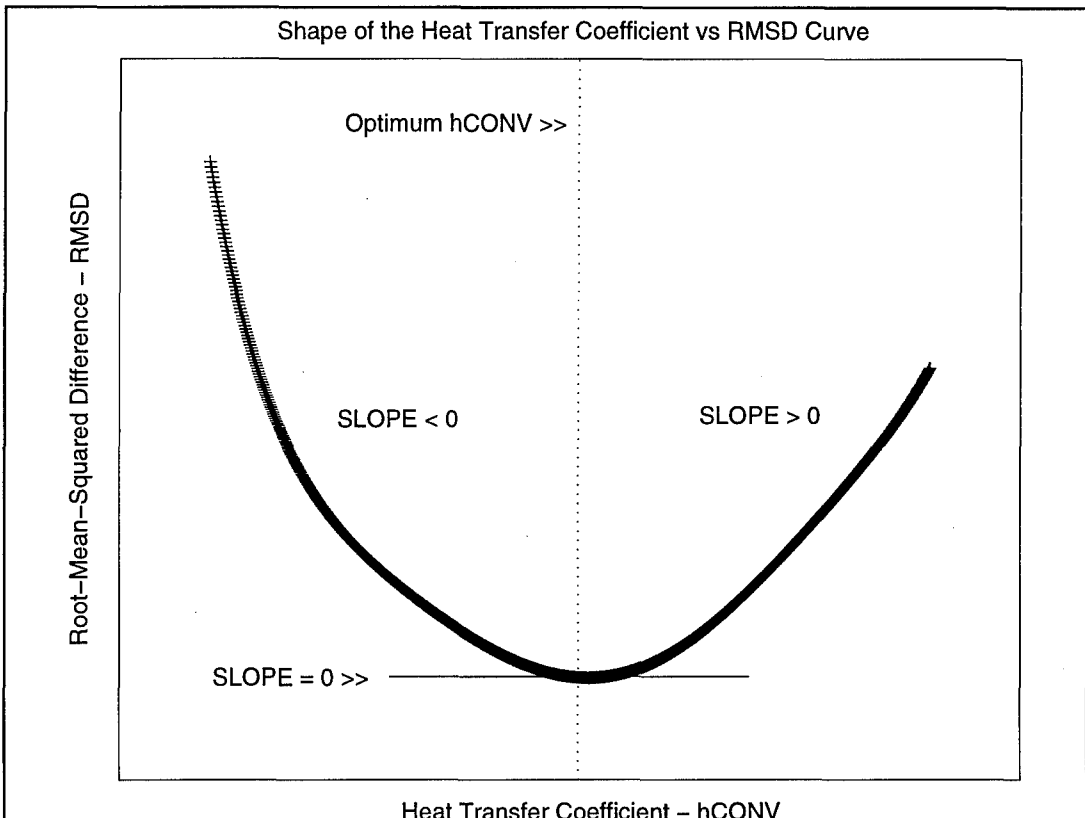


Figure 13. Root-Mean-Squared-Difference as a Function of the Heat Transfer Coefficient

the value of the heat transfer coefficient gives the best fit to the numerical data.

The second problem with the minimum root-mean-squared difference approach is deciding over which time interval to compute the root-mean-squared difference. During the sponge effect delay time, there is not much temperature change in T_{g2} . At late times, the physics of the model no longer fit the physics of the experiment as explained in the Theory section. In order to avoid some amount of arbitrariness, the root-mean-squared difference is evaluated from the end of the delay time

to one matrix thermal time constant or about 50 milliseconds after the occurrence of the maximum slope. This concentrates the comparison to a time interval which includes the maximum slope, i.e. most of the change in T_{g2} has taken place. This completes the description of the three criteria. A brief description of other results calculated by *main* concludes this chapter.

Other Results. Three other important results are returned from the *main* program: 1) the friction factor, 2) the effectiveness of the regenerator, and 3) the theoretical heat transfer based on the maximum slope technique of Pucci, et al. (1967) described above.

The friction factor can be defined in many ways (Kays and London, 1984:36; Miyabe, et al., 1982:1839). The one chosen for this research is developed by Armour and Cannon (1968) specially for woven screens.

$$f = \frac{\Delta P \Phi^2 PS}{L \rho U_g^2} \quad (23)$$

where ΔP is the pressure drop in the regenerator (Pa)

Φ is the porosity

PS is the matrix pore size (m)

L is a length = $Q EL$ where Q is a factor which compensates for the "tortuosity" and EL is the matrix length (m)

ρ is the gas density (kg/m^3)

and U_g is the gas velocity (m/sec)

The ΔP was measured for each test run. The porosity was determined by the following equation:

$$\Phi = 1.0 - \frac{W_{SU}}{\rho_M A EL} \quad (24)$$

where W_{SU} is the mass of the SU (kg)
 ρ_M is the density of the matrix (kg/m^3)
and A is the tube cross-sectional area (m^2)
 EL is the length of the matrix (m)

The pore size was determined to be

$$PS = (((1/MESH) - d_w)^2 (2.0 d_w RF))^{1/3} \quad (25)$$

where $MESH$ is the mesh size (m^{-1})
 d_w is the wire diameter (m)
and RF is the reduction factor

According to Armour and Cannon (1968), for plain weave screens, the length should be the length of the matrix, EL , and Q is set equal to 1.0. The gas density is calculated from a measured average temperature and pressure in the test section, and perfect gas relations. Finally, the mass velocity is the measured mass flow rate divided by the area for flow, $A_f = \Phi A$, divided by the density.

Another parameter, effectiveness, was defined for the purpose of deciding the merits of reducing the thickness of the screens. Effectiveness is defined for regenerators in Chapter II in terms of the ability of the regenerator to

remove the maximum amount of energy from the gas relative to an ideal case. Another effectiveness, $SPEFF$, can be defined for the case of one-directional flow:

$$SPEFF = \frac{\dot{m} C_p SEDT}{W_{SU} C_M} \quad (26)$$

where \dot{m} is the mass flow rate (kg/sec)
 C_p is the specific heat of the gas (J/kg/°C)
 $SEDT$ is the sponge effect delay time (sec)
 W_{SU} is the mass of matrix (kg)
and C_M is the specific heat of the matrix (J/kg/°C)

The numerator is the energy of the gas, with respect to the initial temperature of the regenerator, which flows into the matrix during the delay time. The denominator is the amount of energy required to raise the matrix from its initial temperature to the same final temperature defined by the flow of the gas. If the regenerator uses up all of its thermal capacity to absorb all of the relative energy from the gas during the delay time, the effectiveness is 1.0. More will be said about these three results in Chapter V.

IV. Experimental Apparatus and Procedure

This chapter describes the apparatus and procedures used to gather the experimental data, and the data reduction technique for composing the input data file for each test run.

Apparatus

First, details of the experimental apparatus are given. A diagram is shown in Fig. 14. A detailed list of the equipment for Fig. 14 is given in Table 1.

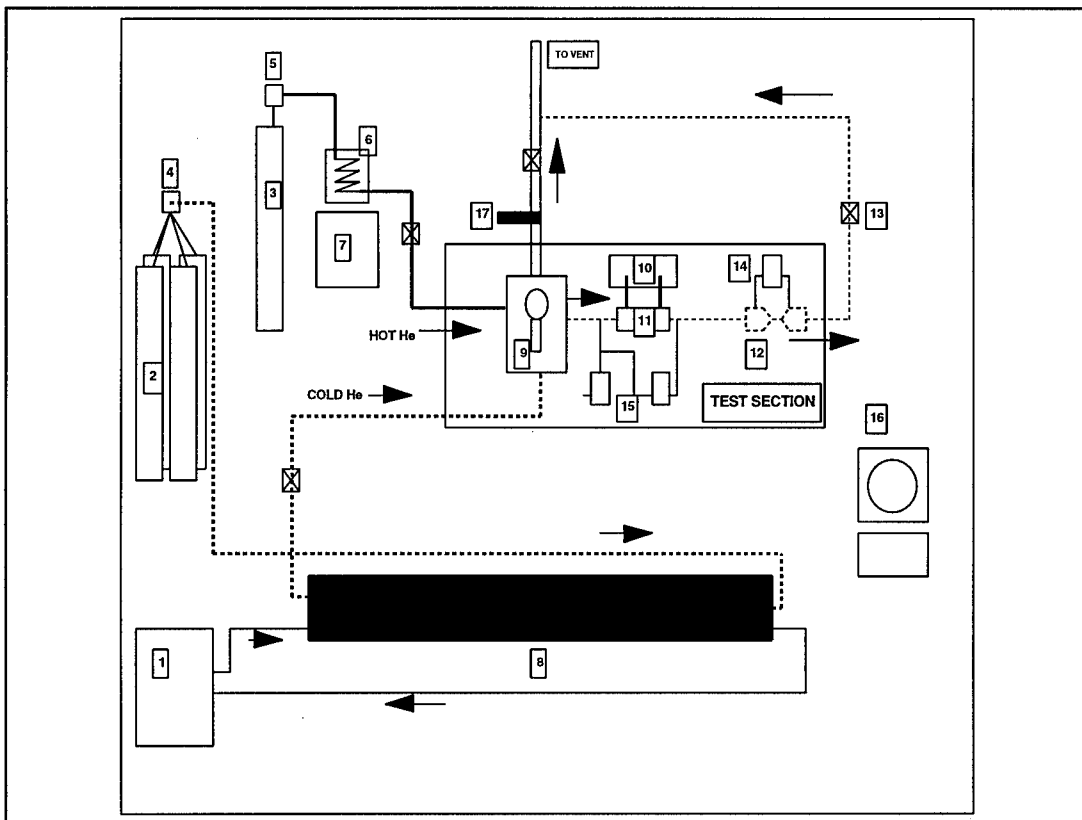


Figure 14. Diagram of Experimental Apparatus

Table 1. Instrumentation List for Fig. 10

ITEM #	DESCRIPTION	SERIAL #
1	Chiller - NESLAB HX-100	A95064014
2	4 Tank Helium Harness - Cold Gas	--
3	Single Helium Tank - Hot Gas	--
4	Regulator - Victor SR - 600	DB 48406
5	Same as Item #4	DB 48407
6	Heating Coil - Hot Water Bath	--
7	Heater - Fisher Thermix 11-493	121 MX 2614
8	Heat Exchanger - Counter Flow	1
9	4 Way Valve - Whitey B-45YF8	--
10	2 X Thermistor - Thermometrix FP07 2 X Motherboard - E & L Instruments	-- --
11	Regenerator	--
12	Flowmeter - Venturi Tube	--
13	4 X Valve - Whitey B-44S6	--
14	Pressure Transducer - Validyne DP10-42	74693
15	Pressure Transducer - Validyne DP15-48 " " " DP15-56	87548 84654
16	Data Acquisition System - Zenith Z-510	4LSBUX7536
17	Thermocouple - Omega .005" Fe-constan Indicator - Omega DP41-TC-A	-- 10984A1-01

The first major subsection of the apparatus is the equipment used to handle the helium. Helium was chosen as the working fluid since 99.995% pure helium was available (small pores in a matrix are easily clogged), and helium is commonly used for the working fluid in cryocoolers, although any clean gas could have been used. The tanks used to hold the helium

gas have 17 MPa, 0.5 m³ capacity and hold about 5 kg. A four-tank harness supplied the cold gas flow. A single tank was used for the hot gas flow. A NESLAB Model HX-100 chiller cooled water to 3° C. The water was pumped into a 3.0 m length section of 25 cm diameter PVC piping. This forms the outer shell of a counter-flow heat exchanger. The helium flowed through approximately 50 meters of coiled copper tubing over which cold water was pumped. The gas could be cooled to 6° C. A Fisher Thermix adjustable-power hot plate was used to heat a steel container filled with water. The hot gas flowed through a 3 m length of 9.5 mm O.D. tubing, coiled 25 cm in diameter, which lay in the hot water. The gas could be heated to 50° C. The gas flowed through the test section due to the pressure in the tanks which was regulated by Victor SR-600 regulators. The mass flow rate was controlled with tandem upstream and downstream needle valves. Except for the tubing of the SU in the test section, the gas flowed through 9.5 mm O.D. copper tubing rated to 34.5 MPa. The tubing, valves, geometry, etc., were chosen to achieve a Reynolds number (based on pore size) between 50 and 600.

The next major subsection of the experimental apparatus is the test section. At the test section entrance is a Whitey Model B-45YF8 four-way valve (Fig. 14). With the valve handle in the vertical position, cold gas flowed through the test section; in the horizontal position, hot gas flowed through

the test section. The flow diverted from the test section was vented to atmosphere; the outflow from the test section was also vented to atmosphere. The central element of the test section is the fixture for holding the screen units (SUs) and instrumentation for pressure and temperature measurements.

One of the two mounting fixtures on either end of an SU is shown in Fig. 15. They were made from 0.0095 m I.D. to 0.0159 m I.D. Swagelok brand male connectors. The connectors were reamed such that the SUs slid far enough down the interior of the opening that the Swagelok gas-tight seal would clamp approximately 0.0032 m from the end of the SU. Three 100 mesh screens were inserted into the upstream connector inlet to act as a mixer and turbulence-generator. Each connector held three measurement devices: 1) a Thermometrix Fastip 1.5×10^{-5} m diameter bead, quick-response, thermistor, 2) a 0.00635 m O.D. flushed-wall, copper tube for pressure measurements, and 3) a TSI brand hot-wire probe (not used for measurements in this report). The three measurement instruments were epoxied into the connectors with specially made holding fixtures. The connectors were slid over the end of the SU to a predetermined position, and then clamped in a leak-proof seal with Swagelok fittings. The SUs were easily removed and replaced for testing.

The design of the SUs is shown in Fig. 16. The SUs are made from 304 stainless steel plain-weave mesh in three sizes:

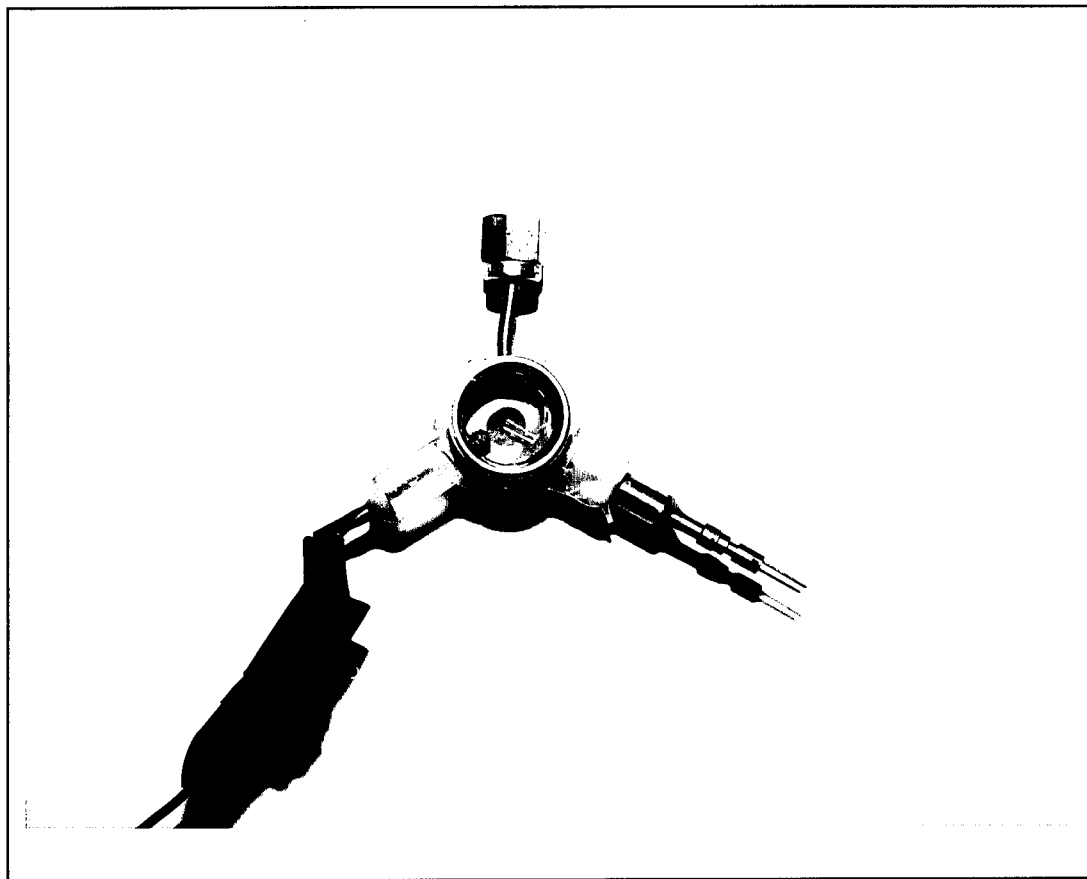


Figure 15. Instrumentation Holders

100, 180, and 250 strands per inch. The screen was rolled by a collandering process (between a stationary rotating pin and a moving table) on a Bridgeport mill to nominal 15%, 30% and 50% reduction in thickness, i.e. reduction factors of 0.85, 0.70, and 0.50. Unrolled screens were also tested. A special tool was used to punch out disks of a diameter that fit snugly inside the stainless steel tube used to hold the regenerator matrix. There are precisely two hundred screens per SU since

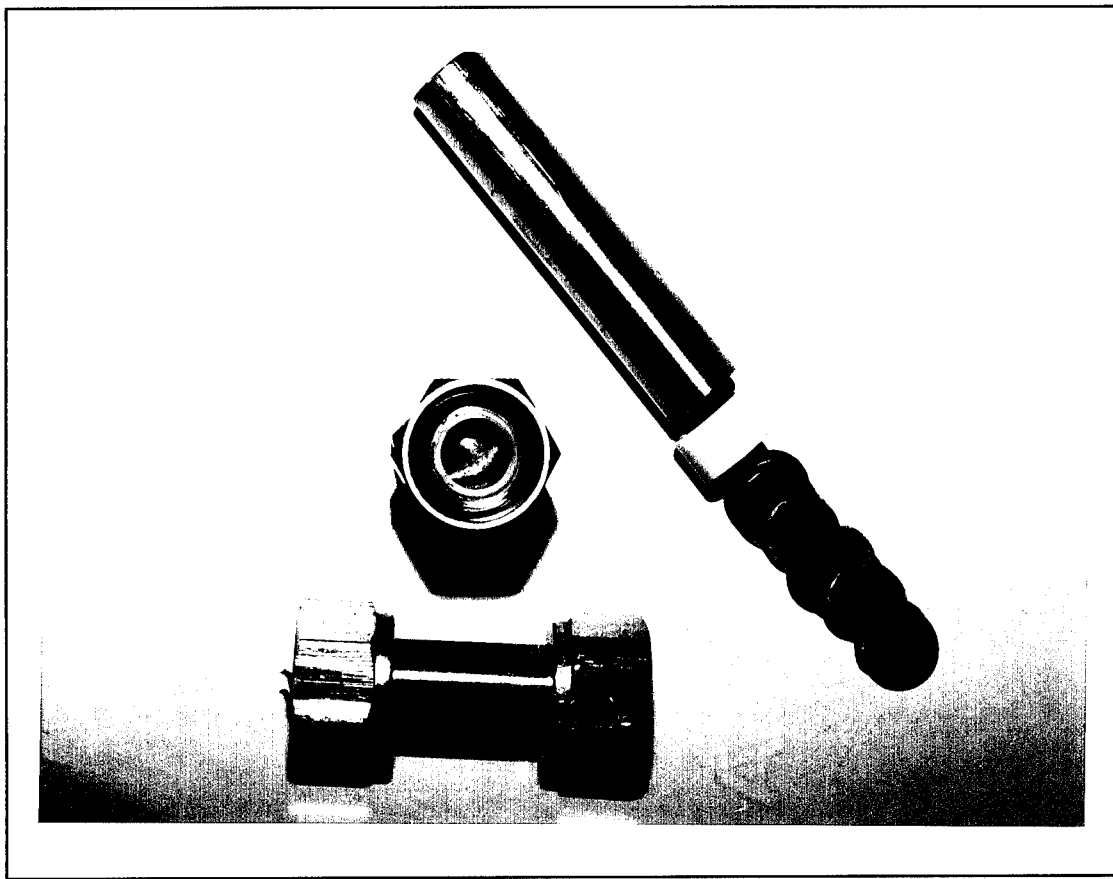


Figure 16. Photo of Screen Unit (S/U)

this allows direct comparison of SU performance. The number two hundred was chosen because studies show (Mikulin, et al., 1972) that this is a sufficient number of screens to eliminate length effects on heat transfer. The screens were cleaned with isopropyl alcohol, dried, and stacked inside a 0.0159 m O.D., 5.1×10^{-4} m thick walled, ASTM-A269 304 stainless steel tube. The weights and lengths of the individual screens and entire SUs were carefully measured with vernier calipers and a Denver Instruments XL-300 electronic scale. A 9.5 mm long

spacer made from PVC tubing was epoxied into each end of the tube to hold the screens in place.

Thirteen SUs were fabricated as listed in Table 2. The first twelve are from the three mesh sizes and four reduction factors.

Table 2. List of Screen Units

S/ U	MESH	Porosity Φ	RF ^a	d_w^b 10^{-5} m	PS ^c 10^{-5} m	EL ^d 10^{-3} m	t_s^e 10^{-5} m	W_{SU}^f gms
1	100	0.677	1.0	11.4	16.5	45.4	22.6	19.0
2	"	0.636	0.86	"	15.6	38.9	19.6	19.1
3	"	0.599	0.70	"	14.6	31.9	15.9	18.8
4	"	0.466	0.50	"	13.1	22.7	11.2	17.5
5	180	0.660	1.0	6.4	9.15	29.5	14.7	12.1
6	"	0.601	0.83	"	8.60	24.5	12.3	12.1
7	"	0.520	0.72	"	8.20	21.2	10.5	12.0
8	"	0.375	0.53	"	7.41	15.7	7.4	11.6
9	250	0.666	1.0	4.1	6.71	17.4	8.6	6.9
10	"	0.598	0.85	"	6.35	14.7	7.4	6.6
11	"	0.541	0.75	"	6.08	13.0	6.5	6.4
12	"	0.399	0.55	"	5.51	9.6	4.7	6.3
13	MIX	0.577	MIX	7.3	9.28	23.1	11.8	12.5

a. Reduction Factor; b. Wire diameter; c. Pore Size; d. Length; e. Screen thickness; f. Mass of the SU

A special SU was also made to investigate an alternate configuration which may achieve the desired result, i.e., less void fraction with comparable compactness factor. The special

SU was made from a random mixture of all the mesh sizes and reduction factors.

Pressure measurements were made at either end of the SU to determine the pressure drop, and subsequently, a friction factor. The pressure at the inlet, P₁, was measured with a Validyne Model DP-1556 34.5 MPa differential pressure transducer. The differential pressure transducer measured the difference between P₁ and atmospheric pressure which was monitored by a Transamerica Delaval Type CEC 2500 Digital Barometer. The pressure drop across the SU was measured with a Validyne Model DP-1548 0.5 MPa differential transducer. Both transducers used a Validyne Model CD-280 six channel exciter.

Temperature measurements were made in three locations. At the inlet and outlet from the SU, a thermistor was used. The thermistor was one leg in a Wheatstone bridge configuration. A Hewlett-Packard Model 6405C DC Power Supply provided 1.0 ± 0.001 VDC across the bridge. This low power voltage was used to minimize self-heating of the thermistors. The major benefit of the bridge was that the other three resistances could be chosen so that the bridge operated near a balanced condition. The smaller the voltage measurement range for the thermistor (± 0.1 VDC was achieved in this case), the greater the amplification by the data acquisition system (DAS), and the better the digital resolution of the

fluctuating component of the signal (Labview for Windows, 1993; 2-8). The third location for temperature measurements was at the entrance to the bypass vent. The temperature there was measured by a 0.127 mm (0.005") diameter Omega iron-constantan thermocouple in conjunction with an Omega Model DP41-TC-A Digital Thermocouple Indicator. The measurement was made to monitor the bypass gas temperature, in particular, to determine when it was hot enough to begin the transient of a test run.

At the exit of the test section, a venturi flowmeter with a 0.0065 m diameter throat was used for measuring the mass flow rate of the gas. The venturi flowmeter had geometrical proportions recommended by ASME standards (ASME, 1971). The pressure drop across the throat was measured with a Validyne Model DP 10-42 34.5 kPa differential pressure transducer using the same exciter mentioned above.

The last major subsection of the experimental set-up is the Data Acquisition System (DAS). Coaxial cables were used to connect the instrument readings (all DC voltages) to a junction board. The board was connected to a Zenith Data Systems Z-Station 510 with a ribbon cable. All amplification and conversions were done internally to the computer, using a National Instruments NI-DAQ driver and an AT-MIO-16 board which is controlled by Labview Version 3.0.1 Virtual Instrument software. Special Labview Virtual Instruments (VI)

were designed and built for calibrations and experimental control. MY_SS_REGENERATORHTC.VI provided steady-state monitoring of conditions in the test section and transient data collection, conversion, and storage. Once the data were stored to a file, they could be transferred via the local area network to a SUN workstation where data reduction was accomplished.

Experimental Procedure

The detailed experimental procedure is shown in Appendix A. A synopsis is given here. The preliminary part of the procedure involved preparing for the test. After a new SU was placed into the test section, a leak test was done around all seals. Foam insulation was placed on any surface open to the room air. Voltages were checked on the thermistor circuits with a Hewlett-Packard Model 34401A Multimeter. Gas levels were maintained high enough to complete the test, and the chiller and heating units were brought to their respective steady state conditions.

The testing procedure began with a data sheet containing the appropriate information for the test run about to begin. The approximate back pressure was set in the tanks and both hot and cold flows were adjusted so that the correct pressure, P_1 , at the entrance to the SU, and the correct mass flow rate were maintained. After approximately four minutes, steady state cold temperatures around $10^\circ C$ prevailed in the SU, and

hot gas temperatures around 35° C prevailed in the vent. Next, the data collection trigger was tripped, and after an approximately three second delay, the four-way valve was manually rotated so that the hot gas was diverted to the SU. Pre-transient conditions were recorded by the DAS, and data were taken during the transient. After approximately 20 seconds, all gas flows were shut off. A graph of the test run data was shown on the computer screen so that the quality of the test run could be ascertained. Post-transient data as well as any pertinent comments were added to the data sheet for the test. The data file was given an identifier, backed-up on tape, and sent to a SUN workstation via a file transfer protocol (ftp) and the local network. The data reduction technique described in the next section was applied to the data before it was loaded into the numerical model for determination of heat transfer and friction coefficients.

Data Reduction Technique

After temperature, pressure, and mass flow data had been gathered for the transient tests, they were converted into a format suitable to determine the heat transfer coefficient. The aim of this section is to describe the steps taken to create a data file that was fed into the FORTRAN program which models the flow. Some important parameters are defined, as well as how they were calculated from the experimental data.

The raw data from the data acquisition system was sent to a Sun Sparc10 workstations via file transfer protocol over the local area network. This data contained temperature traces from the inlet and outlet to the test section, pressure and pressure drop readings from the three pressure stations in the test section, and an average value of the mass flow rate. The data sampling rate and total transient time were also included. These data were loaded into a MATLAB session for manipulation. MATLAB is a high-performance numerical computation and visualization software (MATLAB, 1993). The MATLAB m.files used to perform the data reduction are contained in Appendix B.

The first important parameters determined from the data were the start and finish times of the transient. Each test run lasted ten seconds and data were collected at 10,000 time steps (a sampling frequency of 1 kHz). τ_0 is the start time and τ_f the finish time of the transient which began approximately three seconds after data acquisition began. These data were used to concentrate the matching of the analytical and experimental results during the transient. The raw data for T_{g1} and T_{g2} were filtered with a 20th order finite impulse response (FIR) filter. τ_0 was defined to be the time at which T_{g1} changed by more than two standard deviations (0.4° C) from its running average prior to the transient. τ_f was chosen more subjectively. The MATLAB m.file (trange.m),

written to choose τ_f starts by identifying the data acquisition time that the slope of the T_{g2} trace is greater than five degrees per second. This normally gave a long duration value for the transient duration. The value of τ_f was shortened from the MATLAB calculation to a point after which the maximum slope in the outlet temperature trace had obviously occurred, between ten and fifteen matrix time constants after τ_0 .

Once the beginning of the change in the inlet temperature trace and end of the change in the outlet temperature trace were identified, the next important parameter to find was τ_2 . The time between τ_0 and when the trace of T_{g2} begins to change measurably, τ_2 , is defined as the sponge effect delay time, *SEDT*. The determination of τ_2 was done in the same way as for τ_0 ; by definition, it's located at the data acquisition time step where T_{g2} has changed by more than two standard deviations from its running average since the test run began.

The final important parameters were the magnitude of the maximum slope of the T_{g2} trace and the time step at which it occurred. A MATLAB m.file (*bestpoly.m*) was constructed to find the best polynomial fit to the T_{g2} trace during the time between τ_2 and τ_f . It picked the polynomial of order two through thirty which best fits the experimental data in a root-mean-squared-difference sense. Another m.file

(maxslope.m) calculated the maximum slope of the polynomial, and when it occurred in relation to τ_0 .

The final step in the reduction process was the collection of all the data into a read file for each experimental run. Results from the raw data such as mass flow rate and pressures were assembled at the beginning of the read file. Next, some geometric properties of the individual SUs such as mass, pore size, and length were added to the file. Next, the filtered T_{g1} and T_{g2} traces were appended to the file. Finally, the τ parameters described above were included. All these data were used by the numerical model given in the next section to determine a heat transfer coefficient.

V. Results and Discussion

In this chapter, results which give confidence in the method described in Chapter III, and which prove the hypothesis stated in Chapter I, are presented. Additionally, a section is dedicated to comparisons between the heat transfer coefficients obtained using the three criteria mentioned in Chapter III. How regenerator effectiveness is changed by reducing the screen thickness is shown, and a general discussion about the results is given at the end of the chapter. The numerical values for the test results are listed in Appendix E. Before the test results are shown, some preliminary results and definitions are presented.

Preliminary Results

Four preliminary items are addressed. One is a definition of the Reynolds number; the second is a relation for specific surface area for each matrix; the third is a typical temperature trace from the experimental apparatus; and the fourth is the test run matrix.

During the course of this research, many definitions for the Reynolds number were encountered. Generally, it is defined

$$Re = \frac{\rho U_G L}{\mu} \quad (27)$$

where Re is the Reynolds number
 ρ is the gas density (kg/m^3)
 U_g is the gas velocity (m/sec)
 μ is the dynamic viscosity ($\text{kg}/\text{m/sec}$)
 and L is a characteristic length (m)

The difference between Reynolds numbers is the choice of the characteristic length. The most common characteristic length in the porous media arena is the pore size. The pore size, PS , is defined as the cube root of the average volume of the voids in the medium. In the study of heat transfer and fluid dynamics in pipes and over cylinders, it is also common to see a Reynolds number based on wire diameter or hydraulic radius. For a stacked-screen matrix, the choice is not clear. In an article written by Armour and Cannon (1968), a definition is developed specially for the case of stacked screen matrices. They contend the pressure drop in a matrix is the sum of two terms: 1) a surface shear/drag term which requires an area, and 2) an inertial term due to eddies and sudden enlargements/contractions in the direction of flow which requires a volumetric dimension. The resulting definition for the characteristic length is

$$L_A = \frac{1.0}{A_R^2 PS} \quad (28)$$

where A_r is the surface area per unit volume of unrolled matrix (m^{-1})
and PS is the pore size (m)

This combination of area and linear dimensions was shown by Armour and Cannon to give the best correlations for conditions in a stacked-screen matrix and will be used in the current research unless otherwise stated.

In order to use the Armour and Cannon dimension, the surface area per unit volume needs to be determined for each matrix. This was accomplished using geometrical arguments and measurements of the dimple in the wire left by the rolling process. Wiese (1993:4-2) took electron microscope photographs of the screens which he rolled by the same process (same machine) to the same reduction factors as those used in the current research. The photographs show that the rolling caused the round wire surfaces to be flattened at certain locations in each screen cell (set of four crossing wires). When two screen disks are stacked against one another, the flattened areas cover each other, and these covered areas no longer come in contact with the fluid. Wiese's photographs were used to estimate the area per unit volume for each of the rolled screen matrices. The results and a simple curve-fit are shown in Fig. 17.

To use this plot, the specific area per unit volume for unrolled screens, A_s , is obtained from a geometrical relation developed in Armour and Cannon (1968:418).

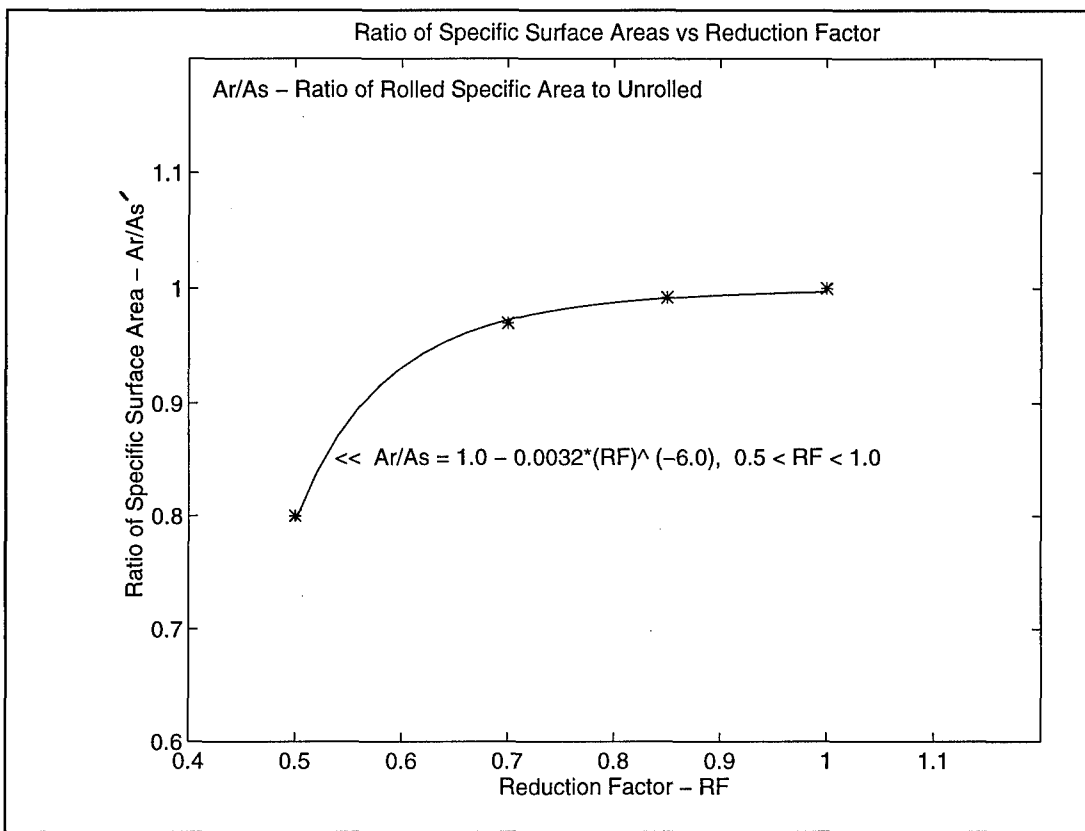


Figure 17. Specific Surface Area vs Reduction Factor

$$A_{s'} = \frac{2.0 \pi [PIT^2 + d_w^2]^{1/2}}{PIT^2} \quad (29)$$

where PIT is the inverse of the mesh number (m)
and d_w is the wire diameter (m)

This value for $A_{s'}$ is multiplied by the appropriate factor shown in Fig. 17 to get the specific area of the rolled screen per unit of unrolled volume, A_r .

The third piece of preliminary information is a plot of a typical inlet and outlet temperature trace. This is shown in Fig. 18. The temperatures of the inlet and outlet gas begin at steady state at around 10° C, and rise quickly to between 30° C and 35° C. The plot shows the filtered data which is input to the numerical model.

The final piece of preliminary information is the test run matrix. This is shown in Table 3. Four pieces of information are given: 1) the test run number, 2) the SU

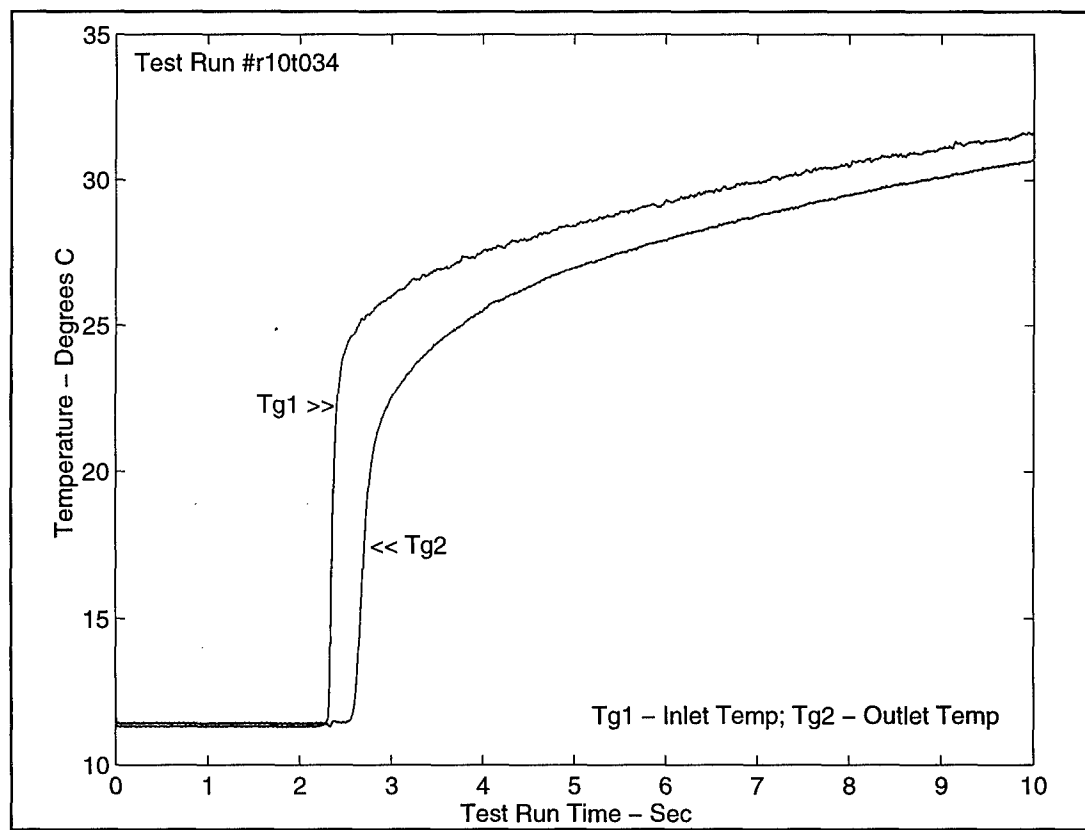


Figure 18. Typical Experimental Temperature Trace

number (the characteristics for which can be found in Table 2), 3) the Reynolds number based on pore size which is more often used in the literature to report operating conditions, and 4) the nominal mass flow rate for each test. The geometries and Reynolds numbers are representative of current operating conditions for regenerative refrigeration cycles.

Comparisons to Published Data

In this section, published data for unrolled screens of similar geometry and flow conditions are compared to the experimental data collected during the current research.

In Fig. 19, the data for the three SUs made from unrolled screens is compared to published correlations for friction factors and Nusselt numbers. In the case of the friction factors, Armour and Cannons's (1968) result, $f = 8.61/Re + 0.52$, was used (solid line). Their study included similar mesh sizes and a Reynolds number range, $1.0 < Re < 100$. The agreement is very good with a mean difference of $\pm 2.5\%$.

The published Nusselt number data (solid line) are due to Hamaguchi (1990), $Nu = 0.42 Re_{dw}^{0.56}$. He also used identical mesh sizes, and a Reynolds number range of $1.0 < Re < 900$. The fit is also good with a mean difference of -13.9% . For the reasons given in Chapter III, i.e. non-exact step-change in inlet temperature and the thermal inertia of the tube, heat transfer results from the current research should be larger than previously published ones. These favorable comparisons

Table 3. Test Run Matrix

Test Run #	Screen Unit #	Reynolds number (Pore Size)	Mass Flow Rate (g/sec)
01	09	50	1.87
02	09	100	3.74
03	10	50	1.87
04	10	100	3.74
05	11	50	1.87
05	11	50	1.87
06	11	100	3.74
07	12	50	1.87
08	12	100	3.74
09	01	250	3.78
10	01	500	7.55
11	02	250	3.78
12	02	500	7.55
13	03	250	3.78
13	03	250	3.78
14	03	500	7.55
15	04	250	3.78
16	04	500	7.55
17	05	100	2.72
17	05	100	2.72
18	05	250	6.80
19	06	100	2.72
20	06	250	6.80
21	07	100	2.72
22	07	250	6.80
23	08	100	2.72
23	08	100	2.72
24	08	250	6.80
25	13	150	2.72
26	13	200	3.78

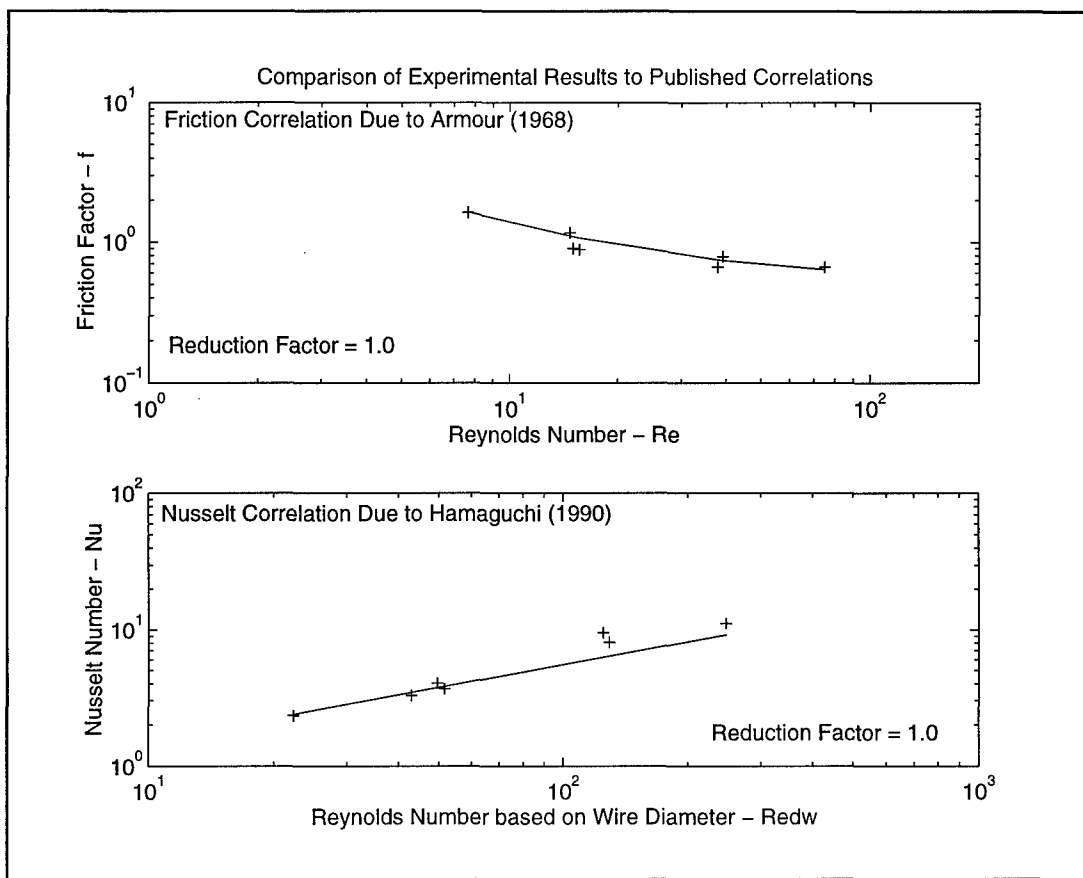


Figure 19. Friction and Nusselt Number Comparisons

give confidence that the method outlined in Chapter III is acceptable and gives believable results for the heat transfer coefficient and friction factors of the unrolled screen matrices, and will also work for the rolled screen matrices.

Repeatability

Another test of confidence for the methodology is repeatability. In Fig. 20, data is shown for both friction factor and Nusselt number for four sets of test runs.

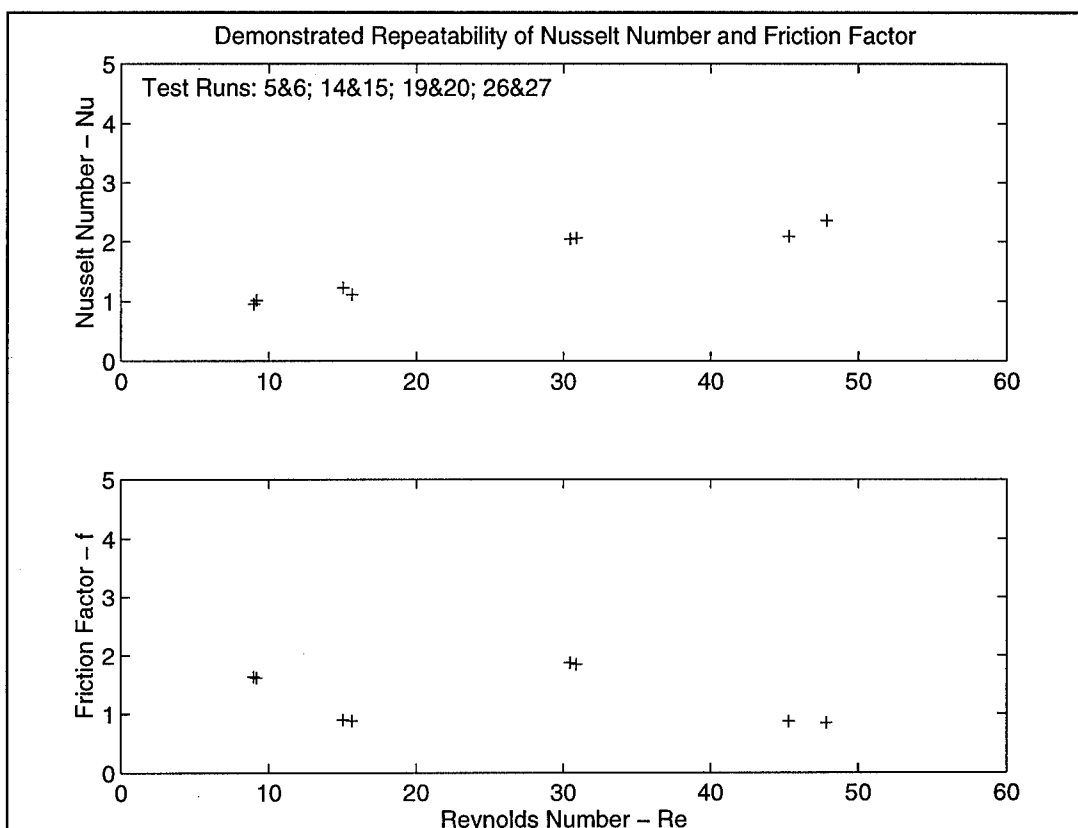


Figure 20. Repeatability of the Data

The test runs were done on different days but with approximately the same operating conditions. The test runs were chosen at random and cover a range of reduction factors and Reynolds numbers. The friction data is particularly good with a mean difference of only 2.0% between the members of each set. The fit for the Nusselt numbers is also good with a mean difference of 8.4% between members of the same set. Since the results can be duplicated so closely from one test run to the next, confidence in the measurements was warranted.

Heat Transfer Coefficient

In this section, the results for the heat transfer coefficient are shown. The Nusselt Number is defined as

$Nu = h_{conv} * L_A / k$, where h_{conv} is the convective heat transfer coefficient, L_A is the Armour and Cannon (1968) dimension, and k is the thermal conductivity of the gas. The general relation is shown in Fig. 21.

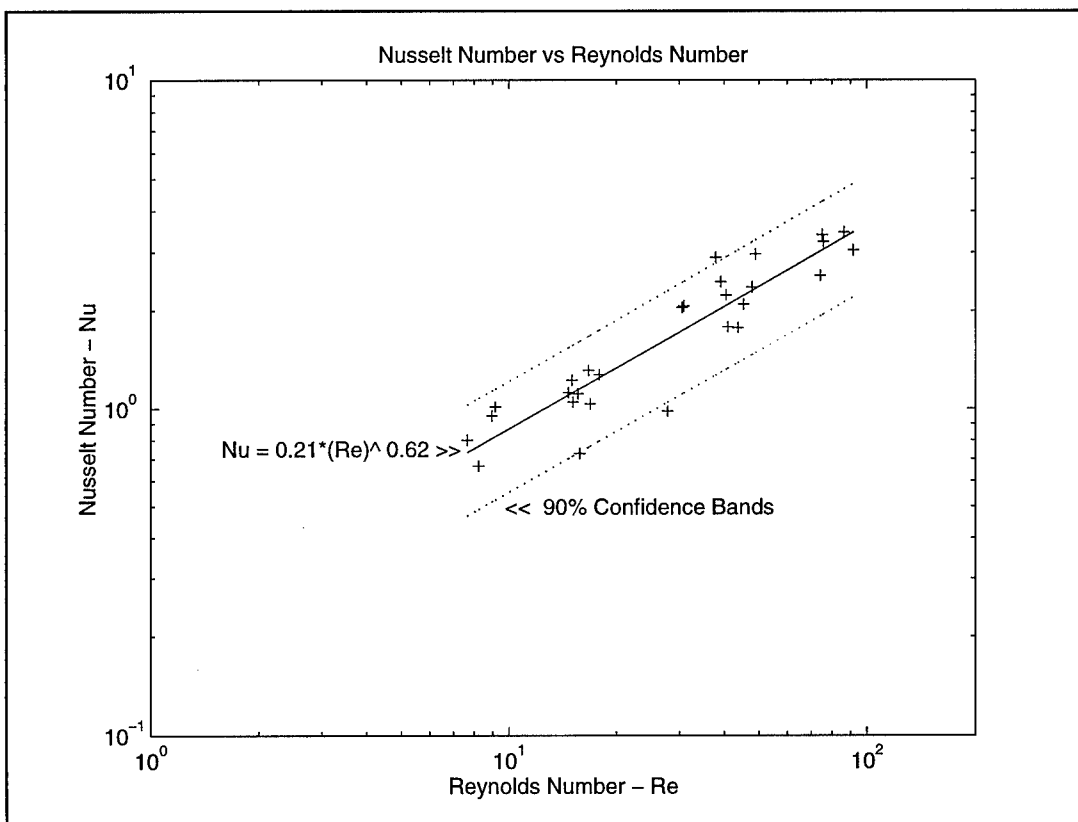


Figure 21. Heat Transfer Results for All SUs

The best fit for the data is a familiar form for heat transfer from a surface to a fluid, $Nu = A * Re^B$, where in this case $A=0.21 \pm 0.049$ and $B=0.62 \pm 0.055$.

One thing seems to be missing from the relation for the Nusselt number. There is no dependence on the reduction factor. During the first attempt to run the data in the numerical model, the surface area of the regenerator was assumed to be the same for the reduced thickness screens as it was for the unrolled screens. When this was the case, the Nusselt number decreased as the reduction factors decreased. When the reduction in area caused by rolling the screens was taken into account, by using a characteristic dimension which included the effects of the surface area, no dependence on the reduction factor by the heat transfer coefficient was observed. It appears no new heat transfer mechanism, e.g., increased turbulence intensity or additional turbulence scale, is introduced by rolling the screens.

In Fig. 22, the reduced Nusselt number, defined as the actual Nusselt number divided by the Nusselt number calculated for an unrolled screen, is shown plotted against the reduction factor. The plot shows within the accuracy of the testing, changing the reduction factor has no effect on the heat transfer except by changing the surface area.

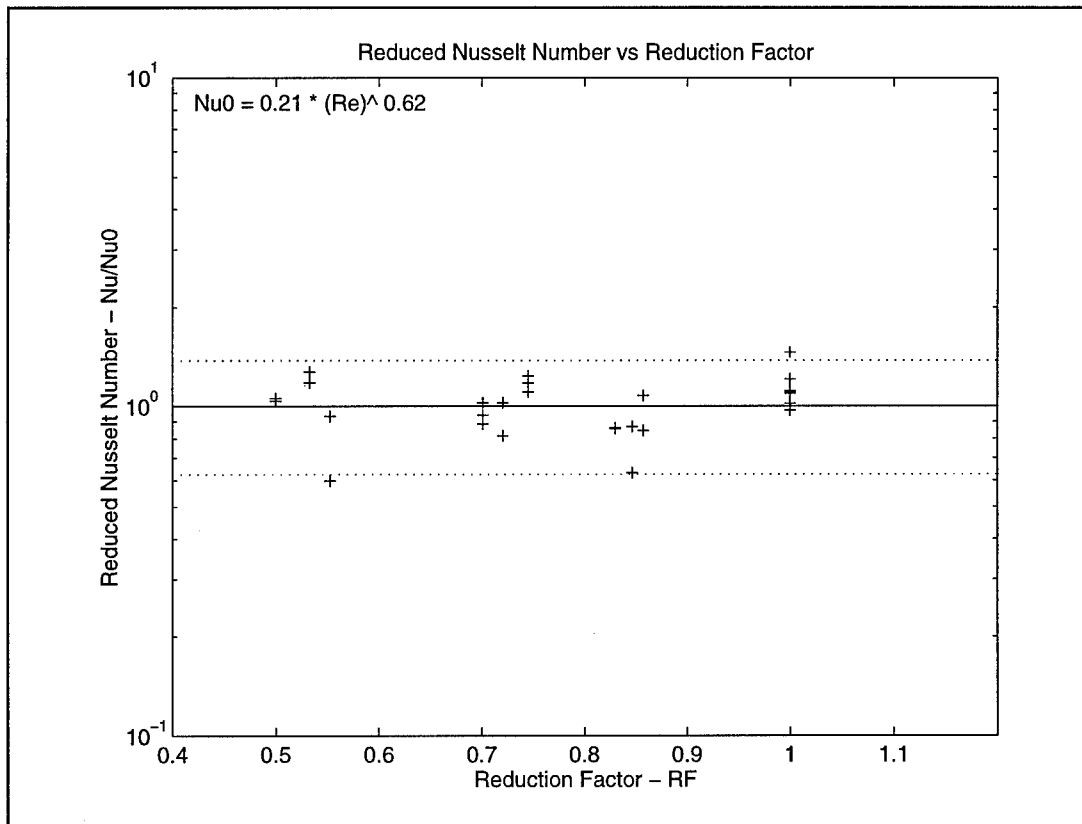


Figure 22. Reduced Nusselt Number as a Function of Reduction Factor

Friction Factor

In this section, the results for the friction factor are given. The behavior of the friction factor differs from the behavior of the Nusselt number. The reduction factor plays a significant role in the value of the pressure drop.

The relation between the friction factor and Reynolds number is shown in Fig. 23. The plotted line is the relationship by Armour and Cannon (1968) for unrolled screens. The first thing to notice about the experimental data is a group of points which are far from the rest in the upper left

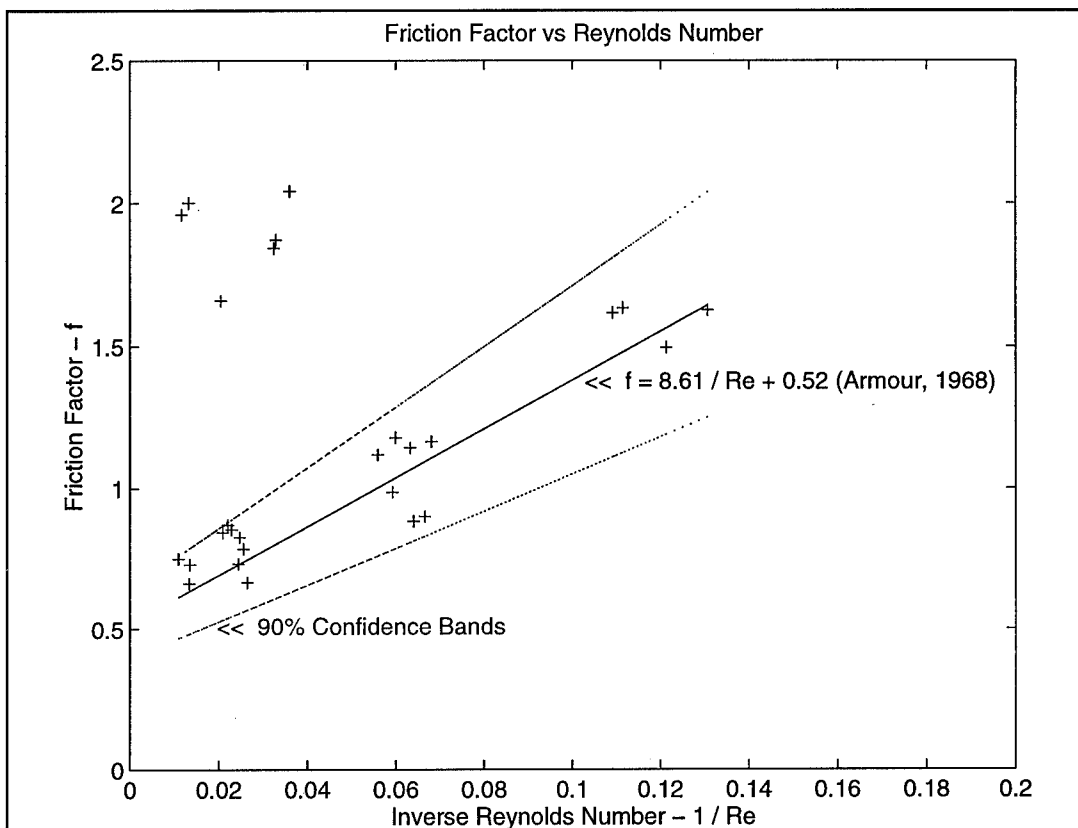


Figure 23. Friction Factor Results for All SUs

hand corner. All of these data points are for test runs with a reduction factor = 0.5. Apparently, reducing the thickness of the screen by 50% causes a large increase in the friction coefficient.

The second thing to notice in Fig. 23 is the remaining data points seem to fall closely to the line for the unrolled relationship. To insure this was the case, the reduced friction factor was plotted against the reduction factor as shown in Fig. 24. The reduced friction factor is defined as the actual friction factor divided by the friction factor for

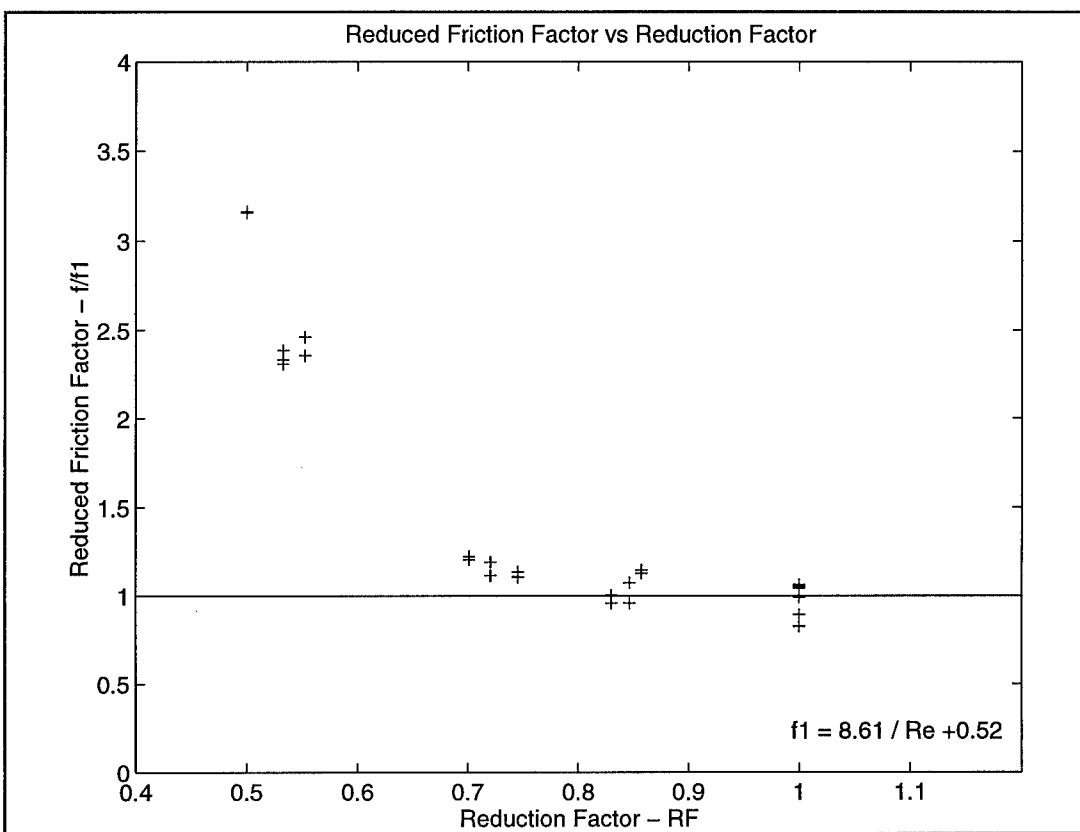


Figure 24. Reduced Friction Factor vs Reduction Factor

the unrolled screens at the same Reynolds number. It appears that the friction factor increases for all values of reduction factor less than 0.7.

A closer look at the friction factor results for $0.7 < RF < 1.0$ is shown in Fig. 25. For $RF = 0.7$, the friction factor increases by approximately 10%. Although the effect of increasing the friction factor is small in this range, it is nonetheless present. These data indicate that the friction factor increases whenever the screens are flattened by 30% or more. This conclusion is consistent with

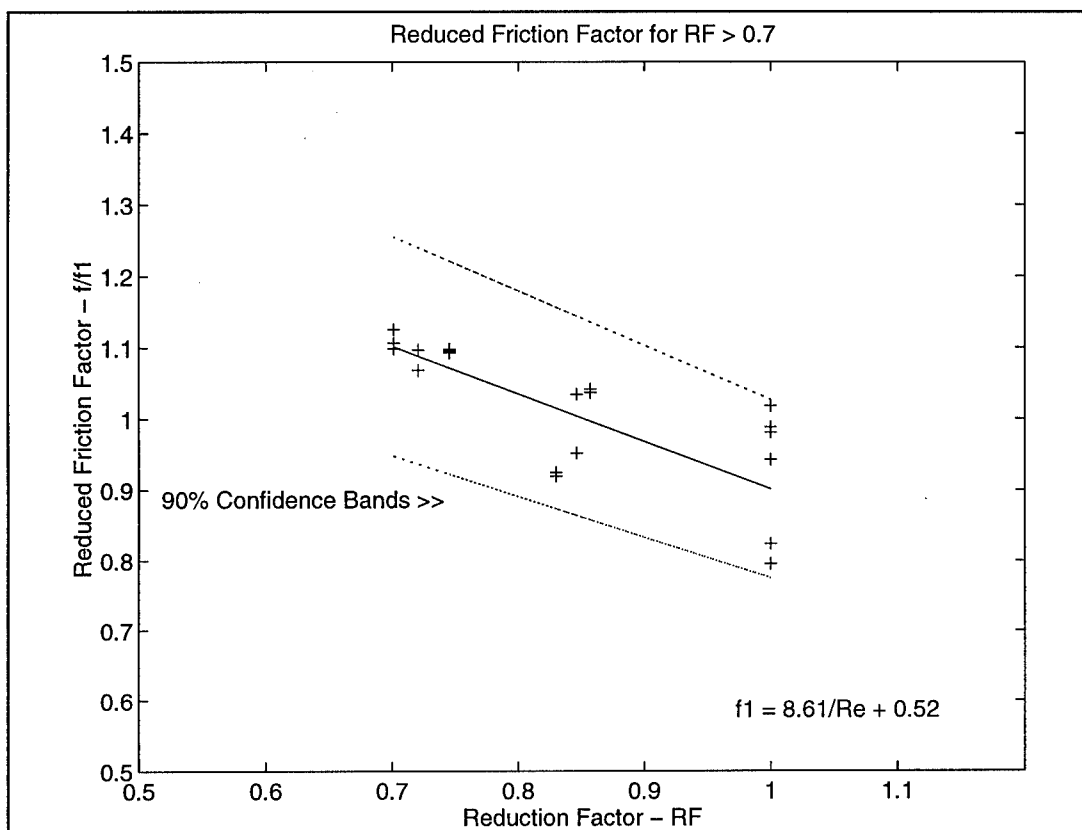


Figure 25. Reduced Friction Factor vs Reduction Factor for RF > 0.7

the results shown in the bottom part of Fig 5. More will be said about this later.

Compactness Factor

The most important result for the purpose of this research is the compactness factor. The compactness factor is a ratio between the heat transfer and pressure drop characteristics of a regenerator. The definition of compactness factor: $CF = j_H/f$, where j_H is the Colburn factor, and f is the friction factor defined in Chapter III. The

Colburn factor is defined: $j_H = St \ Pr^{1/3}$ where St is the Stanton number and Pr is the Prandtl number. The Stanton number is defined: $St = Nu / (Re \ Pr)$ where Nu is the Nusselt number, and Re is the Reynolds number defined above.

In Fig. 26, the results for the compactness factor for all the SUs is shown. While the general trend is lower CF for lower values of the reduction factor, there is no discernable trend which depends on the MESH size.

In Fig. 27, the results for the compactness factor as a function of reduction factor are shown for each mesh size. The results for the unrolled cases compare favorably with published results for the compactness factor (Radebaugh and Louie, 1986:180). For the 100 and 180 mesh screens, the trend is clear, the compactness factor decreases with decreasing reduction factor. Hence, rolling the screens tends to reduce the compactness factor.

For the 250 mesh screens, the compactness factor seems to increase at a reduction factor of 0.7. The data for this case was examined more closely, and whereas the heat transfer coefficient is about what one would expect (compared to the other data), the friction factor is smaller than expected. The reason is not apparent for the discrepancy, and since all the other data follow a predictable trend, it is considered an outlier.

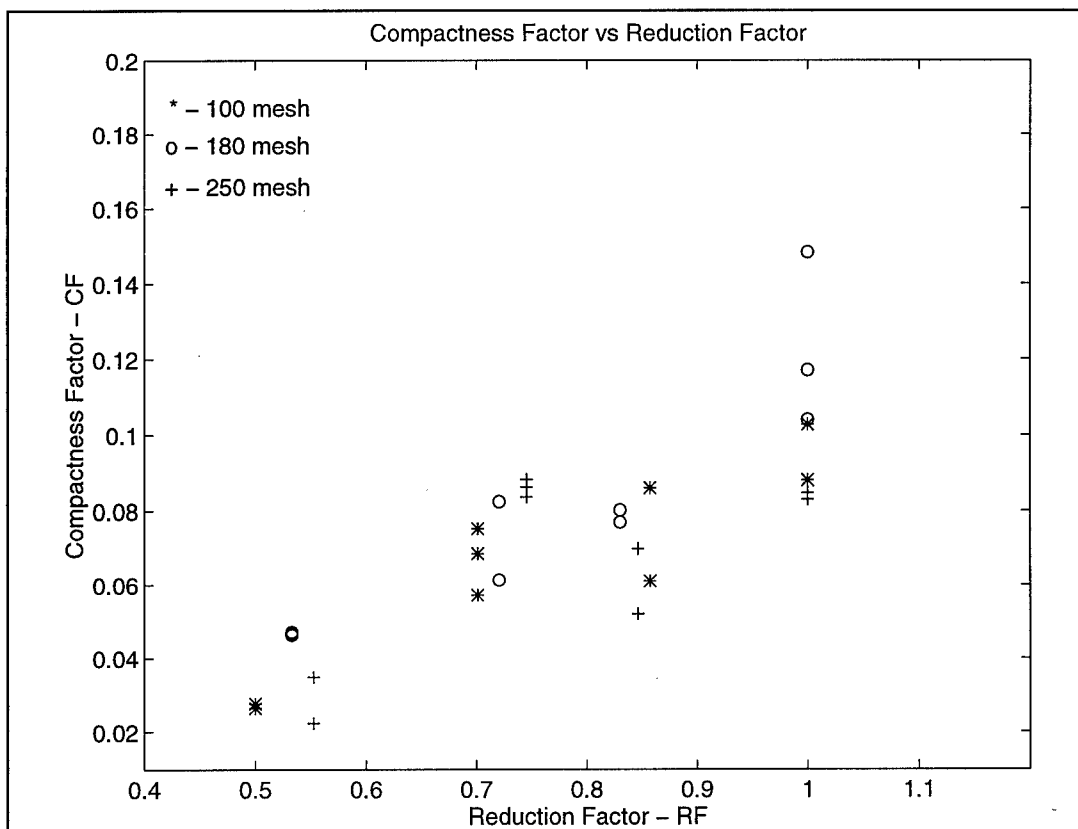


Figure 26 Compactness Factors for All SUs

The entire set of compactness factor data is plotted in Fig. 28 , along with a relationship for determining the compactness factor as a function of the reduction factor. Although the spread in the data is $\pm 50.5\%$, the trend is for smaller compactness factors whenever rolling is done.

In an effort to reduce the spread, the reduced compactness factor was plotted against the reduction factor in Fig. 29. The reduced compactness factor is defined as the ratio of the compactness factor to the compactness factor for unrolled screens based on empirical relations for Nusselt

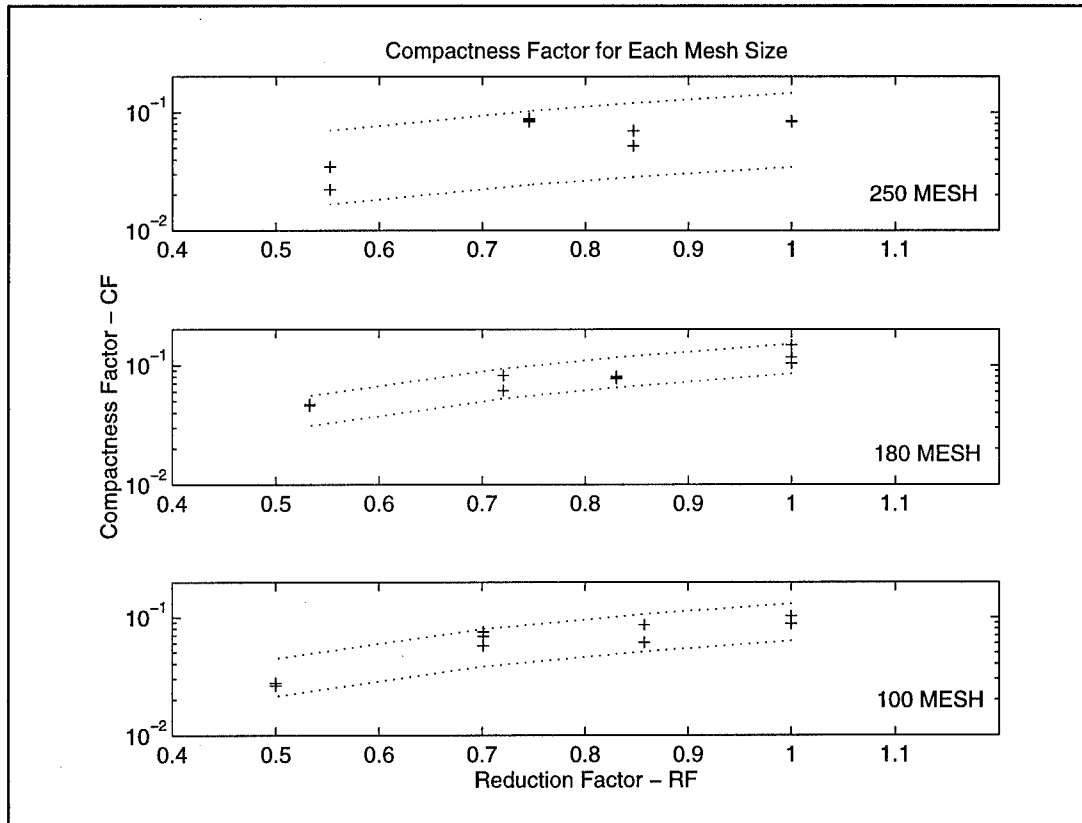


Figure 27. Compactness Factors for Each Screen Size

number and friction factor. The best fit for the data is the curve, Reduced CF = A1 Re^{B1} , where in this case $A1 = 1.22 \pm 0.061$ and $B1 = 1.65 \pm 0.211$. The spread is still moderate (a standard deviation of 21.5% from the best curve fit), but the trend toward reduced compactness factors as the screen thickness gets smaller is still clear. This is the most important result of the current research. Other results are also interesting.

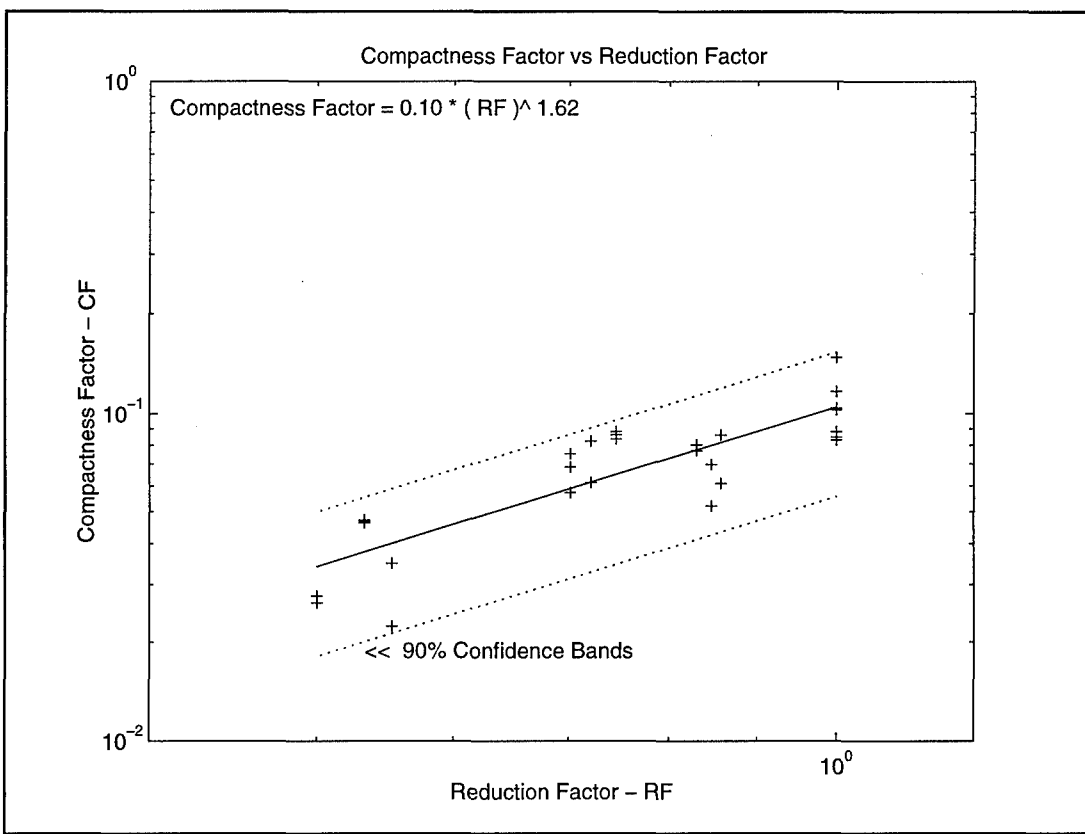


Figure 28. Global Compactness Factor vs Reduction Factor

Criteria Comparisons

Some statements are made in Chapter III about the relative merits of the three criteria used to select the best heat transfer coefficient. The objective of this section is to show the experimental evidence which supports those statements.

To begin, Fig. 30 shows the outlet temperatures from experimental data as well as from the numerical model for three heat transfer coefficients, one based on matching delay time (DT), one based on minimum root-mean-squared difference

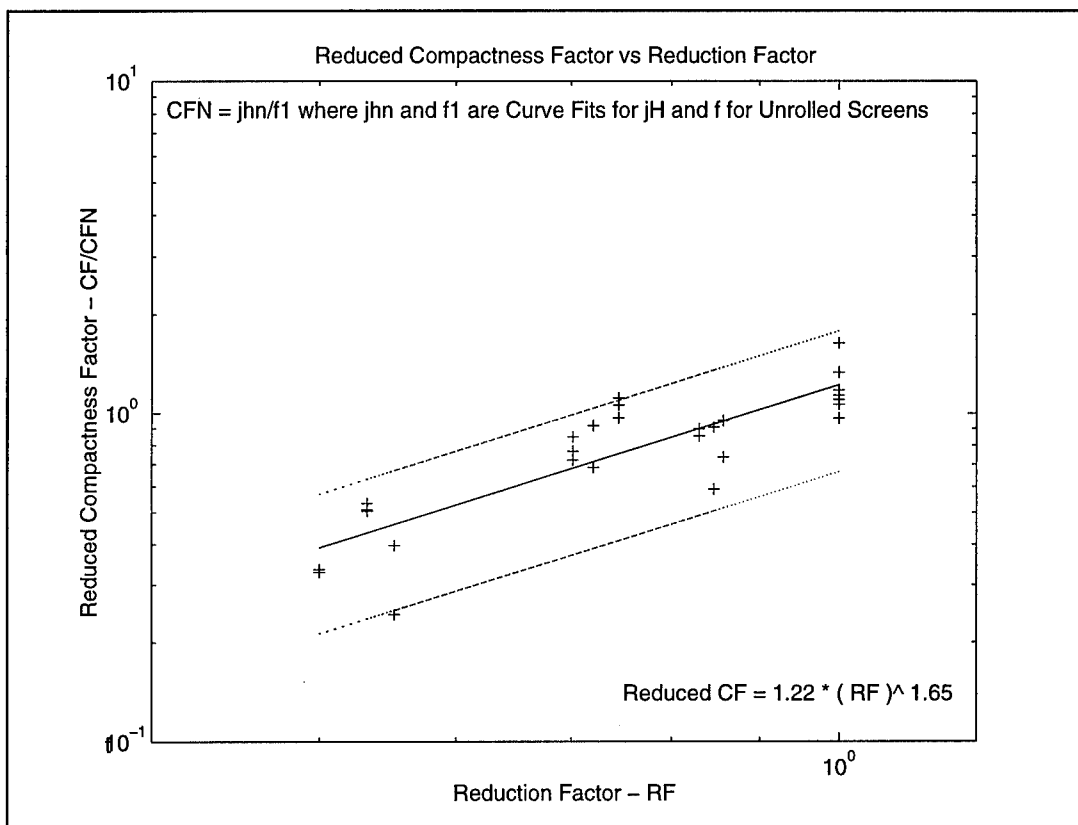


Figure 29. Reduced Compactness Factor vs Reduction Factor

(RMSD), and one based on matching the experimental maximum slope (MS).

In this case, the delay time and root-mean-squared difference results are very close to each other, and match the experimental trace for most of its rise time. The late-time effects of the tube cause the traces to diverge there. The maximum slope results do not match well anywhere. The kind of results shown in Fig. 30 did not happen every time, but they exemplify the types of problems one can encounter unless the

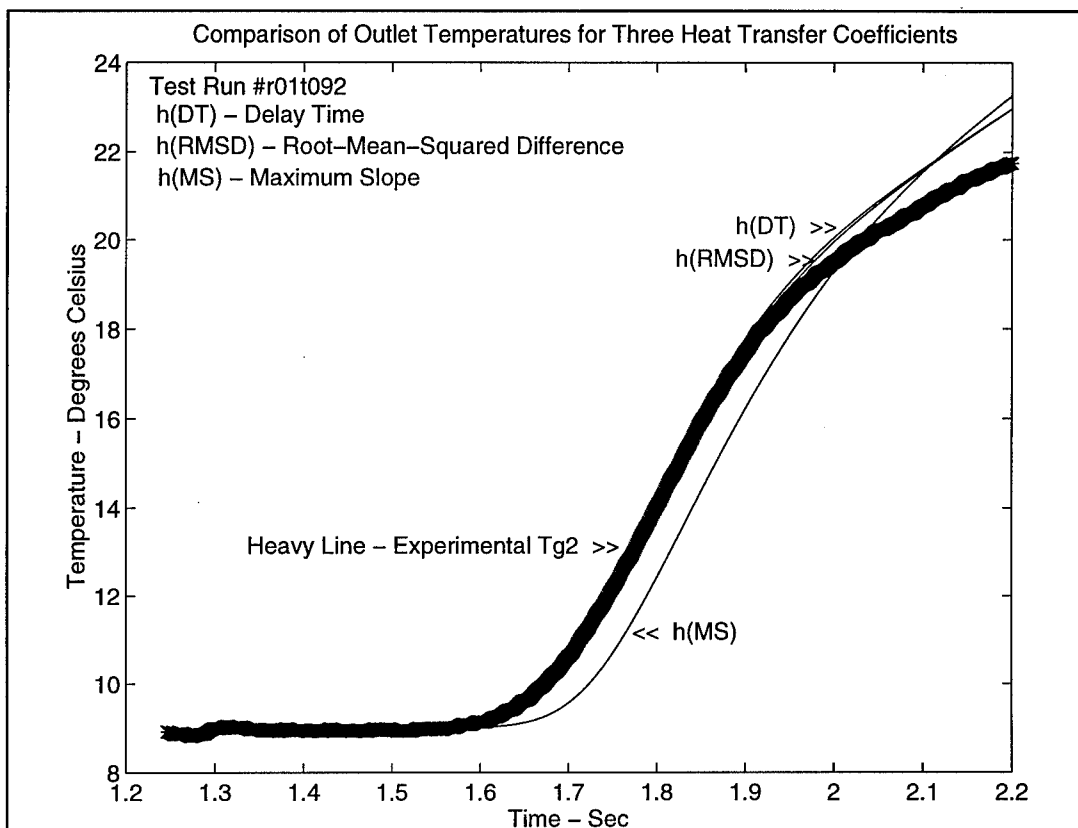


Figure 30. Outlet Temperature Traces for All Three Criteria

improvements to the classical technique made in the current research are included in the approach.

To broaden the conclusions of the previous paragraph, other figures are given below which compare the delay time, minimum root-mean-squared difference, and maximum slope approaches.

The first comparison is shown in Fig. 31 where the delay time and root-mean-squared difference results are plotted against one another. In general, they match each other well with a mean difference of 10.4%. They should match each other

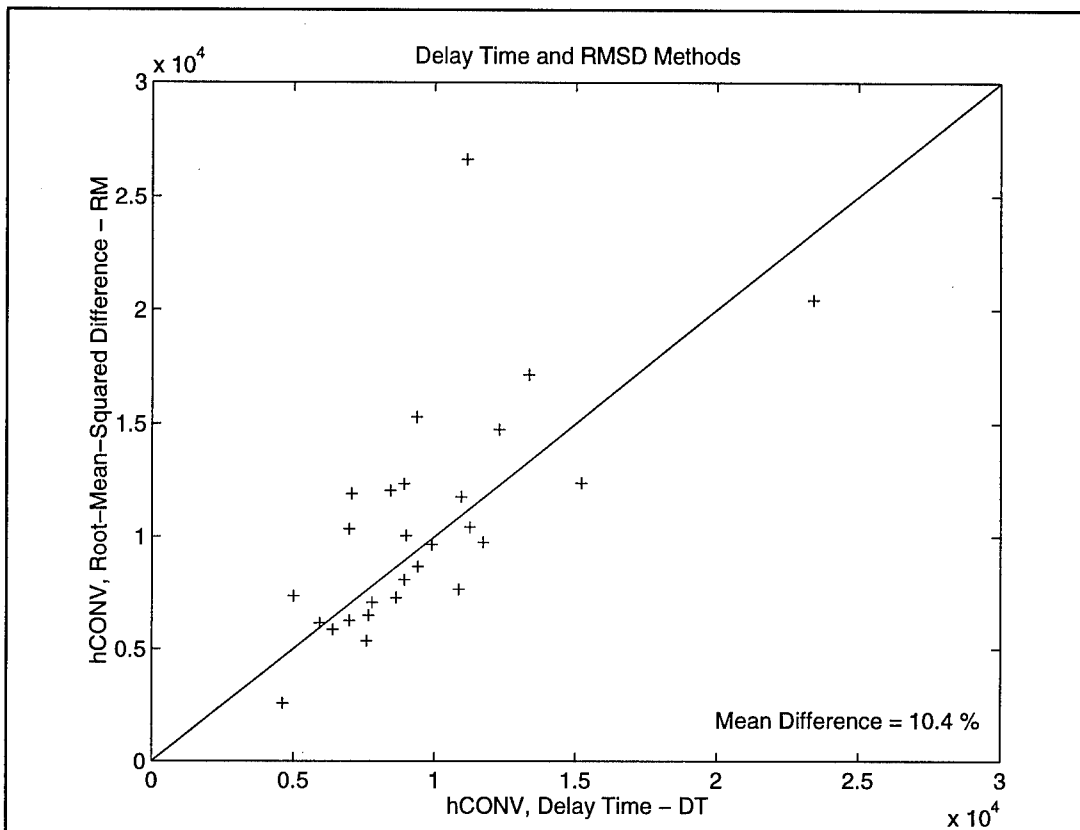


Figure 31. Comparison of Delay Time and Root-Mean-Squared Difference Methods

well if the numerical model is correct during the time when the root-mean-squared differencing is accomplished. The problem becomes choosing the appropriate time frame. On the first run through the data collected for this research, the root-mean-squared differencing was done for the whole period between the beginning of the rise in the outlet temperature trace, τ_2 , to the end of the transient, τ_f . Many of the root-mean-squared difference heat transfer coefficients were badly in error because the experimental outlet temperature traces diverged from the current numerical model results at late

times (as shown above). Only when the root-mean-squared differencing time frame was reduced to the period between the end of the delay time to one matrix thermal time constant after the occurrence of the maximum slope, did the root-mean-squared difference results match the delay time results closely. This time frame is closer to when the physics and the model match each other.

The next comparison is made between the delay time results and those for the theoretical maximum slope in Fig. 32. As expected, the maximum slope approach underestimates the correct answer for the heat transfer coefficient for the reasons given in Chapter III. The literature shows a general problem in accurately matching regenerator heat transfer in numerical models of regenerative systems (Barnes, 1986:513; Hamaguchi, et al, 1991; Hutchinson, 1987; Tew, 1988). The accepted conclusion is that oscillating flow causes an increase in heat transfer coefficient, but some authors who have studied the problem conclude that the heat transfer coefficient is not a function of oscillation frequency (Koester, et al 1990). Perhaps the heat transfer coefficient data which is being used in current models reflect the underestimation of the maximum slope method.

The third comparison shown in Fig. 33 is between the heat transfer coefficient based on delay time and that based on the maximum slope of the outlet temperature trace calculated by

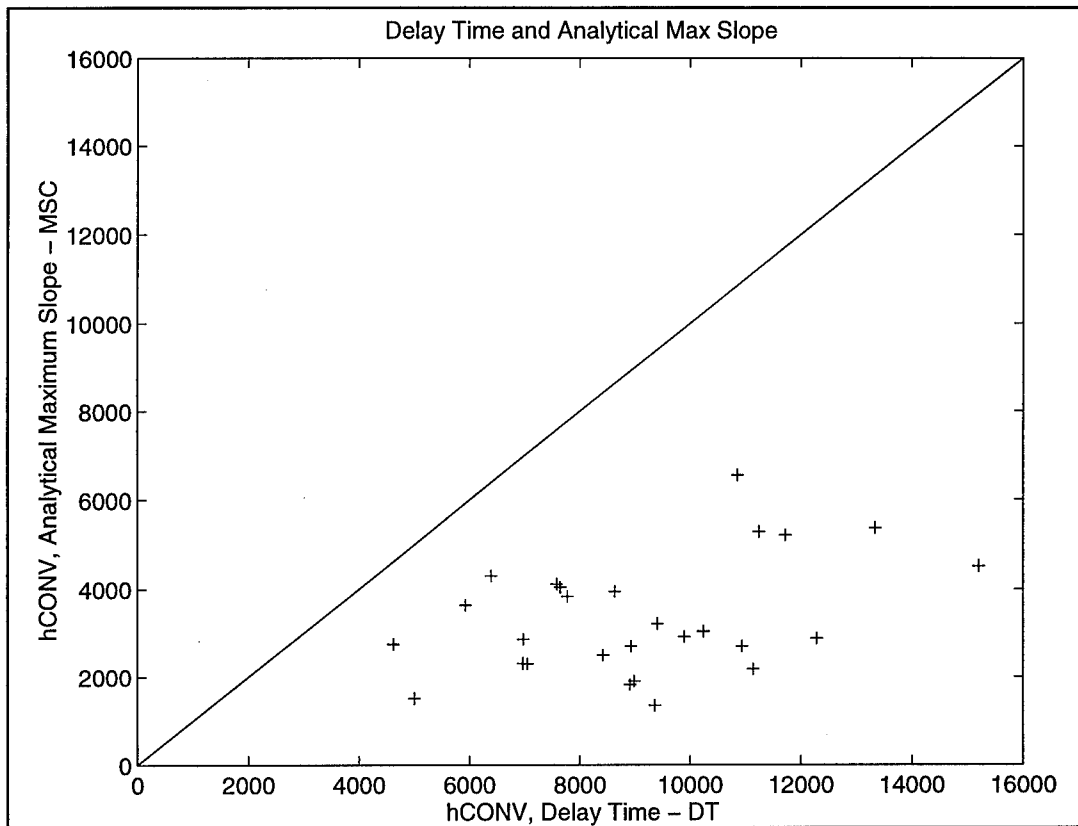


Figure 32. Comparison Between Delay time and Analytical Maximum Slope Results

the current numerical model. This approach is different from the analytical approach due to Pucci, et al. It takes advantage of the contention that the maximum slope of the outlet temperature trace is a unique function of the heat transfer coefficient. The experimentally measured maximum slope is used to choose the heat transfer coefficient by requiring the maximum slope of an outlet temperature trace calculated by *tsie* to match the experimental one. Compared to the delay time results for Nusselt number, eleven of the twenty eight test runs match within 50%. Two comparisons are

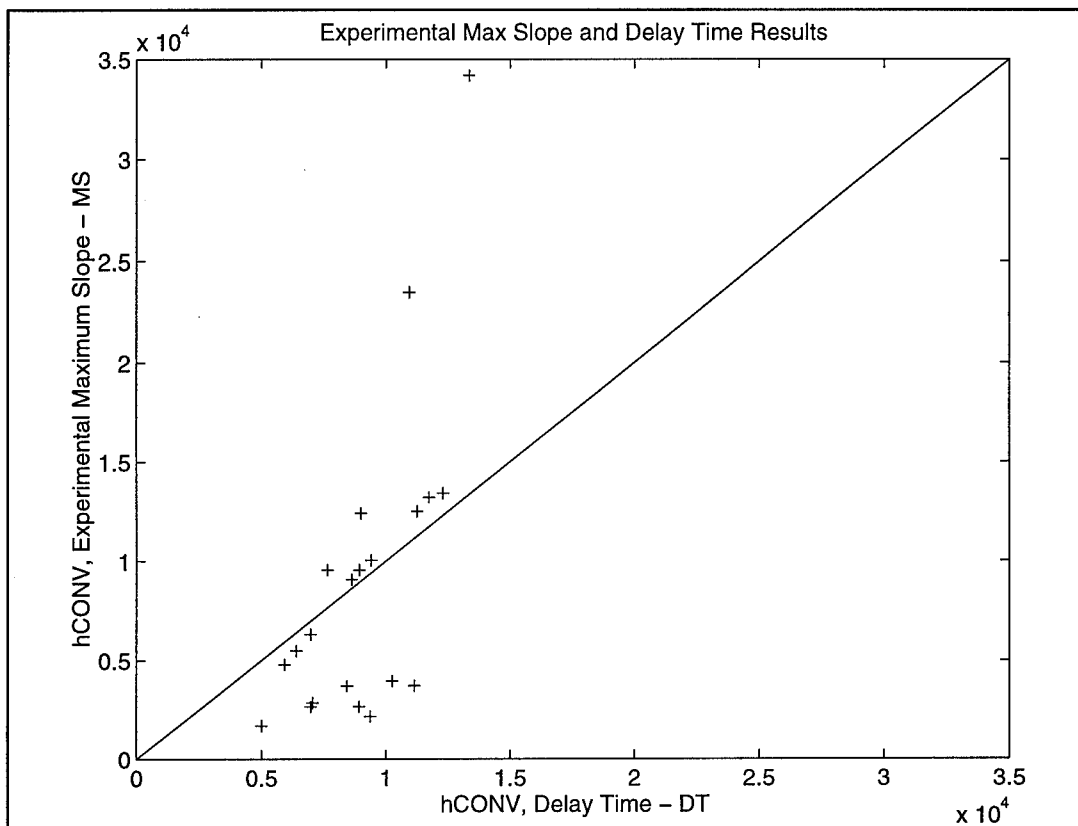


Figure 33. Comparison Between Delay Time and Experimental Maximum Slope Results

100% high, and eight of the results are 66% lower than the delay time results. The balance of the seven test runs did not converge. A value for the heat transfer coefficient could always be calculated with the delay time criteria. Both the large scatter and the inconsistency of using a maximum slope make it an inferior criteria for calculating the heat transfer coefficient.

The final data comparison is shown in Fig. 34. It compares the value of the heat transfer coefficient for the analytical maximum slope case and the numerical maximum slope

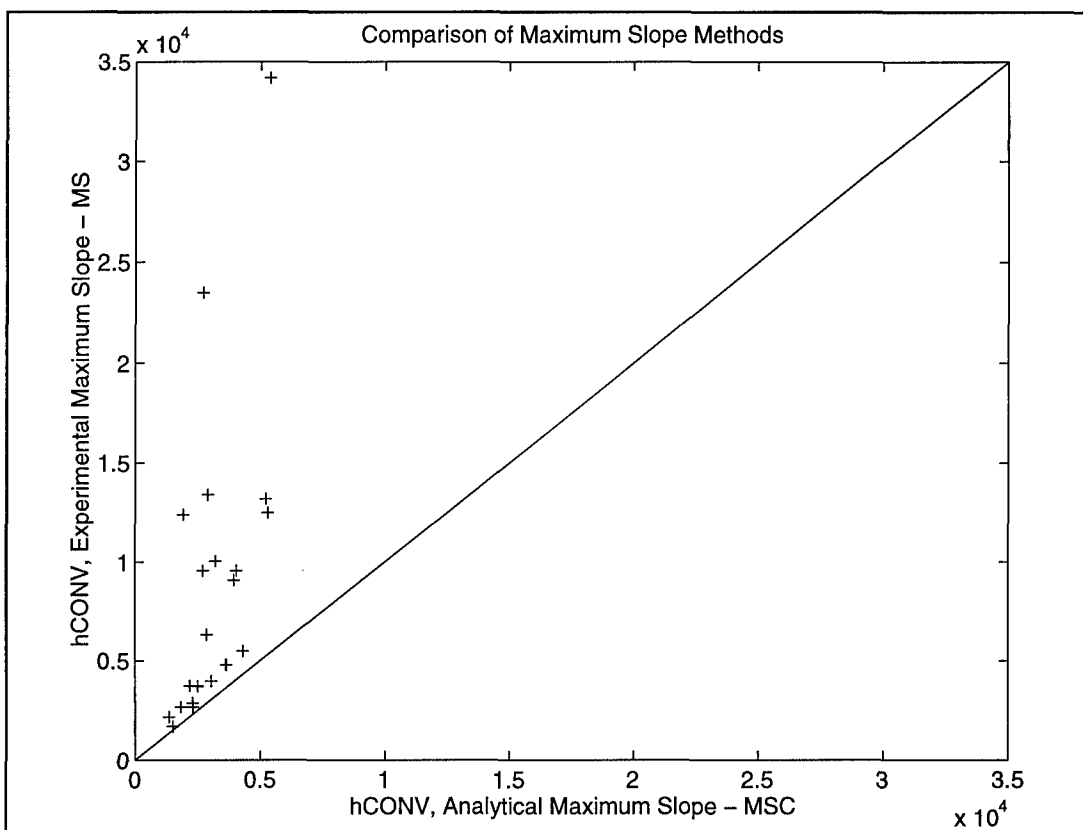


Figure 34. Comparison Between Analytical and Experimental Maximum Slope Results

case. In all cases, the analytical maximum slope predicts a smaller value for the heat transfer coefficient than one determined by an experimentally measured maximum slope. This was expected for the reasons given in Chapter III.

Effectiveness

In Fig. 35, the effectiveness (Eq (26)), and in Fig. 36, the reduced effectiveness, is shown as a function of the reduction factor. Effectiveness is the dominant parameter in cryocooler systems performance as mentioned in Chapter III.

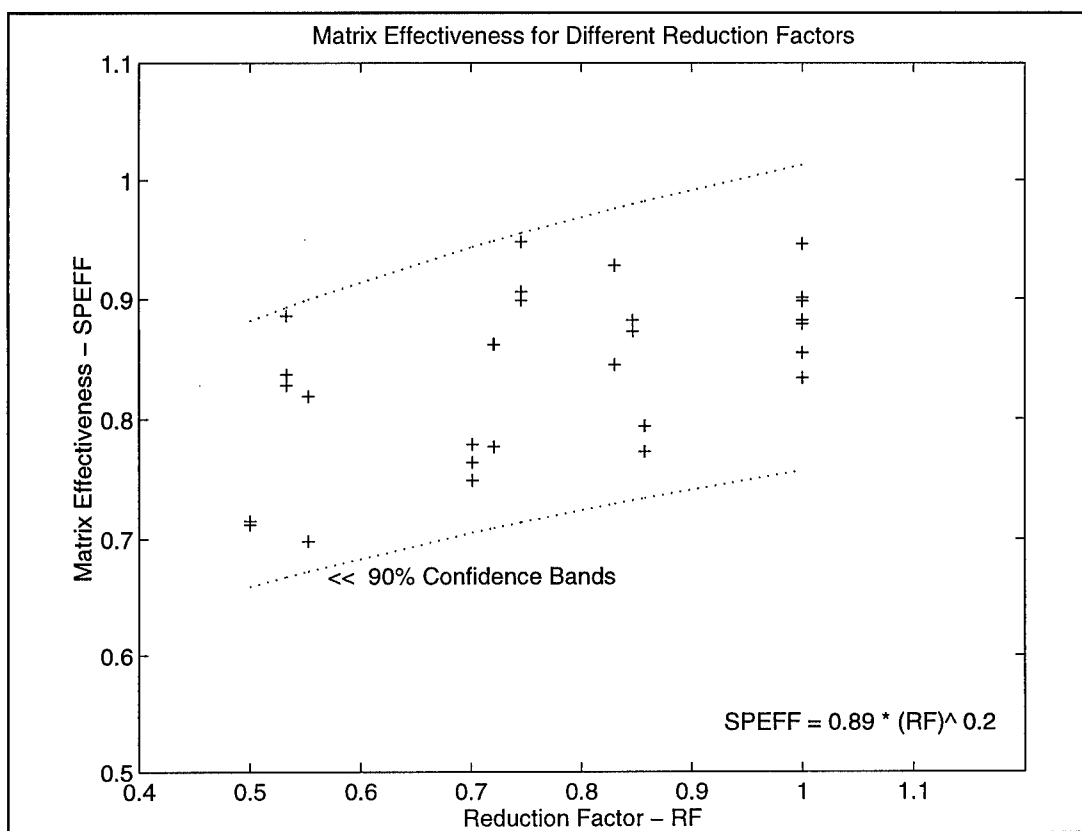


Figure 35. Effectiveness vs Reduction Factor

The figures show a reduction in effectiveness whenever the reduction factor is decreased. In Fig. 35 the best curve fit is $\text{SPEFF} = A_2 \text{Re}^{B_2}$, where $A_2 = 0.89 \pm 0.018$ and $B_2 = 0.20 \pm 0.059$. The effect is small at reduction factors of 0.7 and 0.85, and falls to about a 13% decrement at a reduction factor of 0.5. Again, these results would rule out any benefit of reducing the screen thickness by 50%. The interesting thing about the figures is that one would expect the effectiveness to increase by making pore sizes smaller because of the larger surface area to volume ratio. Rolling the screens does not

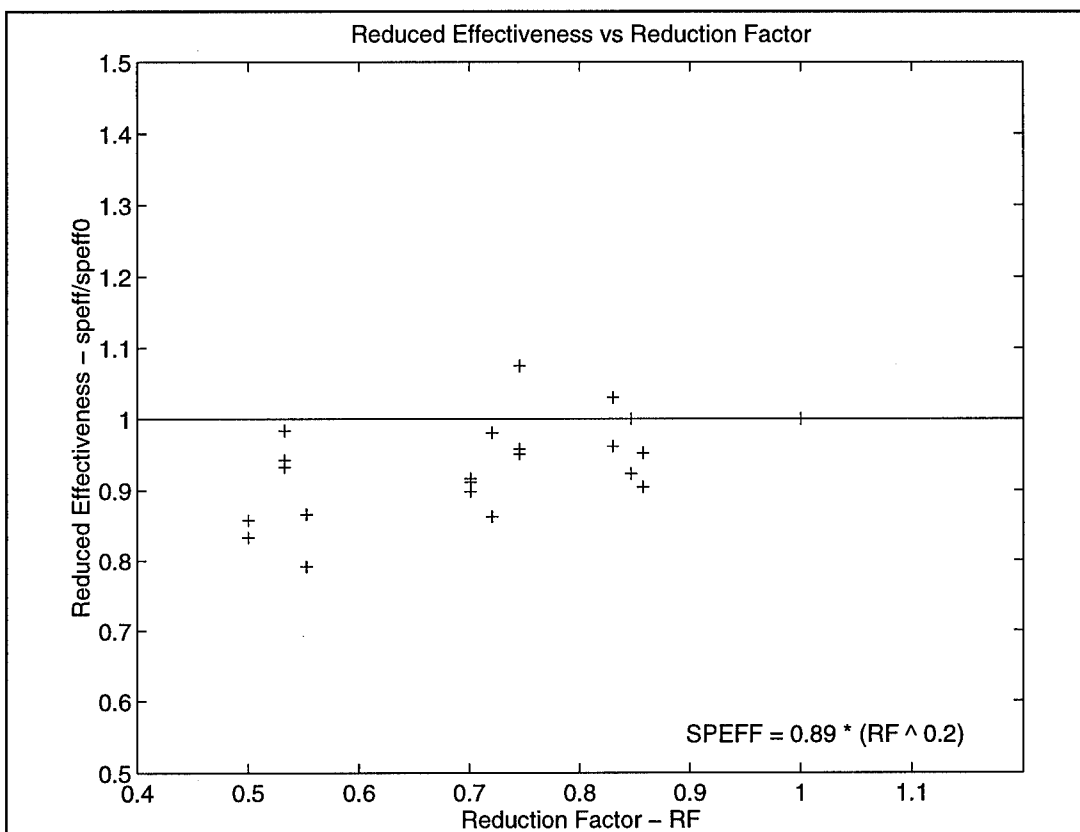


Figure 36. Reduced Effectiveness vs Reduction Factor

change the material properties of the gas or matrix, hence another reason must exist for the decrement. Rolling the screens does reduce the surface area of the matrix since abutted round wires have small areas of contact while flat surfaces cover flat surfaces completely. In Chapter II, large surface-area-to-volume ratios were credited with the large effectiveness of wire-screen matrices, and the area is diminished when flat surfaces are introduced by rolling the screens.

Special SU

In Chapter III, SU #13 was described. It differs from the rest of the SUs since it is made from a combination of different sizes and reduction factors for the screens. Two test runs were accomplished with this regenerator with results shown in Table 4.

Table 4. Comparison of S/U #13 to the Unrolled Case

Test Run	25	26
Experimental f	1.304	1.162
Calculated f (Unrolled Screens)	0.927	0.820
Per Cent Difference	+ 40.7%	+41.7%
Experimental SPEFF	0.668	0.612
SPEFF (Unrolled)	0.782	0.725
Per Cent Difference	- 14.6%	- 15.6%

The purpose of these runs was to gather data for a truly nonhomogeneous matrix and compare it with unrolled screens. Only data for the friction factor is given since the numerical model would have to rely on average values for important parameters to calculate the heat transfer coefficient and the results may be unreliable. In both test runs, the results for the friction are about 40% higher. Since there is no mechanism for enhancing the heat transfer, the compactness factor for this nonhomogeneous matrix must be much smaller

than that for a matrix with unrolled screens and the same porosity, specific surface area, and mass flow rate. Additionally, the *SPEFF* (a measure of effectiveness) is shown to be about 15% lower for both cases. While this study is not exhaustive, it gives further testimony that introducing heterogeneity to the matrix causes a decrease in the compactness factor.

Reynolds Analogy

Due to the lack of heat transfer data for regenerators, some researchers resort to measuring the friction factor and applying Reynolds Analogy (Radebaugh and Louie, 1986:180) to determine the heat transfer coefficient. For Reynolds Analogy to apply to flow in a regenerator, the compactness factor should be a constant (Incropera and Dewitt, 1985: 272-275). If the results for flow in a tube are used, Reynolds analogy states the compactness factor should be 0.125 (Holman, 1968: 146). For the unrolled screens, this is not a bad guess (16.7% high versus the average for the unrolled values) as shown in Fig. 37. But the analogy breaks down at smaller reduction factors, reaching a mean value of 0.031 for $RF = 0.5$. Reynolds analogy works in flow regimes where either surface effects dominate or where inertial effects dominate (*ibid*: 274). But in a regenerator where both are important, the analogy predicts the wrong trend.

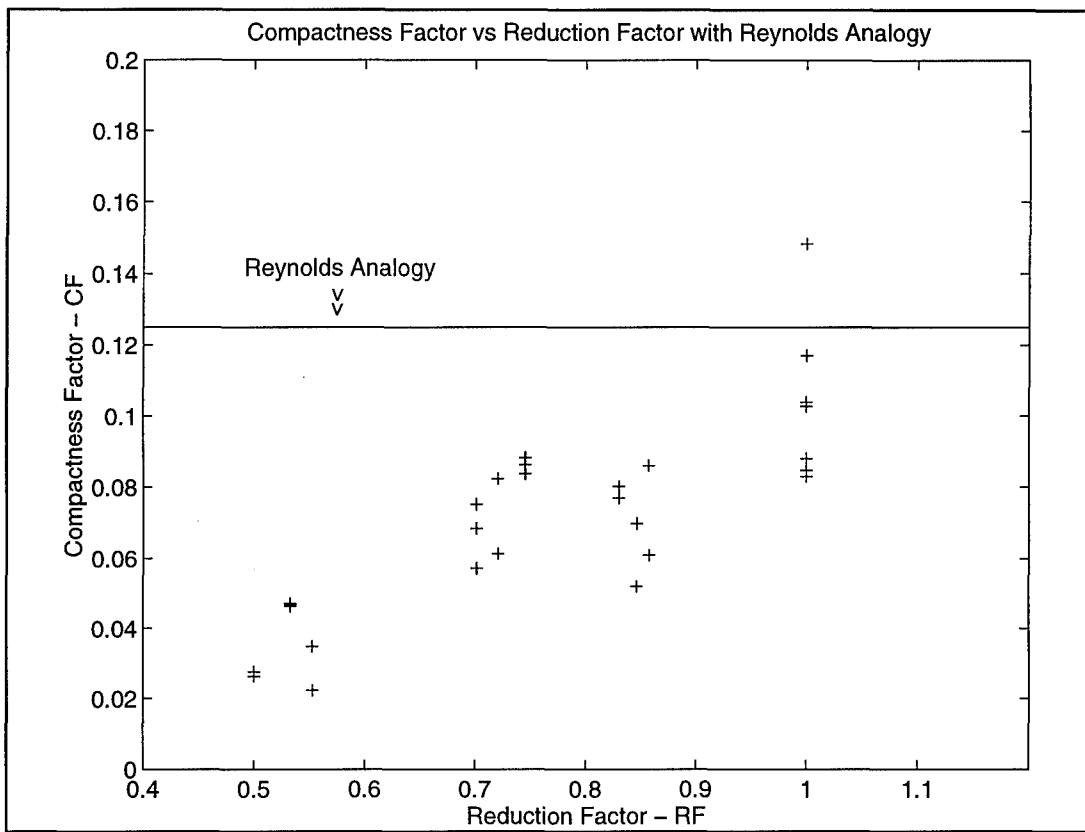


Figure 37. Reynolds Analogy Revisited

Discussion

In this discussion of the results, three topics are addressed. First, the uncertainties for the measurements and parameters is reported. Second, how changes in the most uncertain parameters impacts the results is examined. The section ends with a summary of the results.

Uncertainties. The uncertainties for important parameters and measurements made during the current research are shown in Table 5, along with the source of the estimated value. The calibrations for the mass flow rate, temperature

measurements, and pressure measurements are discussed in Appendix D. The three worst uncertainties are for the density of the steel, the mass flow rate, and the surface area of the matrix.

Table 5. Uncertainties in Measurements

Quantity	Uncertainty	Source
Specific Heats, c_p/c_M	$\pm 2.5\%$	literature
Viscosity, μ	± 3.3	"
Porosity, Φ	± 0.03	worst case
Reduction Factor	± 0.0014	"
Length, EL	$\pm 1.3\%$	"
Area of Tube, A	$\pm 1.7\%$	Measured
Pore Size, PS	$\pm 1.3 \mu\text{m}$	"
Wire Diameter, d_w	"	"
Matrix Mass, W_{SU}	$\pm 0.001g$	"
Delay Time, $SEDT$	$\pm 0.001\text{sec}$	"
Matrix Density, ρ_M	$\pm 10\%$	lit./self test
Gas Density, ρ	$\pm 1\%$	calculated
Mass Flow Rate, \dot{m}	$+7.5\%, -0\%$	calibration
Matrix Surface Area, A_s	$+0, -20\%$	calculated
Temperature, T	$\pm 0.2^\circ\text{C}$	calibration
Pressure, P	$\pm 1\% \text{ of full scale}$	calibration

Effects of Uncertainties. The effect on the data for each of the three worst uncertainties is discussed in this section. The first is the uncertainty of the density of the

steel. Any error in this material property would affect all the data runs similarly, hence, the any conclusions would not change since they are based on a comparison between the characteristics of rolled and unrolled SUs.

The measured mass flow rate uncertainty was calibrated to be $\pm 7.5\%$ for the lowest Reynolds number and $\pm 4.0\%$ at the highest. If the flow velocity is really larger than measured, the effect on the compactness factor can be seen by studying the Armour and Cannon (1968) relation for friction and the curve-fit for the Nusselt number given above. Since the Reynolds numbers would be larger, the friction factor would be smaller. The Nusselt number would be larger proportional to $Re^{0.62}$, hence the Stanton number would be smaller proportional to $Re^{-0.38}$. The ratio between the Colburn factor and the friction factor would make the uncertainty in the compactness factor $\pm 7.8\%$ for the lowest flow rates and $\pm 2.0\%$ for the largest flow rates. Since these spreads are well below the spread in the experimental data ($\pm 37.4\%$), the results are unchanged.

The largest uncertainty is in the surface area of the matrix. This problem was addressed by first assuming there was no surface area lost due to rolling. The effect on the Nusselt number was to make it smaller by a mean difference of 6.1%, compared to the subsequent analysis which included the area correction. The friction factor was unaffected. The

treatment of the area was somewhat conservative since it was assumed all flattened areas were no longer available for heat transfer or surface friction exchanges. Hence, the final answer for the compactness factor lies somewhere between the 6.1% difference between the calculated Nusselt numbers with and without area change, which is within the $\pm 37.4\%$ spread in the plot of compactness factor vs reduction factor.

Summary. The results presented in this chapter give a convincing explanation for the conclusion that flattened screens causes the ratio of heat transfer coefficient to friction factor to decrease. Confidence in the results is warranted because of the favorable comparisons to other data, the repeatability of the test runs, the improvements made in the methodology, the small uncertainties in the measurements, and the immutability of the results given a worse case change in measurements.

The data show that the heat transfer coefficient is unaffected by the rolling of the screens when the reduction in the wetted surface area caused by rolling the screens is taken into account. No enhancement to the heat transfer characteristics of the regenerator is created by introducing flattened surface to the geometry.

The friction factor, however, appears to increase marginally for the larger reduction factors, but substantially for the 50% reduction case. As mentioned in Chapter II, there

are two components to the pressure drop, a surface shear and an inertial component. Although, measurements of these two components were not made, an argument for the observed pressure drop behavior can be made. Reducing the surface area would reduce the surface shear, but decreasing the size of the pores and introducing sharp edges into the geometry would increase the inertial component of the pressure drop. At the higher reduction factors, RF=0.7 or especially RF = 0.85, the inertial component of the pressure drop increases to compensate for the reduction in surface drag forces due to a decrease in surface area which leaves the total pressure drop nearly constant. At a reduction factor of 0.5, there is a large increase in inertial pressure drop. The pore size becomes so small, and the velocity increases so much, the onset of compressibility effects occurs which causes the friction factor to grow much larger.

The combination of the results above leads to the conclusion the compactness factor decreases whenever rolling the screens is done. Hence, the hypothesis presented in Chapter I is proven: Using pressed screens to construct the regenerator matrix decreases the volume of the regenerator, but by doing so, the compactness factor is also reduced.

VI. Conclusions and Recommendations

The purpose of this last chapter is to summarize the current research, and make suggestions for further investigations.

The objective of the research was to measure the heat transfer and friction factor characteristics for a typical stacked-screen regenerator which has had its geometry altered by reducing the thickness of its screens. Regenerative heat exchanger technology is important for space-based energy conversion systems, and any increase in performance which can be achieved by incorporating easily achieved design features should be put to full advantage. Some researchers have reported an improvement in system-level performance of an engine by rolling the screens in a stacked-screen matrix. Although this certainly reduced the dead volume, they did not report whether the improvement in system-level performance was due to the decrease in dead volume, or to an improvement in the operating characteristics of the regenerator, represented by the compactness factor, or to a combination of both. Since the benefits of reduced dead volume have already been documented, a study of the effect on the compactness factor was undertaken for a range of geometries and flow conditions found in current cryocooler systems.

Rolling the screens did reduce the volume of the regenerator, but the results of the current research show

rolling the screens did nothing to enhance the heat transfer. However, the pressure drop increases, particularly for reduction factors of 50%. At larger reduction factors, around 0.85, the decrease in heat transfer and increase in pressure drop are small, which left the compactness factor nearly unchanged. But the effectiveness data indicate any reduction in screen thickness would degrade the effectiveness, the dominant factor for determining cryocooler coefficient of performance. With the friction and heat transfer data presented in Chapter IV, a cryocooler designer could do a trade-off study which includes the influence of effectiveness, pressure drop, and volume reduction, and determine which combination of flow conditions, geometry, and reduction factor gives the optimum performance.

The crux of the matter with regard to the compactness factor is how the geometry of the matrix changed after the screens had been rolled. Rolling the screens caused the smooth, round surfaces of wires to be replaced with flattened areas with abrupt edges. The flattened areas abut one another causing the available wetted surface area to decrease. Reduced wetted surface area reduces the total heat transfer. But the smaller pore sizes and sharp edges causes the total pressure drop to increase. The overall effect of the geometry change is to decrease the compactness factor.

The conclusions concerning heat transfer are due in part to the improved method for determining the heat transfer coefficient in a porous medium used in the current research. The measured inlet temperature profile is used. The sponge effect delay time during which the numerical model and the physics of the flow more closely match one another, is a characteristic of the matrix and is the criteria for choosing the heat transfer coefficient . Also, the significant effect of the tube surrounding the matrix is included in the model. These modifications in the method resulted in generally higher values for the Nusselt number than occurs in other transient step-change techniques.

Further study in four areas warrants attention. First, the same apparatus, data reduction, and numerical model could be used with an oscillating flow of gas to determine if oscillation frequency is a factor in the heat transfer or pressure drop characteristics. This would be particularly interesting because the results could be obtained with the same apparatus and the same technique, a condition not found in current experimentation. Second, since there are ways to increase the surface area of the wire before it is rolled, e.g., by etching or drawing small grooves in the wire, the effectiveness of a regenerator might be increased, even for a rolled screen configuration. Thirdly, since predicting the characteristics of regenerators which are not constructed in

a homogeneous fashion is impossible, a further study of sponge effect delay times could determine the usefulness of comparing regenerators based solely on delay time characteristics as a figure of merit. Finally, analytical studies which include the compactness factor and Reynolds analogy in lieu of experimental heat transfer data to estimate the performance of porous medium regenerators could be repeated to determine how the decreasing trend in compactness factor changes their results. In particular, since heat transfer and friction factor data are now available, a study which incorporates all the influences of effectiveness, pressure drop, and reduced dead volume on the system-level performance should be undertaken to determine the best configuration for a stacked, wire-screen regenerator with reduced thickness screens.

Appendix A: Test Procedures

TEST PROCEDURE

(CAPT TIM MURPHY, AFIT DSY96M, REGENERATOR HEAT TRANSFER STUDY)

RIG SET UP

- TURN ON COOLER/HOT PLATE:
- MAKE SURE ENOUGH HE FOR TEST:
- TURN ON DC POWER SOURCE VI IFA 100 VALIDYNE
- CHECK 1 VDC \pm 0.001 ON THERMISTOR CIRCUIT
- SAFETY EQUIPMENT IN PLACE
- LEAK CHECK WITH SOAPY WATER FOR S/U SWITCHOUT
- WAIT ONE HOUR FOR STEADY STATE
-

TEST RUN

- FILL IN DATA SHEET FOR THIS RUN
- RECORD ROOM TEMPERATURE/PRESSURE ON .VI
- MAKE SURE SAMMPLE FREQUENCY AND BUFFER ARE SET TO 1000/SEC
- ENSURE REGEN.RAW IS EMPTY OF OLD TEST RUN DATA
- CLOSE VENT OUTLET VALVE; 4-WAY VALVE TO HOT FLOW
- RUN HOT HE UNTIL T1/T2 EQUILIBRATE THEN SHUT OFF THE VALVE
- SET TANKS BACK PRESSURE TO APPROPRIATE psia
- ZERO OUT DPVEN DPSU EP1 PRESSURE TRANSDUCERS
- PUT 4-WAY VALVE TO COLD FLOW AND OPEN UPSTREAM VALVE
- ADJUST BOTH VALVE UNTIL P1 AND MDOT ARE ABOUT RIGHT
- PUT 4-WAY TO HOT FLOW AND MATCH COLD FLOW P1 AND MASS FLOW
- TURN 4-WAY BACK TO COLD FLOW AND WAIT FOR TEMPERATURE TO EQUILIBRATE AT ABOUT 10°C
- LET HOT HE TRICKLE UNTIL TEMPERATURE IN VENT IS APPROXIMATELY 35°C
- HIT "SEND DATA TO FILE" ON .VI
- WAIT THREE SECONDS; TURN 4-WAY VALVE TO HOT FLOW
- WAIT 20 SECS; NOTE PRETRANSIENT MEASUREMENTS
- TURN OF GAS FLOW HOT COLD
- NOTE POST TRANSIENT MEASUREMENTS
- OBSERVE DATA TRACE FOR QUALITY; REPEAT IF NECESSARY
- RENAME REGEN.RAW FOR THIS TEST (t**r**.raw)
- MAKE NOTES ABOUT THE TEST RUN ON THE DATA SHEET
- ENTER TEST RUN IN THE LOG BOOK

DATA SHEETS

DATE: _____

TIME: _____

TEST #: _____
SIZE: _____

S/U: _____ P O R E

RE_{PS} : _____

MASS FLOW RATE: _____

ROOM BAROMETRIC PRES (psia): _____ ROOM TEMP. (deg C): _____

HE TANK PRESSURE (psia): _____ B A C K
PRESSURE(psia): _____

DATA FILE NAME: _____

ANEMOMETER OSCILLATIONS ?: _____

PRETRANSIENT: DPSU _____ DOTM _____ DELTA
T1/T2 _____
P1 _____
POST-TRANSIENT: DPVEN _____ DPSU _____
P1 _____
DELTA T1/T2 _____

COMMENTS:
OK? _____

TEST QUALITY

Appendix B: MATLAB m.files

```

function range=trange(tlt2,t)
%The purpose of this function is to take in a range of independent variables,tr,
%and a function, temp ,of the independent variable and determine when a 'change'
%is occurring, e.g. when the slope of the function is more than 1% different
% from the mean slope for the range. This will define a range of the
% independent variable for which a transient is defined.
%
delt=diff(t(1:2));
t1=tlt2(:,1);
t2=tlt2(:,2);
b=fir1(100,.006);
t1f=filtfilt(b,1,t1);
t2f=filtfilt(b,1,t2);
l=length(t1f);
lder=l-1;
lz=lder-220;
lz1=lder-121;
der1=diff(t1f)./diff(t);
der2=diff(t2f)./diff(t);
tav=mean(t1f(21:121));
derav=mean(der2(lz:1z1))
%plot(der2)
%
ti=zeros(1,1);
for i=1:l
    if (t1f(i)-tav) > 1.0;
        ti(i)=-1.0/t(i);
    end
ti(i)=ti(i)+50.;
end
[time k]=sort(ti);
indi=k(1);
tri=t(indi);
%
tf=zeros(1,1);
for j=lz:-1:indi
    if der2(j) > 5.0;
        tf(j)=-1.0*t(j);
    end
end
[time k]=sort(tf);
indf=k(1);
trf=t(indf);
range=[indi indf];
plot((tri:delt:trf),t1(indi:indf),(tri:delt:trf),t2(indi:indf))

```

```
function mslope=maxslope(p,tr)
%This function takes in the coefficients of a polynomial,p, and a range of
%independent variables,tr, and returns the value of the maximum slope in that range
%as well as the location.
ord=length(p)-1;
dor=ord-1
p1=[p(1:ord)];
n=(ord:-1:1);
pd=p1.*n;
der=polyval(pd,tr);
lder=length(der);
plot(der)
[md loc]=sort(der');
lms=tr(loc(lder));
ms=md(lder);
mslope=[ms lms]
```

```
function bestorder=bestpoly(temp,tr)
%This function takes vectors of dependent variables,temp, and
%independent variables,tr, and returns the best order of the
%polynomial which fits the temp data in the range tr based on
%the minimum value of the root mean squared difference.
for i=1:27
    p=polyfit(tr,temp,i);
    f=polyval(p,tr);
    dif=temp-f;
    dif=dif';
    sdif=dif.^2;
    cdif=sum(sdif);
    msdif=cdif/length(dif);
    rms=sqrt(msdif);
    M=mean(dif);
    S=std(dif);
    MS(i,1)=rms;
    MS(i,2)=S;
    MS(i,3)=M;
end
ams=abs(MS)
[ms j]=sort(ams);
ms;
check=j(1,1)-j(1,2);
j
minrmsdif=ms(1,1)
order=j(1,1)
bestorder=polyfit(tr,temp,order)
```

```
function dt=t2dt(t2,T,II,IF)
%This m.file takes in a data file containing the temperatures and times
%of a thermal transient and returns dt, the time it takes for the
%temperature to change "significantly" from its initial value.
%
b=fir1(20,.006);
t2f=filtfilt(b,1,t2);
l=length(t2);
l1=l-100;
ti=ones(l,1);
%
for i=II:IF
    tav=mean(t2f(II:i));
    if t2f(i+50)-tav > 0.4;
        ti(i)=-1.0/i;
    end
end
%
[time k]=sort(ti);
i2=k(1);
tau2=T(i2);
dt=[i2 tau2]
plot(T(i2:IF),t2f(i2:IF))
```

```
function temp=filtlt2(t1,t2)
%
%This m.file takes in the values of the inlet temperature,t1,
%and the outlet temperature,t2, and filters them with a 100
%order fir filter. t1 and t2 are two vectors containing experimenetal
%data.
%
b=fir1(20,.006);
t1fir20=filtfilt(b,1,t1);
t2fir20=filtfilt(b,1,t2);
temp=[t1fir20 t2fir20];
plot(t1fir20)
hold
plot(t2fir20)
hold off
```

Appendix C: FORTRAN Codes - *tsie* and *main*

PROGRAM TSIE
C THIS IS A COMPUTER PROGRAM TO DETERMINE THE TRANSIENT GAS
C TEMPERATURE FOR A WIRE-SCREEN REGENERATOR SUBJECTED
C TO A QUASI STEP CHANGE IN TEMPERATURE AT THE INLET.
C IT USES A STRICTLY EXPLICIT FINITE DIFFERENCE
C SCHEME AT EACH TIME STEP AND INCLUDES THE INTERACTION BETWEEN
C THE GAS AND THE TUBE ALTHOUGH NOT CONDUCTION BETWEEN THE TUBE
C AND THE MATRIX.
C THE WORKING FLUID IS HELIUM AT ROOM TEMPERATURE.
C THE MASS FLOW RATE IS GIVEN AND ASSUMED STEADY.
C THE ENERGY EQUATION FOR INCOMPRESSIBLE FLOW IS USED TO CALCULATE
C THE TEMPERATURE OF THE EXIT GAS.
C DOTM IS THE MASS FLOW RATE (FUNCTION OF TIME ONLY).
C TG0(I) AND TGL(I) ARE THE EXPERIMENTALLY MEASURED GAS TEMPS
C AT THE INLET AND EXIT OF THE REGENERATOR, RESPECTIVELY.
C D IS THE PIPE DIAMETER; EL IS THE REGENERATOR LENGTH.
C POR IS THE POROSITY; I,N ARE THE TIME AND SPACE COUNTERS.
C DH IS THE HYDRAULIC DIAMETER OF THE REGENERATOR MESH.
C DELT, DELX ARE THE TIME AND SPACE INCREMENTS OF THE MODEL.
C SAMPT IS THE EXPERIMENTAL DATA SAMPLING TIME INCREMENT.
C I,J, AND N ARE THE TIME AND SPACE COUNTERS.
C II AND IF ARE THE BEGINNING AND ENDING INDEXES ASSOCIATED WITH
C TAU0 AND TAUF OF THE ACTUAL TRANSIENT.
C JMAX AND NMAX ARE THE MAXIMUM TIME AND SPACE INCREMENTS.
C ITRAN IS THE NUMBER OF TIME INCREMENTS DURING THE ACTUAL
C TRANSIENT, TAUF-TAU0/DELT.
C IO IS THE COUNTER FOR THE EXPERIMENTAL DATA AT THE BEGINNING
C OF THE CURRENT ICOUNT.
C IINT IS THE NUMBER IF CALCULATION TIME INCREMENTS BETWEEN
C EXPERIMENTAL DATA POINTS.
C ICOUNT IS THE COUNTER FOR THE CALCULATION SUBINTERVAL BETWEEN
C DATA POINTS.
C EMU IS THE DYNAMIC VISCOSITY; ENU THE KINEMATIC VISC.
C REPS IS THE REYNOLD'S NUMBER BASED ON PORE SIZE.
C PS IS THE DISTANCE BETWEEN WIRES.
C DP IS THE WIRE DIAMETER.
C PIT IS THE PITCH = DP+PS.
C HTC IS DEFINED AS Q / A/ TG-TR
C TGC(N), TRC(N), AND TTC(N) ARE THE TEMPERATURES OF THE GAS, MATRIX
C AND TUBE WALL DURING THE CURRENT TIME STEP OF THE TRANSIENT.
C TGP(N), TRP(N), AND TPP(N) ARE THE GAS, MATRIX, AND TUBE
C TEMPERATURES DURING THE PREVIOUS TIME STEP OF THE TRANSIENT.
C TG2 IS THE OUTLET GAS TEMPERATURE DETERMINED BT THE MODEL.
C TEMP IS THE INTERPOLATED INLET GAS TEMPERATURE.
C HNU IS THE NUSSELT NUMBER; NU = HTC*DH/KG
C R IS THE GAS CONSTANT FOR THE WORKING FLUID.
C EKG IS THE THERMAL CONDUCTIVITY OF THE GAS.
C EKS IS THE THERMAL CONDUCTIVITY OF THE TUBE MATERIAL.
C A IS THE TOTAL PIPE AREA; AF IS THE AREA FOR FLOW = POR*A.
C AS IS THE SURFACE AREA FOR HEAT TRANSFER PER UNIT VOLUME OF
C THE REGENERATOR MATRIX.
C AST IS THE TUBE AREA FOR HEAT TRANSFER IN ONE DELX.
C ACXT IS THE CROSS SECTIONAL AREA OF THE TUBE WALL.
C CP IS THE SPECIFIC HEAT OF THE GAS AT CONSTANT PRESS.
C CV IS THE SPECIFIC HEAT OF THE GAS AT CONSTANT VOLUME.
C GAMMA IS THE RATIO OF CP/CV.
C SLOPE IS THE MAXIMUM SLOPE OF THE TEMPERATURE TIME
C CURVE AT t = ELOC; LOC IS THE INDEX FOR ELOC.
C RHO IS THE GAS DENSITY = PM/R/TM
C CM IS THE MATRIX HEAT CAPACITY; RHOM THE MATRIX DENSITY.
C WSU IS THE MASS OF THE SCREEN UNIT.
C THK IS THE TUBE THICKNESS.
C MESH IS THE MESH NUMBER (PER INCH, SEE MIYABE.)
C SAMPT IS THE EXPERIMENTAL DATA SAMPLING TIME.
C TTOT IS THE TOTAL DATA TIME, i.e. IMAX = TTOT/SAMPT
C TAU0 AND TAUF ARE BEGINNING AND ENDING TIMES FOR THE ACTUAL

```

C      TRANSIENT.
C      TAU2 IS THE TIME FOR THE SEDT TO END.
C      TOI,TLI ARE THE INITIAL TEMPERATURES AT THE INLET AND OUTLET.
C      THETA IS THE ANGLE OF CONTACT BETWEEN STRANDS OF THE SCREEN.
C      RF IS THE REDUCTION FACTOR FOR THE SCREEN, RF=EL(act)/EL0.
C

C      DOUBLE PRECISION TGC(155),TRC(155),TTC(155),TGP(155),TRP(155),
$TTP(155),DOTM,REPS,HTC,HNU,TGL(20001),TG0(20001),TG2(20001)
      INTEGER I,N,NMAX,JMAX,LOC,II,IF,IO,IINT,ICOUNT,ITRAN,J
      DOUBLE PRECISION R,RHO,TA,TB,TC,TD,CM,RHOM,A,CP,CV,GAM,TIME,THK,
$DELT,DELX,DH,AF,ENU,EMU,POR,EL,D,PI,DP,PS,EKG,EKS,PIT,THETA,
$STE,TF,TH,TJ,PAV,TOI,TLI,TAV,SLOPE,AS,C,TTOT,ELOC,TAU0,TAUF,
$SACXT,AST,SAMPT,TEMP,WSU,SLOPE1,MESH,RF,TG2AV,SEDT,TAU2

C      INTRINSIC COS,MAX,SQRT,ABS,NINT,ATAN
C

C      OPEN THE DATA OUTPUT FILE
      OPEN(50, FILE='tss.in', STATUS='UNKNOWN')
      OPEN(52,FILE='tss.out', STATUS='UNKNOWN')
      OPEN(53,FILE='tsie.dat', STATUS='UNKNOWN')

C      INPUT FLOW PARAMETERS AND NUMERICAL VARIABLES.
C      INPUT THE WIRE DIAMETER AND PORE SIZE
      READ(50,102) DP,PS
      WRITE(53,*) 'DP =', DP, 'PS = ', PS

C      INPUT REGENERATOR LENGTH AND MASS
      READ(50,102) EL,WSU
      WRITE (53,*) 'LENGTH = ', EL, 'WEIGHT = ', WSU

C      WRITE(*,*) ' INPUT THE HEAT TRANSFER COEFFICIENT,HTC,AND DELT '
      READ(*,*) HTC,DELT
      WRITE(53,*) ' HTC EQUALS ',HTC,' DELT = ',DELT

C      INPUT THE MESH NUMBER
      READ(50,103) MESH
      WRITE(53,*) MESH, 'MESH'

C      THE TUBE DIAMETER AND THICKNESS ARE CONSTANT
      D=0.014859
      THK=0.000508

C      ENTER THE NUMBER OF SPACE INCREMENTS
      WRITE(*,*) ' INPUT THE NUMBER OF SPACE INCREMENTS'
      READ(*,*) NMAX
      WRITE(53,*) ' NMAX = ', NMAX

C      R IS THE GAS CONSTANT FOR HELIUM IN J/Kg*K
      R=2077.

C      DETERMINE THE MAXIMUM THE SPACE INCREMENTS.
      DELX=EL/(NMAX-1)

C      ADD TWO SPACE INCREMENTS TO THE TOTAL.
      NMAX=NMAX+2

C      EKG IS THE THERMAL CONDUCTIVITY OF HELIUM,W/m-K. (SEE KAYS)
      EKG=0.155

C      EKS IS THE THERMAL CONDUCTIVITY OF 304 SS,W/m-K. (SEE INCROPERA)
      EKS=14.9

C      NEED A VALUE FOR EMU FOR THE HELIUM (Pa*SEC).
      EMU=1.95E-05

C      RHO IS THE DENSITY OF THE GAS, ASSUMED CONSTANT

```

```

READ(50,102)PAV,TAV
WRITE(53,*) 'PAV = ', PAV, ' TAV = ', TAV
RHO=(PAV*6895.)/R/(TAV+273.)
C
C DETERMINE THE KINEMATIC VISCOSITY.
ENU=EMU/RHO
C
C DEFINE PI
PI=4.0*ATAN(1.0)
C
C NEED THE TOTAL AREA OF THE PIPE.
A=PI*D**2/4.0
C
C NEED THE CROSS SECTIONAL AREA OF THE TUBE WALL,ACXT.
ACXT=PI*(D+THK/2.0)*THK
C
C NEED A VALUE FOR THE THERMAL CAPACITY OF THE MATRIX
C MATERIAL IN J/KG/K
CM=477.0
C
C NEED A VALUE FOR THE DENSITY OF THE MATRIX IN KG/M3.
RHOM=7100.
C
C NEED A VALUE FOR THE HEAT CAPACITY OF THE GAS IN J/KG/K.
CP=5193.
C
C NEED A VALUE FOR GAMMA AND CV.
CV=CP-R
GAM=CP/CV
C
C NEED A VALUE FOR HEAT TRANSFER AREA, AS. (SEE MIYABE/ARMOUR)
C ENTER THE REDUCTION FACTOR.
READ(50,103) RF
PIT=DP+PS
C DETERMINE THE CONTACT ANGLE.
THETA=ATAN(DP/PIT)
WRITE(53,*) ' RF= ',RF
ASP=PI*(SQRT(PIT**2+DP**2)-(DP*THETA**2/PI))/PIT**2
C
C CORRECT FOR THE REDUCTION FACTOR (SEE NOTES.)
IF (RF.LT.0.65) THEN
  ASP=ASP*0.8
  GO TO 15
ELSEIF (RF.LT.0.8) THEN
  ASP=ASP*0.97
  GO TO 15
ELSEIF (RF.LT.0.95) THEN
  ASP=ASP*0.9992
  GO TO 15
ELSE
  GO TO 15
ENDIF
15 CONTINUE
AS=ASP*A*(DELX/RF)
ATOT=AS*EL/DELX
WRITE(53,*) 'HEAT TRANSFER AREA EQUALS ',AS,' m2'
C
C DETERMINE THE POROSITY (SEE MIYABE 1982).
POR=1.0-(WSU/RHOM/A/EL)
WRITE(53,*) POR,'POR'
C
C DETERMINE THE FLOW AREA.
AF=POR*PI*D**2/4.0
C
C NEED THE TUBE HEAT TRANSFER AREA, AST.
AST=PI*D*DELX*POR

```

```

C
C      DEFINE THE HYDRAULIC DIAMETER.
C      DH=POR/(AS/A/DELX)
C      WRITE(53,*) 'THE HYDRAULIC RADIUS IS ',DH,' m2'
C
C      INPUT THE SAMPLING FREQUENCY ( = 1/SAMPT).
C      READ(50,102) SAMPT,TTOT
C      WRITE(53,*) SAMPT,TTOT,'SAMPT and ttot'
C      INPUT THE TOTAL TIME FOR THE TRANSIENT - IN SECONDS
C      JMAX=NINT(TTOT/SAMPT)
C      WRITE(53,*) JMAX,' JMAX='
105    FORMAT(I9)
C
C      DEFINE THE COURANT NUMBER C.
C      C=DELX/DELT
C      WRITE(53,*) '      THE COURANT NUMBER IS   ',C
C
C      N=1
C      J=1
C      I=1
C
C      READ IN THE MASS FLOW RATE AND THE INLET TEMPERATURES WHICH
C      APPROXIMATE A STEP CHANGE.
C      READ(50,103) DOTM
C      WRITE(53,*) DOTM, ' = dotm '
C      DO 43 J=1,JMAX
C      READ(50,104) TG0(J),TGL(J)
43    CONTINUE
C      WRITE(53,*) TG0(56),TGL(56),' tg0(56),tgl(56)'
C
C      DETERMINE THE INDEX OF THE BEGINNING OF THE ACTUAL TRANSIENT,II,
C      AND THE END OF THE ACTUAL TRANSIENT,IF.
C
C      READ(50,102) TAU0,TAUF
C      WRITE(53,*) TAU0,TAUF,' TAU0,TAUF '
C      II=NINT(TAU0/SAMPT)+1
C      IF=NINT(TAUF/SAMPT)+1
C      WRITE(53,*) II,IF,' II,IF '
C
C      DETERMINE THE NUMBER OF INCREMENTS BETWEEN DATA POINTS,IINT, AND
C      THE NUMBER OF TIME INCREMENTS DURING THE ACTUAL TRANSIENT, ITRAN.
C      IINT=NINT(SAMPT/DELT)
C      ITRAN=NINT((TAUF-TAU0)/DELT)+1
C      WRITE(53,*) IINT,ITRAN,' IINT,ITRAN '
C
C      SET THE INITIAL CONDITION FOR THE GAS AND MATRIX AT A LINEAR
C      DISTRIBUTION BETWEEN TOI AND TLI. TOI IS A MEAN
C      INITIAL INLET TEMP. TLI IS THE MEAN INITIAL OUTLET TEMPERATURE.
C      THE MATRIX RUNS FROM N=2 TO N=NMAX-1.
C      TOI=0.0
C      DO 37 J=(II-20),(II-1)
C      TOI=TOI+TG0(J)
37    CONTINUE
C      TOI=TOI/20.
C      TLI=0.0
C      DO 36 J=(II-20),(II-1)
C      TLI=TLI+TGL(J)
36    CONTINUE
C      TLI=TLI/20.
C      WRITE(53,*) ' TOI= ',TOI,' TLI= ',TLI
C      DO 26 N=2,NMAX-1
C      TRP(N)=(TLI-TOI)/(NMAX-3)*(N-2)+TOI
C      TGP(N)=TRP(N)
C      TTP(N)=TRP(N)
26    CONTINUE
C

```

```

C      SET THE INITIAL CONDITIONS AT THE END POINTS.
TRP (1)=TOI
TGP (1)=TOI
TTP (1)=TOI
TRP (NMAX)=TLI
TGP (NMAX)=TLI
TTP (NMAX)=TLI
C      DETERMINE THE REYNOLDS NUMBER AND NUSSELT NUMBER.
REPS=RF*PS*DOTM/AF/ENU/RHO
HNU=HTC*DH/EKG
WRITE (53,*) ' DOTM= ',DOTM,' REPS= ',REPS,' HNU= ',HNU
WRITE (53,*) DP,AF,RHO, ' DP,AF,RHO'
C      DEFINE SOME OTHER CONSTANTS NEEDED BELOW.
TA=2.0*AS*HTC/DOTM/CP
TB=2.0*RHO*AF*C/DOTM/GAM
TC=HTC*AS/C/CM/RHOM/ (A*(1-POR))
TJ=2.0*HTC*AST/DOTM/CP
TD=TB-TA-TJ
TE=EKS/DELX/RHOM/CM/C
TF=HTC*AST/RHOM/CM/ACXT/C
TH=1.0-2.0*TE-TF
WRITE (53,*) TA,TB,TC,TD,TE,TF,TH,TJ,' TA,TB,TC,TD,TE,TF,TH,TJ '
C      START THE INTERPOLATION COUNTER, ICOUNT, AND SET THE INITIAL
C      INTERPOLATION MARKER, IO.
IO=II
ICOUNT=1
TG2 (IO)=TGP (NMAX)
C      DO 31 I=2,ITRAN
C
IF (ICOUNT.EQ.IINT) THEN
  IO=IO+1
  ICOUNT=0
ENDIF
C      INTERPOLATE THE VALUE OF THE INCOMING GAS TEMPERATURE.
TEMP=((TG0 (I+1)-TG0 (IO))/IINT)*ICOUNT+TG0 (IO)
C      SET THE TEMPERATURE OF THE GAS AT THE INLET TO THE MATRIX
C      EQUAL TO THE INTERPOLATED EXPERIMENTAL TG0 .
TGC (1)=TEMP
C      DETERMINE THE VALUE OF TG AND TM AT THE NEXT LOCATION.
DO 22 N=2,NMAX-1
C
TGC (N)=(TGP (N-1)-TGP (N+1)+TA*TRP (N)+TJ*TTP (N)+TD*TGP (N)) / TB
TRC (N)=TC*TGP (N)+TRP (N)*(1.0-TC)
TTC (N)=TE*TTP (N+1)+TE*TTP (N-1)+TF*TGP (N)+TH*TTP (N)
C      CONTINUE
C
SET THE TEMPERATURE OF THE GAS/MATRIX AT THE EXIT.
TGC (NMAX)=TGC (NMAX-1)
TRC (NMAX)=TRC (NMAX-1)
TTC (NMAX)=TTC (NMAX-1)
C      PUT AN ADIABATIC CONDITION AT THE FRONT OF THE TUBE AND MATRIX.
TRC (1)=TRC (2)
TTC (1)=TTC (2)
C      SET THE CURRENT TIME STEP TEMPS TO THE PREVIOUS ONES.
DO 55 J=1,NMAX
TGP (J)=TGC (J)

```

```

      TRP (J)=TRC (J)
      TTP (J)=TTC (J)
55    CONTINUE
C
      IF (ICOUNT.EQ.0) THEN
        TG2 (I0)=TGC (NMAX)
        IF (ABS (TG2 (I0)).GT.100.) THEN
          WRITE (*, *) 'STABILITY PROBLEM OCCURRING'
          STOP
        ENDIF
      ENDIF
C
      ICOUNT=ICOUNT+1
C
31    CONTINUE
C
C
      CHECK FOR THE MAXIMUM SLOPE AND ELOC.
      SLOPE1=0.0
      DO 71 J=(II+5), (IF-5)
      SLOPE=(TG2 (J-2)+8.0*TG2 (J+1)-8.0*TG2 (J-1)-TG2 (J+2)) /12.0/SAMPT
      IF (SLOPE.GE.SLOPE1) THEN
        SLOPE1=SLOPE
        LOC=J
      ENDIF
71    CONTINUE
      ELOC=(LOC-1)*SAMPT
      WRITE (53, *) SLOPE1, ' SLOPE1', ELOC, ' ELOC '
C
C
      DETERMINE THE SPONGE EFFECT DELAY TIME, SEDT.
      TG2AV=TLI
      DO 83 J=II, IF
      TG2AV=(TG2AV*(J-II+20)+TG2 (J)) /(J-II+21)
      IF ((TG2 (J+50)-TG2AV).GE.0.4) THEN
        SEDT=(J-II)*SAMPT
        TAU2=TAU0+SEDT
        GO TO 84
      ENDIF
83    CONTINUE
84    CONTINUE
C
      WRITE (53, *) ' SEDT ', SEDT, '*****TAU2 Equals', TAU2
C
      OUTPUT THE TG AND TRs
      DO 57 J=II, IF
      TIME=(J-1)*SAMPT
      WRITE (52, 106) TIME, TG2 (J), TGL (J)
57    CONTINUE
C
C
      WRITE (53, 107) MESH, REPS, HNU, RF
      OUTPUT IMPORTANT PARAMETERS
      WRITE (53, *) ' EL , POR , DELX , MESH '
      WRITE (53, *) EL, POR, DELX, MESH
C
101    FORMAT(F15.8,1x,F15.8,1x,F15.8,1x,F15.8)
102    FORMAT(F15.8/F15.8)
103    FORMAT(F15.8)
104    FORMAT(F15.8,1X,F15.8)
106    FORMAT(F15.8,1X,F15.8,1x,F15.8)
107    FORMAT(4F15.8)
      STOP
      END

```

PROGRAM MAIN3C
C THIS IS A COMPUTER PROGRAM TO DETERMINE THE HEAT
C TRANSFER COEFFICIENT AND FRICTION FACTOR FOR A WIRE-SCREEN
C REGENERATOR SUBJECTED TO A QUASI-STEP CHANGE
C IN INLET TEMPRATURE.
C THE WORKING FLUID IS HELIUM AT LARGE PRESSURES (5-20 ATM).
C THE MASSFLOW RATE IS GIVEN (MEASURED) AND ASSUMED STEADY.
C A FINITE DIFFERENCE SOLUTION TO THE ENERGY EQUATION FOR
C INCOMPRESSIBLE FLOW IS USED TO CALCULATE THE TEMPERATURE
C OF THE GAS AND MATRIX AS A FUNCTION OF TIME AND SPACE.
C THE VALUES OF THE HTC ARE DETERMINED ITERATIVELY BY MATCHING
C THREE CRITERIA:
C 1) THE SIZE AND LOCATION OF THE MAXIMUM SLOPE OF THE
C TEMP-TIME CURVE OF THE TRANSIENT.
C 2) THE TIME IT TAKES FOR THE OUTLET GAS TEMPERATRUE
C TO DEVIATE SIGNIFICANTLY FROM THE INITIAL REGENERATOR
C TEMPERATURE, THE SPONGE EFFECT DELTA T, SEDT.
C 3) THE ROOT-MEAN-SQUARE DIFFERENCE OF THE EXPERIMENTAL
C AND CALCULATED OUTLET TEMPERATURES.
C A FUNCTION SUBPROGRAM NAMED ZEROIN IS USED TO FIND THE
C SOLUTION OF $F(X)=0$. ANOTHER FUNCTION SUBPROGRAM,
C FUNSMS/DT/RM, IS USED TO DETERMINE THE MAXIMUM SLOPE, SEDT, AND
C ROOT-MEAN-SQUARE-DIFFERENCE, RMSD, OF THE CALCULATED
C OUTLET TEMPERATURE PROFILE, TG2, FROM THE EXPERIMENTAL ONE,
C GIVEN THE INPUT TEMPERATURE-TIME TRACE AND A GUESS AT
C THE HEAT TRANSFER COEFFICIENT, HTC.
C FUNSMS/DT/RM IS A NUMERICAL SOLUTION FOR THE TRANSIENT
C TEMPERATURE DISTRIBUTION FOR STEADY INCOMPRESSIBLE
C FLOW THROUGH A WIRE-SCREEN REGENERATOR SUBJECTED TO
C A QUASI-STEP CHANGE IN TEMPERATURE BETWEEN TOI AND TLI.
C DOTM IS THE MASS FLOW RATE (FUNCTION OF TIME ONLY).
C TGC(N), TRC(N), AND TTC(N) ARE THE GAS, REGENERATOR, AND TUBE
C TEMPERATURES DURING THE CURRENT TIME-STEP OF THE TRANSIENT.
C TGP(N), TRC(N), AND TTC(N) ARE THE GAS, REGENERATOR, AND TUBE
C TEMPERATURES DURING THE PREVIOUS TIME-STEP.
C TG0(I) AND TGL(I) ARE THE EXPERIMENTALLY MEASURED GAS
C TEMPERATURES AT THE INLET AND EXIT RESPECTIVELY.
C TG2(I) IS THE CALCULATED OUTLET TEMPERATURE.
C TAV, PAV ARE THE EXPERIMENTALLY MEASURED AVERAGE TEMPERATURE
C AND PRESSURE OF THE GAS DURING THE TRANSIENT.
C D IS THE PIPE DIAMETER; EL IS THE REGENERATOR LENGTH.
C POR IS THE POROSITY; I, J, N ARE THE TIME AND SPACE COUNTERS.
C DH IS THE HYDRAULIC DIAMETER OF THE REGENERATOR MESH.
C DELT, DELX ARE THE TIME AND SPACE INCREMENTS DURING THE ACTUAL
C TRANSIENT.
C JMAX AND NMAX ARE THE MAXIMUM TIME AND SPACE INCREMENTS OF
C THE TOTAL DATA SAMPLE.
C ITRAN IS THE NUMBER OF TIME INCREMENTS DURING THE ACTUAL
C TRANSIENT, $(\text{TAUF}-\text{TAU0})/\text{DELT}$.
C IO IS THE COUNTER FOR THE EXPERIMENTAL DATA AT THE BEGINING
C OF THE CURRENT ICOUNT.
C IINT IS THE NUMBER OF CALCULATION TIME INCREMENTS BETWEEN
C EXPERIMENTAL DATA POINTS.
C ICOUNT IS THE COUNTER FOR THE CALCULATION SUBINTERVALS
C BETWEEN EXPERIMENTAL DATA POINTS.
C II AND IF ARE THE TIME INDEX OF THE START AND END OF THE ACTUAL
C TRANSIENT ASSOCIATED WITH ITRAN.
C EMU IS THE DYNAMIC VISCOSITY; ENU THE KINEMATIC VISCOSITY.
C REPS IS THE REYNOLDS NUMBER BASED ON PORE SIZE.
C REDW IS THE REYNOLDS NUMBER BASED ON WIRE DIAMETER.
C CD IS A DRAG COEFFICIENT USED IN F3C.
C PS IS THE DISTANCE BETWEEN WIRES IN THE SCREENS.
C PSC IS THE ACTUAL PORE SIZE; $\text{PSC} = (\text{PS}^2 \cdot \text{PS}^2 \cdot \text{DP} \cdot \text{RF})^{0.33333}$.
C DP IS THE WIRE DIAMETER.
C PIT IS THE PITCH = DP+PS.
C HTC IS DEFINED AS Q / A / TG-TR

C R IS THE GAS CONSTANT FOR THE WORKING FLUID.
 C EKG IS THE THERMAL CONDUCTIVITY OF THE GAS.
 C EKS IS THE THERMAL CONDUCTIVITY OF THE 304 STAINLESS STEEL.
 C A IS THE CROSS SECTIONAL AREA OF THE PIPE.
 C AF IS THE FLOW AREA OF THE REGENERATOR; AF = POR*A.
 C ASP IS THE SURFACE AREA FOR HEAT TRANSFER PER UNIT VOLUME.
 C AS IS THE HEAT TRANSFER AREA PER SPACE INCREMENT.
 C ATOT IS THE TOTAL HEAT TRANSFER AREA IN THE SCREEN UNIT.
 C AST IS THE SURFACE AREA OF THE TUBE FOR HEAT TRANSFER.
 C ACXT IS THE CROSS SECTIONAL AREA OF TUBE WALL FOR CONDUCTION.
 C CP IS THE SPECIFIC HEAT OF THE GAS AT CONSTANT PRESS.
 C CV IS THE SPECIFIC HEAT OF THE GAS AT CONSTANT VOLUME.
 C GAM IS THE RATIO OF CP/CV.
 C HTCMS IS THE HEAT TRANSFER COEFFICIENT DETERMINED BY
 USING THE MAXIMUM SLOPE CRITERIA.
 C HTCDT IS THE HEAT TRANSFER COEFFICIENT DETERMINED BY
 USING THE SPONGE EFFECT DELAY TIME CRITERIA.
 C HTCRM IS THE HEAT TRANSFER COEFFICIENT DETERMINED BY
 USING THE ROOT MEAN SQUARE DIFFERENCE CRITERIA.
 C HTCMAX,HTCMIN ARE BOUNDING GUESSES FOR HTC IN ZEROIN.
 C HTCSTAB IS A BOUNDING HTC FOR STABILITY.
 C TOL IS A TOLERANCE USED IN ZEROIN.
 C ESLOPE AND ELOC ARE THE MAGNITUDE AND LOCATION IN TIME OF
 THE MAXIMUM SLOPE OF THE EXPERIMENTAL TIME-TEMP CURVE.
 C LOC IS THE INDEX OF ELOC.
 C CSLOPE IS THE MAXIMUM SLOPE OF THE TEMPERATURE-TIME CURVE
 AT TIME EQUALS ELOC CALCULATED FROM THE MODEL.
 C RHO IS THE GAS DENSITY.
 C CM IS THE MATRIX HEAT CAPACITY; RHOM THE MATRIX DENSITY.
 C THK IS THE TUBE WALL THICKNESS; WSU THE MASS OF THE SCREEN UNIT.
 C SCTHK IS THE THICKNESS OF A SCREEN.
 C MESH IS THE MESH OF THE SCREENS (PER INCH; SEE MIYABE.)
 C SAMPT IS THE EXPERIMENTAL DATA SAMPLING TIME.
 C TIME IS THE TIME DURING THE CALCULATED SUBINTERVAL.
 C TTOT IS THE TOTAL DATA SAMPLING TIME, I.E. JMAX=TTOT/SAMPT.
 C TAU0 AND TAUF ARE THE BEGINNING AND ENDING TIMES FOR THE
 ACTUAL TRANSIENT.
 C TAU2 IS THE TIME AT THE END OF THE SEDT; I2 IS ITS INDEX.
 C TOI AND TLI ARE THE INITIAL TEMPERATURES AT THE INLET AND OUTLET.
 C THETA IS THE ANGLE OF CONTACT BETWEEN STRANDS OF THE SCREEN.
 C RF IS THE REDUCTION FACTOR FOR THE SCREEN; RF=EL(ACT)/ELO.
 C RMSD IS A ROOT MEAN SQUARE DIFFERENCE.
 C DPSU IS THE AVERAGE EXPERIMENTALLY MEASURED PRESSURE DROP
 THROUGH THE REGENERATOR.
 C F1/2/3E AND F1/2/3C ARE EXPERIMENTAL AND CALCULATED FRICTION
 FACTORS.
 C USTAR IS A VELOCITY BASED ON THE RATIO OF FRONTAL AREA FOR
 FLOW TO THE TOTAL AREA.
 C BETA IS THE RATIO OF THE MINIMUM FLOW AREA TO THE TOTAL AREA.
 C ARP IS AN AREA FACTOR USED FOR FRICTION FACTOR F2CARP.
 C ELARM IS A LENGTH DEFINED BY ARMOUR.
 C REARM IS A REYNOLDS NUMBER BASED ON ELARM.
 C F2CARP IS ARMOUR'S FRICTION FACTOR FOR ROUND WIRE SCREENS.
 C
 DOUBLE PRECISION TG0(20001), TGL(20001), TG2(20001)
 INTEGER I,N,NMAX,JMAX,LOC,II,IF,I2,IINT,ITRAN,J
 DOUBLE PRECISION R,RHO,CM,RHOM,A,CP,CV,GAM,DELT,ACXT,ARP,
 \$DELT,DELX,DH,AF,ENU,EMU,POR,EL,D,PI,DP,PS,EKG,SAMPT,SEDT,
 \$TAV,TOL,AS,C,PIT,TOI,TLI,PAV,HTC,THK,EKS,WSU,THETA,HTCSTAB,ASP,
 \$ESLOPE,ELOC,HTCMAX,HTCMIN,REPS,TAU0,TAUF,MESH,RF,AST,
 \$HTCMS,HTCDT,HTCRM,SZERMS,SZERRM,TAU2,FUNSMS,FUNSDT,FUNSRM,
 \$DPSU,F1E,F2E,F3E,F1C,F2C,F3C,USTAR,Q,ATOT,SCTHK,BETA,CD,REDW,
 \$REARM,ELARM,F2CARP,PSC
 C
 COMMON TG0,TGL,DELT,AS,CP,DELX,SAMPT,RHO,AF,C,CM,GAM,DELT,THK,
 \$POR,RHOM,TOI,TLI,DP,ENU,EKG,DH,PS,II,IF,IINT,ITRAN,

```

$D, PI, A, ACXT, AST, EKS, NMAX, LOC
C
C      EXTERNAL SZERMS, SZERDT, SZERRM, FUNSMS, FUNSDT, FUNSRM
C      INTRINSIC COS, MAX, SQRT, ABS, NINT, ATAN
C
C      OPEN THE DATA INPUT/OUTPUT FILES.
C      OPEN(50, FILE='mss.in', STATUS='UNKNOWN')
C      OPEN(52, FILE='mss.out', STATUS='UNKNOWN')
C      OPEN(53, FILE='final.dat', STATUS='UNKNOWN')
C
C      INPUT FLOW PARAMETERS AND NUMERICAL VARIABLES.
C      INPUT THE WIRE DIAMETER AND PORE SIZE.
C      READ(50,102) DP,PS
C      WRITE(*,*) 'DP = ', DP, 'PS = ', PS
C
C      INPUT REGENERATOR LENGTH AND WEIGHT.
C      READ(50,102) EL,WSU
C      WRITE (*,*) 'LENGTH = ',EL,' WEIGHT = ', WSU
C
C      INPUT THE DELT FOR THE TRANSIENT.
C      WRITE(*,*) ' INPUT DELT '
C      READ(*,*) DELT
C
C      INPUT THE MESH NUMBER
C      READ(50,103) MESH
C      WRITE(*,*) 'MESH = ', MESH
C
C      THE TUBE DIAMETER AND THICKNESS ARE CONSTANT.
C      D=0.014859
C      THK=0.000508
C
C      WRITE(*,*) ' INPUT THE MAXIMUM SPACE INCREMENTS'
C      READ(*,*) NMAX
C      WRITE(*,*) 'NMAX = ', NMAX
C
C      R IS THE GAS CONSTANT FOR HELIUM IN J/Kg*K
C      R=2077.
C
C      DETERMINE THE SPACE INCREMENTS.
C      DELX=EL/ (NMAX-1)
C      WRITE(*,*) DELX,' DELX'
C
C      ADD TWO SPACE INCREMENTS TO THE TOTAL.
C      NMAX=NMAX+2
C
C      EKG IS THE THERMAL CONDUCTIVITY OF HELIUM. (SEE KAYS).
C      EKG=0.155
C
C      EKS IS THE THERMAL CONDUCTIVITY OF 304 SS, W/m-K. (INCROPERA)
C      EKS=14.9
C
C      NEED A VALUE FOR EMU FOR THE HELIUM (Pa*SEC).
C      EMU=1.95E-05
C
C      RHO IS THE DENSITY OF THE GAS, ASSUMED CONSTANT, BASED ON THE
C      AVERAGE TEMPERATURE AND PRESSURE AT THE VENTURI DURING THE
C      TRANSIENT.
C      READ(50,102) PAV, TAV
C      WRITE(*,*) 'PAV = ', PAV, ' TAV = ', TAV
C      RHO=(PAV*6895.)/R/(TAV+273.)
C
C      DETERMINE THE KINEMATIC VISCOSITY.
C      ENU=EMU/RHO
C
C      DEFINE PI
C      PI=4.0*ATAN(1.)

```

```

C NEED THE CROSS-SECTIONAL AREA OF THE PIPE.
C A=PI*D**2/4.0
C NEED THE CROSS-SECTIONAL AREA OF THE TUBE WALL.
C ACXT=PI*(D+THK/2.0)*THK
C NEED A VALUE FOR THE THERMAL CAPACITY OF THE MATRIX
C MATERIAL IN J/KG/K.
C CM=477.0
C NEED A VALUE FOR THE DENSITY OF THE MATRIX IN KG/M3.
C RHOM=7100.
C NEED A VALUE FOR THE HEAT CAPACITY OF THE GAS IN J/KG/K.
C CP=5193.
C NEED A VALUE FOR GAM AND CV.
C CV=CP-R
C GAM=CP/CV
C NEED A VALUE FOR HEAT TRANSFER AREA, AS. (SEE MY NOTES)
C ENTER THE REDUCTION FACTOR.
READ(50,103) RF
PIT=DP+PS
C DETERMINE THE CONTACT ANGLE, THETA.
THETA=ATAN(DP/PIT)
C WRITE(*,*) ' THETA, PIT, RF ', THETA,PIT,RF
C DETERMINE THE SURFACE AREA PER UNIT ORIGINAL VOLUME.
ASP=PI*(SQRT(PIT**2+DP**2)-(DP*THETA**2/PI))/PIT**2
C CORRECT THE SPECIFIC AREA FOR REDUCTION FACTOR. (SEE NOTES)
IF (RF.LT.0.65) THEN
  ASP=ASP*0.8
  GO TO 15
ELSEIF (RF.LT.0.8) THEN
  ASP=ASP*0.970
  GO TO 15
ELSEIF (RF.LT.0.95) THEN
  ASP=ASP*0.9992
  GO TO 15
ELSE
  GO TO 15
ENDIF
15 CONTINUE
AS=ASP*A*(DELX/RF)
ATOT=AS*EL/DELX
WRITE(*,*) ' THE TOTAL HEAT TRANSFER AREA IS ', ATOT
C DETERMINE THE POROSITY (SEE MIYABE 1982).
POR=1.0-(WSU/RHOM/A/EL)
C WRITE(*,*) POR, ' THE POROSITY IS'
C DETERMINE THE FLOW AREA.
AF=POR*PI*D**2/4.0
C NEED THE TUBE HEAT TRANSFER AREA.
AST=PI*D*DELX*POR
C DEFINE THE HYDRAULIC DIAMETER.
DH=EL*AF/ATOT
WRITE(*,*) ' DH =',DH
C FIND THE NUMBER OF DATA POINTS PER TRANSIENT, JMAX.
C INPUT THE SAMPLING TIME AND TOTAL NUMBER OF EXPERIMENTAL POINTS.

```

```

      READ(50,102) SAMPT,TTOT
      JMAX=INT(TTOT/SAMPT)
      WRITE(*,*) JMAX, ' JMAX'

      C
      C DEFINE THE COURANT NUMBER.
      C=DELX/DELT
      WRITE (*,*) C, ' THE COURANT NUMBER IS '

      C
      N=1
      I=1
      J=1

      C
      C ENTER THE EXPERIMENTALLY MEASURED VALUES OF DOTM AND THE
      C GAS TEMPERATURES WHERE TG0 APPROXIMATES A STEP CHANGE.
      READ(50,103) DOTM
      DOTM = 1.1*DOTM
      WRITE(*,*) ' DOTM = ',DOTM
      DO 21 J=1,JMAX
      READ(50,104) TG0(J),TGL(J)
21    CONTINUE

      C
      C DETERMINE THE INDEX OF THE BEGINNING OF THE ACTUAL TRANSIENT
      C II, AND THE END OF THE ACTUAL TRANSIENT, IF.
      C
      READ(50,102) TAU0,TAUF
      II=NINT(TAU0/SAMPT)+1
      IF=NINT(TAUF/SAMPT)+1
      WRITE(*,*) TAU0,TAUF,II,IF,'*****' TAU0,TAUF,II,IF'

      C
      C DETERMINE THE INDEX FOR THE END OF THE SEDT.
      READ(50,103) TAU2
      I2=NINT(TAU2/SAMPT)+1
      WRITE(*,*) 'TAU2 AND I2 ARE ', TAU2,I2
      SEDT=(I2-II)*SAMPT

      C
      C DETERMINE THE NUMBER OF INCREMENTS BETWEEN DATA POINTS, IINT, AND
      C THE NUMBER OF TIME INCREMENTS DURING THE ACTUAL TRANSIENT, ITRAN.
      IINT=NINT(SAMPT/DELT)
      ITRAN=NINT((TAUF-TAU0)/DELT)+1
      WRITE(*,*) IINT,ITRAN,' IINT,ITRAN'

      C
      C DETERMINE THE INITIAL MEAN TEMPERATURE AT BOTH THE OUTLET
      C AND INLET, TLI AND TOI.
      TLI=0.0
      DO 37 J=(II-20),(II-1)
      TLI=TLI+TGL(J)
37    CONTINUE
      TLI=TLI/20.

      C
      TOI=0.0
      DO 36 J=(II-20),(II-1)
      TOI=TOI+TG0(J)
36    CONTINUE
      TOI=TOI/20.
      WRITE(*,*) TLI,TOI,' TLI,TOI '

      C
      C ENTER THE MAXIMUM EXPERIMENTALLY MEASURED SLOPE, ESLOPE,
      C OF THE OUTLET GAS AND ITS LOCATION ON THE TIME-TEMP CURVE.
      READ(50,102) ESLOPE,ELOC
      LOC=NINT(ELOC/SAMPT)+1
      WRITE(*,*) ESLOPE,ELOC,LOC,' *****ESLOPE,ELOC,LOC'

      C
      C ENTER THE EXPERIMENTALLY MEASURED VALUES OF THE PRESSURE
      C DROP THROUGH THE REGENERATOR, DPSU, AND THE SCREEN THICKNESS.
      READ(50,102) DPSU,SCTHK
      WRITE(*,*) ' THE DPSU IS ',DPSU,' SCTHK IS ',SCTHK

```

```

C
C
C USE ZEROIN TO DETERMINE THE HTC GIVEN BOUNDING VALUES OF
C THE HTC AND THE LOCATION AND MAGNITUDE OF THE EXPERIMENTALLY
C MEASURED MAXIMUM SLOPE AND SEDT OF THE TRANSIENT.
C TOL=5.0E+1
C
C SIGNIFY THE MAXIMUM HTC FOR THIS CONDITION.
HTCSTAB=C*CP*RHO*AF/(AS+AST)/GAM
C WRITE(*,*) 'THE MAXIMUM HTC FOR STABILITY IS ABOUT ',HTCSTAB
C
C INPUT THE GUESSES FOR HTCMIN AND HTCMAX
WRITE(*,*) ' INPUT HTCMIN AND HTCMAX '
READ(*,*) HTCMIN,HTCMAX
WRITE(*,*) ' HTCMIN=',HTCMIN,' HTCMAX=',HTCMAX
C
C DETERMINE THE HTCs BASED ON THE THREE CRITERIA.
HTCRM=SZERRM(HTCMIN,HTCMAX,FUNSRM,TOL,I2)
HTCMS=SZERMS(HTCMIN,HTCMAX,FUNSMS,TOL,ESLOPE)
HTCDT=SZERDT(HTCMIN,HTCMAX,FUNSDT,TOL,I2,TAU2)
WRITE(*,*) HTCDT,' = HTCDT'
C
C DETERMINE THE FRICTION FACTORS.
C
C CHANGE THE PRESSURE DROP TO PASCALS.
DPSU=DPSU*6895.0
C
C F1 IS ACCORDING TO CHEN; 200 IS THE NUMBER OF SCREENS.
BETA=(1.0-DB/PIT)**2
USTAR=DOTM/RHO/A/BETA
C WRITE(*,*) ' USTAR = ',USTAR
REPS=PS*USTAR/ENU
F1E=2.0*DPSU/200./RHO/USTAR**2
F1C=49.78/REPS**0.968+0.318
C
C F2 IS DUE TO ARMOUR AND CANNON; Q IS A TORTUOUSITY FACTOR.
Q=1.
PSC=(PS**2*2.*DP*RF)**(1./3.)
ELARM=1.0/(ASP**2*PSC)
REARM=DOTM*ELARM/A/EMU
ARP=PI*SQRT(PIT**2+DP**2)/PIT**2
F2E=DPSU*POR**2*PSC*A**2*RHO/Q/EL/DOTM**2
F2CARP=8.61*EMU*ARP**2*PSC*A/DOTM+0.52
F2C=8.61/REARM+0.52
WRITE(*,*) ' REARM = ',REARM,' ELARM = ',ELARM
C
C F3 IS THE SAME AS WIESE DUE TO KAYS/LONDON.
REDW=DP*USTAR/ENU
CD=10.0**((1.1/(POR**2)/REDW**2*(0.254))-(0.54/POR))
F3E=DPSU*(AF**3)*RHO*DP*RHOM/2.0/DOTM**2/WSU
F3C=CD*(DH/SCTHK)*(POR/BETA)**2
WRITE(*,*) ' F1E F2E F3E '
WRITE(*,106) F1E,F2E,F3E
WRITE(*,*) ' F1C F2C F3C '
WRITE(*,106) F1C,F2C,F3C
C
C OUTPUT THE RESULTS TO FILE.
REPS=PS*DOTM/AF/EMU
C
WRITE(53,107)
WRITE(53,105) HTCMS,ESLOPE,HTCDT,SEDT
WRITE(53,108)
WRITE(53,105) HTCRM,MESH,REPS,RF
WRITE(53,*) ' F1E F2E F3E '
WRITE(53,106) F1E,F2E,F3E

```

```

        WRITE(53,*)          F1C           F2C           F3C'
        WRITE(53,106) F1C,F2C,F3C
        WRITE(53,*) 'DELT= ',DELT,' NMAX= ',NMAX
        WRITE(53,*) ' POR = ',POR,' DH= ',DH
C
102   FORMAT(F15.8/F15.8)
103   FORMAT(F15.8)
104   FORMAT(F15.8,1X,F15.8)
105   FORMAT(4F15.8)
106   FORMAT(F15.8,1X,F15.8,1X,F15.8)
107   FORMAT(5X,'HTCMS',9X,'ESLOPE',10X,'HTCDT',10X,'SEDT')
108   FORMAT(5X,'HTCRM',11X,'MESH',11X,'REPS',12X,'RF')
        STOP
        END
C
C ****
C
C THIS SUBROUTINE FINDS THE VALUE OF HTC WHICH BEST FITS THE
C VALUE OF ESLOPE.
C
C DOUBLE PRECISION FUNCTION SZERMS(HTCMIN,HTCMAX,FUNSMS,TOL,
$ESLOPE)
        DOUBLE PRECISION HTCMIN,HTCMAX,FUNSMS,TOL,ESLOPE
C
C A ZERO OF THE FUNCTION F(X) IS COMPUTED IN THE INTERVAL AX,BX
C
C INPUT
C
C AX      LEFT ENDPOINT OF INITIAL INTERVAL
C BX      RIGHT ENDPOINT OF INITIAL INTERVAL
C F       FUNCTION SUBPROGRAM WHICH EVALUATES F(X) FOR ANY X IN
C          THE INTERVAL AX,BX
C TOL     DESIRED LENGTH OF THE INTERVAL OF UNCERTAINTY OF THE
C          FINAL RESULT
C
C
C OUTPUT
C
C ZEROIN ABCISSA APPROXIMATING A ZERO OF F IN THE INTERVAL AX,BX
C
C IT IS ASSUMED THAT F(AX) AND F(BX) HAVE OPPOSITES SIGNS
C WITHOUT A CHECK. ZEROIN RETURNS A ZERO X IN THE GIVEN INTERVAL
C AX,BX TO WITHIN A TOLERANCE 4*MACHEPS*ABS(X) + TOL, WHERE MACHEPS
C IS THE RELATIVE MACHINE PRECISION.
C THIS FUNCTION SUBPROGRAM IS A SLIGHTLY MODIFIED TRANSLATION OF
C THE ALGOL 60 PROCEDURE ZERO GIVEN IN R. BRENT, ALGORITHMS FOR
C MINIMIZATION WITHOUT DERIVATIVES, PRENTICE-HALL, INC.(1973)
C
C
C DOUBLE PRECISION A,B,C,D,E,EPS,FA,FB,FC,TOL1,XM,P,Q,R,S
C
C EXTERNAL FUNSMS
C
C COMPUTE EPS, THE RELATIVE MACHINE PRECISION
C
C
EPS =1.0
61  EPS=EPS/2.0
    TOL1 = 1.0 + EPS
    IF(TOL1.GT.1.0)GO TO 61
C
C INITIALIZATION
C
A=HTCMIN
B=HTCMAX
FA=FUNSMS (A,ESLOPE)
FB=FUNSMS (B,ESLOPE)

```

```

      WRITE(*,*) 'fa= ',FA,' fb= ',FB
C
      IF((FA/FB).GT.0.0) GO TO 71
C
C BEGIN STEP
C
62    C=A
      FC=FA
      D=B-A
      E=D
63    IF(ABS(FC).GE.ABS(FB))GO TO 64
      A=B
      B=C
      C=A
      FA=FB
      FB=FC
      FC=FA
C
C CONVERGENCE TEST
C
64    TOL1 = 2.0*EPS*ABS(B) + 0.5*TOL
      XM = 0.5*(C-B)
      IF(ABS(XM).LE.TOL1)GO TO 69
      IF(FB.EQ.0.0)GO TO 69
C
C IS BISECTION NECESSARY?
C
      IF(ABS(E).LT.TOL1)GO TO 67
      IF(ABS(FA).LE.ABS(FB))GO TO 67
C
C IS QUADRATIC INTERPOLATION POSSIBLE?
C
      IF(A.NE.C)GO TO 65
C
C LINEAR INTERPOLATION
C
      S=FB/FA
      P=2.0*XM*S
      Q=1.0-S
      GO TO 60
C
C INVERSE QUADRATIC INTERPOLATION
C
65    Q=FA/FC
      R=FB/FC
      S=FB/FA
      P=S*(2.0*XM*Q*(Q-R)-(B-A)*(R-1.0))
      Q = (Q - 1.0)*(R - 1.0)*(S - 1.0)
C
C ADJUST SIGNS
C
60    IF(P.GT.0.0)Q = -Q
      P = ABS(P)
C
C IS INTERPOLATION ACCEPTABLE?
C
      IF((2.0*P).GE.(3.0*XM*Q - ABS(TOL1*Q)))GO TO 67
      IF(P.GE.ABS(0.5*E*Q))GO TO 67
      E=D
      D=P/Q
      GO TO 68
C
C BISECTION
C
67    D=XM
      E=D

```

```

C
C COMPLETE STEP
C
68      A=B
FA=FB
IF (ABS(D).GT.TOL1) B = B + D
IF (ABS(D).LE.TOL1) B = B + SIGN(TOL1,XM)
FB = FUNSMS(B,ESLOPE)
WRITE(*,*) ' New Value of B ',B
IF ((FB*(FC/ABS(FC))).GT.0.0) GO TO 62
GO TO 63
C
C DONE
C
69      SZERMS = B
RETURN
71      WRITE(*,*) 'FUNSMS (BAX) /FUNSMS (BBX) .GT. 0.0'
STOP
END
C
C ****
C
C THIS FUNCTIOM SUBPROGRAM DETERMINES THE VALUE OF
C ESLOPE-CSLOPE FOR A GIVEN HTC.
C
C DOUBLE PRECISION FUNCTION FUNSMS (HTC,ESLOPE)
C THIS IS A FUNCTION SUBROUTINE WHICH DETERMINES THE VALUE
C OF THE DIFFERENCE BETWEEN THE EXPERIMENTAL AND CALCULATED
C MAXIMUM SLOPE OF THE TIME-TEMPERATURE CURVE TRANSIENT.
C IT IS USED TO GET THE BEST VALUE FOR HTC IN CONJUNCTION
C WITH THE FUNCTION SZERMS (HTCMIN,HTCMAX,FA/FB,TOL).
C msie.f IS THE CONTROLING PROGRAM UNIT. SEE PROGRAM tsie.f
C FOR OTHER DETAILS.
C
C TA, TB, TC, TD, TE, TF, TH, TI ARE CONSTANTS USED IN CALCULATIONS.
C CSLOPE IS THE CALCULATED MAXIMUM SLOPE.
C ESLOPE IS THE EXPERIMENTALLY MEASURED SLOPE.
C LOC IS THE LOCATION OF THE MAX SLOPE.
C
C
C      DOUBLE PRECISION TGC(155),TRC(155),TTC(155),TGP(155),TRP(155),
$TTP(155),TG0(20001),TGL(20001),TG2(20001)
      INTEGER I,N,NMAX,II,IF,LOC,I0,ITRAN,IINT,ICOUNT,J
      DOUBLE PRECISION RHO,TA,TB,TC,TD,CM,RHOM,A,CP,GAM,
$DELT,DELX,DH,AF,ENU,POR,D,PI,DP,PS,EKG,EKS,HNU,
$TE,TF,TH,TJ,TOI,TLI,CSLOPE,ESLOPE,SAMPT,
$SAS,C,HTC,DOTM,REPS,TEMP,THK,ACXT,AST
C
C      COMMON TG0,TGL,DOTM,AS,CP,DELX,SAMPT,RHO,AF,C,CM,GAM,DELT,THK,
$POR,RHOM,TOI,TLI,DP,ENU,EKG,DH,PS,II,IF,IINT,ITRAN,
$D,PI,A,ACXT,AST,EKS,NMAX,LOC
C
C      INTRINSIC COS,MAX,SQRT,ABS,NINT,ATAN
C      AT THE INITIAL TIME, THE REGENERATOR AND GAS ARE AT A
C      STEADY STATE INITIAL TEMPERATURE.
C
C      SET THE INITIAL CONDITION OF THE REGENERATOR AND GAS AT A
C      LINEAR DIFTRIBUTION BETWEEN TOI AND TLI.
      TRP(1)=TOI
      TGP(1)=TOI
      TTP(1)=TOI
C      THE MATRIX RUNS FROM N=2 TO NMAX-1.
      DO 26 N=2,NMAX-1
      TRP(N)=(TLI-TOI)/(NMAX-3)*(N-2)+TOI
      TGP(N)=TRP(N)
      TTP(N)=TRP(N)

```

```

26      CONTINUE
      TRP (NMAX)=TLI
      TGP (NMAX)=TLI
      TTP (NMAX)=TLI
C
C      AT SOME EARLY TIME, THE TEMPERATURE AT N=1 IS IMPULSIVELY
C      CHANGED TO A WARMER TEMPERATURE.
C
C      N=1
C      I=1
C
C      DETERMINE THE REYNOLDS AND NUSSELT NUMBER.
      REPS=PS*DOTM/AF/ENU/RHO
      HNU=HTC*DH/EKG
C      WRITE (*,*) AST, DOTM, REPS, HNU, ' AST, DOTM, REPS, HNU'
C      WRITE (*,*) DP, AF, ENU, RHO, HNU, EKG, ' DP, AF, ENU, RHO, HNU, EKG'
C
C      DEFINE SOME OTHER CONSTANTS NEEDED BELOW.
      TA=2.0*AS*HTC/DOTM/CP
      TB=2.0*RHO*AF*C/DOTM/GAM
      TC=HTC*AS/C/CM/RHOM/(A*(1-POR))
      TJ=2.0*HTC*AST/DOTM/CP
      TD=TB-TA-TJ
      TE=EKS/DELX/RHOM/CM/C
      TF=HTC*AST/RHOM/CM/ACXT/C
      TH=1.0-2.0*TE-TF
C      WRITE (*,*) TA, TB, TC, TD, TE, TF, TH, TJ, ' ta, tb, ...'
C
C      START THE INTERPOLATION COUNTER, ICOUNT, AND SET THE INITIAL
C      INTERPOLATION MARKER, I0.
      I0=II
      ICOUNT=1
      TG2 (I0)=TGP (NMAX)
C
C      DO 31 I=2, ITRAN
C
C      IF (ICOUNT.EQ.IINT) THEN
C          I0=I0+1
C          ICOUNT=0
C      ENDIF
C
C      INTERPOLATE THE VALUE OF THE INCOMING GAS BETWEEN EXPERIMENTALLY
C      MEASURED DATA POINTS.
      TEMP=((TG0(I0+1)-TG0(I0))/IINT)*ICOUNT+TG0(I0)
C
C      SET THE INLET TEMPERATURE OF THE GAS AT THE INLET TO THE MATRIX
C      EQUAL TO THE INTERPOLATED EXPERIMENTAL TG0.
      TGC (1)=TEMP
C
C      DETERMINE THE VALUE OF TG, TR, AND TT AT THE NEXT LOCATION.
      DO 32 N=2, NMAX-1
C
      TGC (N)=(TGP (N-1)-TGP (N+1)+TA*TRP (N)+TJ*TTP (N)+TD*TGP (N))/TB
      TRC (N)=TC*TGP (N)+TRP (N)*(1.0-TC)
      TTC (N)=TE*TTP (N+1)+TE*TTP (N-1)+TF*TGP (N)+TH*TTP (N)
32    CONTINUE
C
C      SET THE TEMPERATURE OF THE GAS/MATIX AS IT LEAVES.
      TGC (NMAX)=TGC (NMAX-1)
      TRC (NMAX)=TRC (NMAX-1)
      TTC (NMAX)=TTC (NMAX-1)
C
C      PUT AN ADIABATIC CONDITION AT THE FRONT OF THE TUBE AND MATRIX.
      TRC (1)=TRC (2)
      TTC (1)=TTC (2)
C

```

```

C      SET THE CURRENT TIME STEP TEMPERATURES TO THE PREVIOUS OPES.
C      DO 55 J=1,NMAX
C      TGP (J)=TGC (J)
C      TRP (J)=TRC (J)
C      TPP (J)=TTC (J)
55    CONTINUE
C
C      LET TG2 EQUAL THE CALCULATED TEMPERATURE AT THE SAME TIMES
C      AS THE EXPERIMENTAL TEMPERATURES AT THE EXIT.
C      IF (ICOUNT.EQ.0) THEN
C          TG2 (I0)=TGC (NMAX)
C      ENDIF
C
C      CHECK FOR INSTABILITY.
C      IF (ABS(TG2(I0)).GE.100.) THEN
C          WRITE (*,*) ' INSTABILITY OCCURRING'
C          STOP
C      ENDIF
C
C      ICOUNT=ICOUNT+1
C
31    CONTINUE
C
C      FIND THE VALUE OF THE SLOPE AT I=LOC.
C
C      WRITE (*,*) LOC
C      CSLOPE=(TG2(LOC-2)+8.0*TG2(LOC+1)-8.0*TG2(LOC-1)
C      $-TG2(LOC+2))/12.0/SAMPT
C      WRITE (*,*) CSLOPE,'CSLOPE*****'
C
C      FUNSMS=CSLOPE-ESLOPE
C      WRITE (*,*) 'FUNSMS = ',FUNSMS
C      RETURN
C      END
C
C      ****
C
C      THIS SUBROUTINE FINDS THE VALUE OF HTC WHICH BEST FITS THE
C      VALUE OF THE EXPERIMENTALLY MEASURED SEDT.
C
C      DOUBLE PRECISION FUNCTION SZERDT(HTCMIN,HTCMAX,FUNSDT,TOL,I2,
$TAU2)
C      DOUBLE PRECISION HTCMIN,HTCMAX,FUNSDT,TOL,TAU2
C      INTEGER I2
C
C      A ZERO OF THE FUNCTION F(X) IS COMPUTED IN THE INTERVAL AX,BX
C
C      INPUT
C
C      AX      LEFT ENDPOINT OF INITIAL INTERVAL
C      BX      RIGHT ENDPOINT OF INITIAL INTERVAL
C      F       FUNCTION SUBPROGRAM WHICH EVALUATES F(X) FOR ANY X IN
C              THE INTERVAL AX,BX
C      TOL     DESIRED LENGTH OF THE INTERVAL OF UNCERTAINTY OF THE
C              FINAL RESULT
C
C
C      OUTPUT
C
C      ZEROIN ABCISSA APPROXIMATING A ZERO OF F IN THE INTERVAL AX,BX
C
C      IT IS ASSUMED THAT F(AX) AND F(BX) HAVE OPPOSITES SIGNS
C      WITHOUT A CHECK.  ZEROIN RETURNS A ZERO X IN THE GIVEN INTERVAL
C      AX,BX TO WITHIN A TOLERANCE 4*MACHEPS*ABS(X) + TOL, WHERE MACHEPS
C      IS THE RELATIVE MACHINE PRECISION.
C      THIS FUNCTION SUBPROGRAM IS A SLIGHTLY MODIFIED TRANSLATION OF

```

```

C THE ALGOL 60 PROCEDURE ZERO GIVEN IN R. BRENT, ALGORITHMS FOR
C MINIMIZATION WITHOUT DERIVATIVES, PRENTICE-HALL, INC.(1973)
C
C DOUBLE PRECISION A,B,C,D,E,EPS,FA,FB,FC,TOL1,XM,P,Q,R,S
C
C EXTERNAL FUNSDT
C
C COMPUTE EPS, THE RELATIVE MACHINE PRECISION
C
C EPS =1.0
61 EPS=EPS/2.0
TOL1 = 1.0 + EPS
IF(TOL1.GT.1.0)GO TO 61
C
C INITIALIZATION
C
A=HTCMIN
B=HTCMAX
FA=FUNSDT(I2,A,TAU2)
FB=FUNSDT(I2,B,TAU2)
WRITE(*,*) ' fa= ',FA,' fb= ',FB
C
IF((FA/FB).GT.0.0) GO TO 71
C
C BEGIN STEP
C
62 C=A
FC=FA
D=B-A
E=D
63 IF(ABS(FC).GE.ABS(FB))GO TO 64
A=B
B=C
C=A
FA=FB
FB=FC
FC=FA
C
C CONVERGENCE TEST
C
64 TOL1 = 2.0*EPS*ABS(B) + 0.5*TOL
XM = 0.5*(C-B)
IF(ABS(XM).LE.TOL1)GO TO 69
IF(FB.EQ.0.0)GO TO 69
C
C IS BISECTION NECESSARY?
C
IF(ABS(E).LT.TOL1)GO TO 67
IF(ABS(FA).LE.ABS(FB))GO TO 67
C
C IS QUADRATIC INTERPOLATION POSSIBLE?
C
IF(A.NE.C)GO TO 65
C
C LINEAR INTERPOLATION
C
S=FB/FA
P=2.0*XM*S
Q=1.0-S
GO TO 60
C
C INVERSE QUADRATIC INTERPOLATION
C
65 Q=FA/FC
R=FB/FC

```

```

S=FB/FA
P=S* (2.0*XM*Q* (Q-R)-(B-A)*(R-1.0))
Q = (Q - 1.0)*(R - 1.0)*(S - 1.0)
C
C ADJUST SIGNS
C
60      IF (P.GT.0.0) Q = -Q
        P = ABS(P)
C
C IS INTERPOLATION ACCEPTABLE?
C
        IF ((2.0*P).GE.(3.0*XM*Q - ABS(TOL1*Q))) GO TO 67
        IF (P.GE.ABS(0.5*E*Q)) GO TO 67
        E=D
        D=P/Q
        GO TO 68
C
C BISECTION
C
67      D=XM
        E=D
C
C COMPLETE STEP
C
68      A=B
        FA=FB
        IF (ABS(D).GT.TOL1) B = B + D
        IF (ABS(D).LE.TOL1) B = B + SIGN(TOL1,XM)
        FB = FUNSDT(I2,B,TAU2)
        WRITE(*,*) ' The New Value of fb is ',B
        IF ((FB*(FC/ABS(FC))).GT.0.0) GO TO 62
        GO TO 63
C
C DONE
C
69      SZERDT = B
        RETURN
71      WRITE(*,*) 'FUNSDT(BAX)/FUNSDT(BBX).GT.0.0'
        STOP
        END
C
C*****DOUBLE PRECISION FUNCTION FUNSDT(I2,HTC,TAU2)
C THIS IS A FUNCTION SUBROUTINE WHICH DETERMINES THE VALUE
C OF THE DIFFERENCE BETWEEN THE EXPERIMENTAL AND CALCULATED
C SPONGE EFFECT DELAY TIME, SEDT, OF THE TIME-TEMPERATURE
C CURVE TRANSIENT.
C IT IS USED TO GET THE BEST VALUE FOR HTC IN CONJUNCTION
C WITH THE FUNCTION SZERDT(HTCMIN,HTCMAX,FA/FB,TOL).
C msie3c.f IS THE CONTROLLING PROGRAM UNIT. SEE PROGRAM tsie.f
C FOR OTHER DETAILS.
C
C TA,TB,TC,TD,TE,TF,TH,TI ARE CONSTANTS USED IN CALCULATIONS.
C CSEDT IS THE CALCULATED SEDT.
C SEDT IS THE EXPERIMENTALLY MEASURED SEDT.
C TAU2 IS THE TIME AT THE END OF THE SEDT.
C I2 IS THE INDEX FOR TAU2; I2C IS THE CALCULATED I2.
C
C
C DOUBLE PRECISION TGC(155),TRC(155),TTC(155),TGP(155),TRP(155),
$TTTP(155),TG0(20001),TGL(20001),TG2(20001)
        INTEGER I,N,NMAX,II,IF,I2,I0,ITRAN,IINT,ICOUNT,LOC,I2C,J,K
        DOUBLE PRECISION RHO,TA,TB,TC,TD,CM,RHOM,A,CP,GAM,
        SDELT,DELX,DH,AF,ENU,POR,D,PI,DP,PS,EKG,EKS,
        STE,TF,TH,TJ,TOI,TLI,SAMPT,TG2AV,

```

```

SAS,C,HTC,DOTM,REPS,TEMP,THK,ACXT,AST,SEDT,CSEDT,TAU2
C
COMMON TG0,TGL,DOTM,AS,CP,DELX,SAMPT,RHO,AF,C,CM,GAM,DELT,THK,
$POR,RHOM,TOI,TLI,DP,ENU,EKG,DH,PS,II,IF,IINT,ITRAN,
$D,PI,A,ACXT,AST,EKS,NMAX,LOC
C
INTRINSIC COS,MAX,SQRT,ABS,NINT,ATAN
C
AT THE INITIAL TIME, THE REGENERATOR AND GAS ARE AT A
C
STEADY STATE INITIAL TEMPERATURE.
C
SET THE INITIAL CONDITION OF THE REGENERATOR AND GAS AT A
C
LINEAR DIFTRIBUTION BETWEEN TOI AND TLI.
TRP(1)=TOI
TGP(1)=TOI
TTP(1)=TOI
C
THE MATRIX RUNS FROM N=2 TO NMAX-1.
DO 26 N=2,NMAX-1
TRP(N)=(TLI-TOI)/(NMAX-3)*(N-2)+TOI
TGP(N)=TRP(N)
TTP(N)=TRP(N)
26
CONTINUE
TRP(NMAX)=TLI
TGP(NMAX)=TLI
TTP(NMAX)=TLI
C
AT SOME EARLY TIME, THE TEMPERATURE AT N=1 IS IMPULSIVELY
C
CHANGED TO A WARMER TEMPERATURE.
C
N=1
I=1
C
DETERMINE THE REYNOLDS AND NUSSELT NUMBER.
REPS=PS*DOTM/AF/ENU/RHO
HNU=HTC*DHS/EKG
C
WRITE(*,*) AST, DOTM, REPS, HNU, ' AST, DOTM, REPS, HNU'
C
WRITE(*,*) DP, AF, ENU, RHO, HNU, EKG, ' DP, AF, ENU, RHO, HNU, EKG'
C
DEFINE SOME OTHER CONSTANTS NEEDED BELOW.
TA=2.0*AS*HTC/DOTM/CP
TB=2.0*RHO*AF*C/DOTM/GAM
TC=HTC*AS/C/CM/RHOM/(A*(1-POR))
TJ=2.0*HTC*AST/DOTM/CP
TD=TB-TA-TJ
TE=EKS/DELX/RHOM/CM/C
TF=HTC*AST/RHOM/CM/ACXT/C
TH=1.0-2.0*TE-TF
C
WRITE(*,*) TA, TB, TC, TD, TE, TF, TH, TJ, 'ta,tb,..'
C
START THE INTERPOLATION COUNTER, ICOUNT, AND SET THE INITIAL
C
INTERPOLATION MARKER, IO.
IO=II
ICOUNT=1
TG2(IO)=TGP(NMAX)
C
DO 31 I=2,ITRAN
C
IF(ICOUNT.EQ.IINT) THEN
    IO=IO+1
    ICOUNT=0
ENDIF
C
INTERPOLATE THE VALUE OF THE INCOMING GAS BETWEEN EXPERIMENTALLY
C
MEASURED DATA POINTS.
TEMP=((TG0(IO+1)-TG0(IO))/IINT)*ICOUNT+TG0(IO)
C
SET THE INLET TEMPERATURE OF THE GAS AT THE INLET TO THE MATRIX

```

```

C EQUAL TO THE INTERPOLATED EXPERIMENTAL TG0.
TGC(1)=TEMP

C DETERMINE THE VALUE OF TG, TR, AND TT AT THE NEXT LOCATION.
DO 32 N=2,NMAX-1

C
TGC(N) = (TD*TGP(N)+TGP(N-1)-TGP(N+1)+TA*TRP(N)+TJ*TPP(N)) / TB
TRC(N)=TC*TGP(N)+TRP(N)*(1.0-TC)
TTC(N)=TE*TPP(N+1)+TE*TPP(N-1)+TF*TGP(N)+TH*TPP(N)

32 CONTINUE

C SET THE TEMPERATURE OF THE GAS/MATRIX AS IT LEAVES.
TGC(NMAX)=TGC(NMAX-1)
TRC(NMAX)=TGC(NMAX-1)
TTC(NMAX)=TTC(NMAX-1)

C PUT AN ADIABATIC CONDITION AT THE FRONT OF THE TUBE AND MATRIX.
TRC(1)=TRC(2)
TTC(1)=TTC(2)

C SET THE CURRENT TIME STEP TEMPERATURES TO THE PREVIOUS OPES.
DO 55 J=1,NMAX
TGP(J)=TGC(J)
TRP(J)=TRC(J)
TPP(J)=TTC(J)

55 CONTINUE

C LET TG2 EQUAL THE CALCULATED TEMPERATURE AT THE SAME TIMES
C AS THE EXPERIMENTAL TEMPERATURES AT THE EXIT.
IF (ICOUNT.EQ.0) THEN
    TG2(I0)=TGC(NMAX)
ENDIF

C CHECK FOR INSTABILITY.
IF (ABS(TG2(I0)).GE.100.) THEN
    WRITE(*,*) 'INSTABILITY OCCURRING'
    STOP
ENDIF

C ICOUNT=ICOUNT+1

31 CONTINUE

C FIND THE VALUE OF THE CSEDT.
DO 85 J=II,IF
TG2AV=0.0
    DO 87 K=II,J
    TG2AV=TG2AV+TG2(K)

87 CONTINUE
TG2AV=TG2AV/(J-II+1)
IF ((TG2(J+50)-TG2AV).GT.0.4) THEN
CSEDT=(J-II)*SAMPT
I2C=J
GO TO 86
ENDIF

85 CONTINUE
86 CONTINUE

C DETERMINE THE VALUE OF SEDT.
SEDT=(I2-II)*SAMPT

C
FUNSDT=I2C-I2
WRITE(*,*) 'FUNSDT = ',FUNSDT
WRITE(*,*) 'CSEDT = ',CSEDT,' SEDT= ',SEDT
RETURN
END

```

```

C
C ****
C
C THIS SUBROUTINE FINDS THE VALUE OF HTC WHICH MINIMIZES THE
C ROOT MEAN SQUARE DIFFERENCE BETWEEN THE CALCULATED AND
C EXPERIMENTAL VALUES OF THE OUTLET TEMPERATURE AFTER SEDT.
C
C DOUBLE PRECISION FUNCTION SZERRM(HTCMIN,HTCMAX,FUNSRM,TOL,I2)
C DOUBLE PRECISION HTCMIN,HTCMAX,FUNSRM,TOL
C INTEGER I2
C
C A ZERO OF THE FUNCTION F(X) IS COMPUTED IN THE INTERVAL AX,BX
C
C INPUT
C
C AX LEFT ENDPOINT OF INITIAL INTERVAL
C BX RIGHT ENDPOINT OF INITIAL INTERVAL
C F FUNCTION SUBPROGRAM WHICH EVALUATES F(X) FOR ANY X IN
C THE INTERVAL AX,BX
C TOL DESIRED LENGTH OF THE INTERVAL OF UNCERTAINTY OF THE
C FINAL RESULT
C
C OUTPUT
C
C ZEROIN ABCISSA APPROXIMATING A ZERO OF F IN THE INTERVAL AX,BX
C
C IT IS ASSUMED THAT F(AX) AND F(BX) HAVE OPPOSITES SIGNS
C WITHOUT A CHECK. ZEROIN RETURNS A ZERO X IN THE GIVEN INTERVAL
C AX,BX TO WITHIN A TOLERANCE 4*MACHEPS*ABS(X) + TOL, WHERE MACHEPS
C IS THE RELATIVE MACHINE PRECISION.
C THIS FUNCTION SUBPROGRAM IS A SLIGHTLY MODIFIED TRANSLATION OF
C THE ALGOL 60 PROCEDURE ZERO GIVEN IN R. BRENT, ALGORITHMS FOR
C MINIMIZATION WITHOUT DERIVATIVES, PRENTICE-HALL, INC.(1973)
C
C DOUBLE PRECISION A,B,C,D,E,EPS,FA,FB,FC,TOL1,XM,P,Q,R,S
C
C EXTERNAL FUNSRM
C
C COMPUTE EPS, THE RELATIVE MACHINE PRECISION
C
C EPS =1.0
61 EPS=EPS/2.0
      TOL1 = 1.0 + EPS
      IF(TOL1.GT.1.0)GO TO 61
C
C INITIALIZATION
C
      A=HTCMIN
      B=HTCMAX
      FA=FUNSRM(I2,A)
      FB=FUNSRM(I2,B)
      WRITE(*,*) ' fa= ',FA,' fb= ',FB
C
      IF((FA/FB).GT.0.0) GO TO 71
C
C BEGIN STEP
C
62 C=A
      FC=FA
      D=B-A
      E=D
      IF(ABS(FC).GE.ABS(FB))GO TO 64
      A=B
      B=C

```

```

C=A
FA=FB
FB=FC
FC=FA
C
C CONVERGENCE TEST
C
64      TOL1 = 2.0*EPS*ABS(B) + 0.5*TOL
        XM = 0.5*(C-B)
        IF(ABS(XM).LE.TOL1)GO TO 69
        IF(FB.EQ.0.0)GO TO 69
C
C IS BISECTION NECESSARY?
C
        IF(ABS(E).LT.TOL1)GO TO 67
        IF(ABS(FA).LE.ABS(FB))GO TO 67
C
C IS QUADRATIC INTERPOLATION POSSIBLE?
C
        IF(A.NE.C)GO TO 65
C
C LINEAR INTERPOLATION
C
        S=FB/FA
        P=2.0*XM*S
        Q=1.0-S
        GO TO 60
C
C INVERSE QUADRATIC INTERPOLATION
C
65      Q=FA/FC
        R=FB/FC
        S=FB/FA
        P=S*(2.0*XM*Q*(Q-R)-(B-A)*(R-1.0))
        Q = (Q - 1.0)*(R - 1.0)*(S - 1.0)
C
C ADJUST SIGNS
C
60      IF(P.GT.0.0)Q = -Q
        P = ABS(P)
C
C IS INTERPOLATION ACCEPTABLE?
C
        IF((2.0*P).GE.(3.0*XM*Q - ABS(TOL1*Q)))GO TO 67
        IF(P.GE.ABS(0.5*E*Q))GO TO 67
        E=D
        D=P/Q
        GO TO 68
C
C BISECTION
C
67      D=XM
        E=D
C
C COMPLETE STEP
C
68      A=B
        FA=FB
        IF(ABS(D).GT.TOL1) B = B + D
        IF(ABS(D).LE.TOL1) B = B + SIGN(TOL1,XM)
        FB = FUNSRM(I2,B)
        WRITE(*,*) ' The New Value of B is ',B
        IF((FB*(FC/ABS(FC))).GT.0.0)GO TO 62
        GO TO 63
C
C DONE

```

```

C
C 69      SZERRM = B
C 71      RETURN
C         WRITE(*,*) 'FUNSRM(BAX) /FUNSRM(BBX) .GT. 0.0'
C         STOP
C         END
C
C ****
C
C      DOUBLE PRECISION FUNCTION FUNSRM(I2,HTC)
C      THIS IS A FUNCTION SUBROUTINE WHICH DETERMINES THE VALUE
C      OF THE ROOT MEAN SQUARE DIFFERENCE BETWEEN THE EXPERIMENTAL
C      AND CALCULATED VALUES OF THE OUTLET TEMPERATURE
C      OF THE TIME-TEMPERATURE CURVE TRANSIENT.
C      IT IS USED TO GET THE BEST VALUE FOR HTC IN CONJUNCTION
C      WITH THE FUNCTION SZERRM(HTCMIN,HTCMAX,FA/FB,TOL).
C      msie3c.f IS THE CONTROLLING PROGRAM UNIT. SEE PROGRAM tsie.f
C      FOR OTHER DETAILS.
C
C      TA,TB,TC,TD,TE,TF,TH,TI ARE CONSTANTS USED IN CALCULATIONS.
C      I2 IS THE INDEX OF THE TIME AT THE END OF THE SEDT.
C      RMSD/1/2 ARE ROOT MEAN SQUARED DIFFERENCES.
C
C      DOUBLE PRECISION TGC(155),TRC(155),TTC(155),TGP(155),TRP(155),
C      $TTP(155),TG0(20001),TGL(20001),TG2(20001)
C      INTEGER I,N,NMAX,II,IF,I2,I0,ITRAN,IINT,ICOUNT,LOHI,LOC
C      DOUBLE PRECISION RHO,TA,TB,TC,TD,CM,RHOM,A,CP,GAM,
C      $DELT,DELX,DH,AF,ENU,POR,D,PI,DP,PS,EKG,EKS,
C      $TE,TF,TH,TJ,TOI,TLI,SAMPT,
C      $AS,C,HTC,DOTM,REPS,TEMP,THK,ACXT,AST,RMSD,RMSD1,RMSD2,DT
C
C      COMMON TG0,TGL,DOTM,AS,CP,DELX,SAMPT,RHO,AF,C,CM,GAM,DELT,THK,
C      $POR,RHOM,TOI,TLI,DP,ENU,EKG,DH,PS,II,IF,IINT,ITRAN,
C      $D,PI,A,ACXT,AST,EKS,NMAX,LOC
C
C      INTRINSIC COS,MAX,SQRT,ABS,NINT,ATAN
C
C      FIND THE SLOPES OF THE RMSD VERSUS HTC CURVE AT HTC AND
C      HTC + 10.0.
C
C      LOHI=1
82      N=1
      I=1
C      AT THE INITIAL TIME, THE REGENERATOR AND GAS ARE AT A
C      STEADY STATE INITIAL TEMPERATURE.
C
C      SET THE INITIAL CONDITION OF THE REGENERATOR AND GAS AT A
C      LINEAR DIFTRIBUTION BETWEEN TOI AND TLI.
      TRP(1)=TOI
      TGP(1)=TOI
      TTP(1)=TOI
C      THE MATRIX RUNS FROM N=2 TO NMAX-1.
      DO 26 N=2,NMAX-1
      TRP(N)=(TLI-TOI)/(NMAX-3)*(N-2)+TOI
      TGP(N)=TRP(N)
      TTP(N)=TRP(N)
26      CONTINUE
      TRP(NMAX)=TLI
      TGP(NMAX)=TLI
      TTP(NMAX)=TLI
C
C      AT SOME EARLY TIME, THE TEMPERATURE AT N=1 IS IMPULSIVELY
C      CHANGED TO A WARMER TEMPERATURE.
C
C      DETERMINE THE REYNOLDS AND NUSSELT NUMBER.

```

```

REPS=PS*DOTM/AF /ENU/RHO
HNU=HTC*DH/EKG
C   WRITE(*,*) AST, DOTM, REPS, HNU, ' AST, DOTM, REPS, HNU'
C   WRITE(*,*) DP, AF, ENU, RHO, HNU, EKG, ' DP, AF, ENU, RHO, HNU, EKG'
C
C   DEFINE SOME OTHER CONSTANTS NEEDED BELOW.
TA=2.0*AS*HTC/DOTM/CP
TB=2.0*RHO*AF*C/DOTM/GAM
TC=HTC*AS/C/CM/RHOM/(A*(1-POR))
TJ=2.0*HTC*AST/DOTM/CP
TD=TB-TA-TJ
TE=EKS/DELX/RHOM/CM/C
TF=HTC*AST/RHOM/CM/ACXT/C
TH=1.0-2.0*TE-TF
C   WRITE(*,*) TA, TB, TC, TD, TE, TF, TH, TJ, 'ta,tb,..'
C
C   START THE INTERPOLATION COUNTER, ICOUNT, AND SET THE INITIAL
C   INTERPOLATION MARKER, I0.
I0=II
ICOUNT=1
TG2(I0)=TGP(NMAX)
C
DO 31 I=2, ITRAN
C
IF(ICOUNT.EQ.IINT) THEN
  I0=I0+1
  ICOUNT=0
ENDIF
C
C   INTERPOLATE THE VALUE OF THE INCOMING GAS BETWEEN EXPERIMENTALLY
C   MEASURED DATA POINTS.
TEMP=((TG0(I0+1)-TG0(I0))/IINT)*ICOUNT+TG0(I0)
C
C   SET THE INLET TEMPERATURE OF THE GAS AT THE INLET TO THE MATRIX
C   EQUAL TO THE INTERPOLATED EXPERIMENTAL TG0.
TGC(1)=TEMP
C
C   DETERMINE THE VALUE OF TG, TR, AND TT AT THE NEXT LOCATION.
DO 32 N=2,NMAX-1
C
TGC(N)=(TD*TGP(N)+TGP(N-1)-TGP(N+1)+TA*TRP(N)+TJ*TTP(N))/TB
TRC(N)=TC*TGP(N)+TRP(N)*(1.0-TC)
TTC(N)=TE*TTP(N+1)+TE*TTP(N-1)+TF*TGP(N)+TH*TTP(N)
32 CONTINUE
C
C   SET THE TEMPERATURE OF THE GAS/MATRIX AS IT LEAVES.
TGC(NMAX)=TGC(NMAX-1)
TRC(NMAX)=TGC(NMAX-1)
TTC(NMAX)=TTC(NMAX-1)
C
C   PUT AN ADIABATIC CONDITION AT THE FRONT OF THE TUBE AND MATRIX.
TRC(1)=TRC(2)
TTC(1)=TTC(2)
C
C   SET THE CURRENT TIME STEP TEMPERATURES TO THE PREVIOUS OPES.
DO 55 J=1,NMAX
TGP(J)=TGC(J)
TRP(J)=TRC(J)
TTP(J)=TTC(J)
55 CONTINUE
C
C   LET TG2 EQUAL THE CALCULATED TEMPERATURE AT THE SAME TIMES
C   AS THE EXPERIMENTAL TEMPERATURES AT THE EXIT.
IF(ICOUNT.EQ.0) THEN
  TG2(I0)=TGC(NMAX)
ENDIF

```

```
C  
C      CHECK FOR INSTABILITY.  
C      IF (ABS(TG2(I0)).GE.100.) THEN  
C          WRITE(*,*) ' INSTABILITY OCCURRING'  
C          STOP  
C      ENDIF  
C  
C      ICOUNT=ICOUNT+1  
C  
31    CONTINUE  
C  
C      DETERMINE THE ROOT MEAN SQUARED DIFFERENCE.  
C      DT = 0.0  
C      DO 81 J=I2, (LOC+50)  
C          DT=(TGL(J)-TG2(J))**2+DT  
81    CONTINUE  
C          RMSD=SQRT(DT/(IF-I2+1))  
C  
C      RECORD THE VALUE OF RMSD AND RUN FOR ANOTHER HTC.  
C      IF (LOHI.EQ.1) THEN  
C          RMSD1=RMSD  
C          LOHI=2  
C          HTC=HTC+10.  
C          GO TO 82  
C      ELSE  
C          RMSD2=RMSD  
C      ENDIF  
C  
C      DEFINE FUNSRM AS THE LOCAL SIMPLE DIFFERENCE DERIVATIVE.  
C  
C      FUNSRM = (RMSD2-RMSD1)/10.  
C  
C      WRITE(*,*) 'FUNSRM = ',FUNSRM,' RMSD1,RMSD2 ARE ',RMSD1,RMSD2  
C      RETURN  
C      END
```

Appendix D: Calibrations

This section describes the calibration of the three most important experimental measurements: 1) temperatures, 2) pressure drops, and 3) mass flow rate.

Temperature Calibration

The thermistors at the inlet and outlet were calibrated in-situ with a small iron-constantan thermocouple. The thermocouple was mounted midway in a three inch empty tube which was being supported at each end with the instrumentation connectors. The cooler or heater was turned on, and the system was allowed to come to equilibrium at seven different temperatures in the range 5-35°C. A Labview calibration VI (My_Termistor_Calibration.VI) was designed to read the value of the thermocouple temperature and the voltage across the thermistor bridge, and save this data to a file. Some hysteresis was noted in going from cold-to-hot and then hot-to-cold, so a one directional calibration was performed. It was done going from cold temperatures to hot temperatures, since the actual tests all had a transient from cold-to-hot.

The collection of voltages and related temperatures were saved to a data file and a least-square curve fit was done. The calibration data were inserted into an equation (Doebelin, 1983: 609-613) which has been shown to describe accurately the

behavior of thermistors over temperature ranges less than 50°C:

$$\frac{1.0}{T} = A_1 (\ln R_T)^3 + A_2 (\ln R_T)^2 + A_3 (\ln R_T) + A_4 \quad (30)$$

where R_T is the resistance of the thermistor (Ohms)
 A_i are constants determined by the calibration
 $A_1 = 2.59 \times 10^{-5}$
 $A_2 = -1.94 \times 10^{-4}$
 $A_3 = 7.74 \times 10^{-4}$
 $A_4 = 2.24 \times 10^{-3}$
and T is the temperature (°C)

This equation was used in conjunction with the equation describing the voltage drop for one leg of a Wheatstone bridge. A curve fit was made over the range 5°C to 35°C for each of the two thermistors. The resulting curve matched the data to $\pm 0.2^\circ\text{C}$.

Pressure Drop

The three Validyne differential pressure transducers were calibrated with a dead weight tester. A known pressure was imposed across the diaphragm of each transducer and the resulting voltage output was recorded. The calibration showed a linear relation between voltage output and pressure. The voltage range for each transducer was 0 - 10 VDC. A least-squares curve fit was performed for each transducer and the coefficients were incorporated into the Labview VI which

monitors the tests. These linear curve fit equations matched the transducer calibration data to less a standard deviation of than 1% of full range for all three cases.

Mass Flow Rate

The mass flow rate was determined by a relationship which includes the measured pressure drop across the venturi tube constriction, ΔP_{VEN} , the density of the gas, and some parameters of the geometry of the venturi tube (Benedict, 1984: Chapter 21). The accuracy of the relation for mass flow rate was checked with an independent experiment. A stagnation chamber with a nozzle outlet was connected in-line with the venturi tube. The gas flow in the stagnation chamber was idealized as having zero velocity, and gasdynamic relations for nozzle flow from stagnation to atmospheric were used to determine the mass flow rate out of the cell at equilibrium. A Labview VI was devised to compare the venturi tube results to those from the pressure cell. If a nozzle efficiency of 0.95 is used for the stagnation chamber outlet, the venturi tube arrangement measured the flow rate to within $\pm 7.0\%$ at the lowest flow rates, and to within $\pm 4.0\%$ at the highest Reynolds number.

Appendix E: Test Data

In this appendix, the final values of the Reynolds number, Nusselt number, friction factor, compactness factor, reduction factor, and effectiveness for the twenty eight test runs are included.

Re	Nu	f	CF	RF	SPEFF
7.6543	0.8010	1.6281	0.0830	1.0000	0.9460
14.6904	1.1218	1.1638	0.0847	1.0000	0.8820
8.2452	0.6672	1.4964	0.0698	0.8465	0.8730
15.8082	0.7285	1.1426	0.0521	0.8465	0.8820
8.9725	0.9508	1.6349	0.0837	0.7456	0.8990
9.1630	1.0130	1.6179	0.0882	0.7456	0.9060
16.6818	1.3136	1.1780	0.0863	0.7456	0.9480
15.1212	1.0475	2.5664	0.0348	0.5526	0.8190
27.8053	0.9822	2.0428	0.0223	0.5526	0.6980
39.1208	2.4477	0.7860	0.1027	1.0000	0.8340
75.0169	3.3876	0.6623	0.0880	1.0000	0.8550
40.4648	2.2300	0.8273	0.0860	0.8574	0.7940
74.0514	2.5543	0.7299	0.0610	0.8574	0.7730
45.3124	2.0922	0.8700	0.0685	0.7013	0.7490
47.8531	2.3574	0.8449	0.0753	0.7013	0.7640
91.5990	3.0476	0.7507	0.0572	0.7013	0.7790
75.5909	3.2338	2.0015	0.0276	0.5000	0.7150
86.2827	3.4506	1.9613	0.0263	0.5000	0.7120
15.6136	1.1117	0.8838	0.1040	1.0000	0.8790
15.0196	1.2263	0.9003	0.1170	1.0000	0.8980
37.8461	2.8948	0.6658	0.1483	1.0000	0.9010
16.8837	1.0339	0.9857	0.0802	0.8302	0.8450
40.9000	1.7855	0.7321	0.0770	0.8302	0.9280
17.8880	1.2749	1.1168	0.0824	0.7207	0.8620
43.7263	1.7756	0.8548	0.0613	0.7207	0.7770
30.4596	2.0455	1.8725	0.0463	0.5328	0.8280
30.8783	2.0618	1.8439	0.0467	0.5328	0.8370
48.8819	2.9644	1.6604	0.0471	0.5328	0.8860

Bibliography

Anderson, D.A. et al. Computational Fluid Mechanics and Heat Transfer. Taylor & Francis Publishers, 1984.

Armour, J.C. and Cannon, J.N. "Fluid Flow through Woven Screens," AICHE Journal, 14 n.3: 415-420 (May, 1968).

ASME. Fluid Meters, Their Theory and Application (6th Edition). New York: ASME Press, 1971.

Atrey, M.D., et al. "Microcomputer Aided Cyclic Analysis of the Stirling Cryocooler with Different Regenerator Meshes," Cryogenics, 30: 236-240 (September Supplement, 1990).

Barnes, C. and Reader, G.T. "An Investigation into the Effect of Various Regenerators on the Performance of a Stirling Engine," Proceedings of the 21st IECEC, 1: 512-518 (1986).

Brent, R.P. Algorithms for Minimization without Derivatives. Englewood Cliffs, New Jersey: Prentice-Hall, 1973.

Chan, C.K. et al, "Overview of Cryocooler Technologies for Spaced-Based Electronics and Sensors," Adv. in Cryogenic Engr., 35: 1239-1250 (1990).

Daney, D.E. and Radebaugh, R. "Non-Ideal Regenerator Performance - the Effect of Void Volume Fluid Heat Capacity," Cryogenics, 24: 499-501 (1984).

Dekker, T.J. "Finding a Zero by Means of Successive Linear Interpolation," Constructive Aspects of the Fundamental Theorem of Algebra. New York: Wiley Interscience, 1969.

Doebelin, E.O. Measurement Systems (Third Edition). New York: McGraw-Hill Book Co., 1983.

Forsythe, G.E., et al. Computer Methods for Mathematical Computations. Englewood Cliffs, N.J.: Prentice-Hall, 1977.

Koester G. et al. "Oscillatory Flow Test Results in Stirling Engines Heat Exchangers: Final Report," NTIS HC/MF A13 182288CR (May 1990).

Hamaguchi, K. et al. "Effects of Regenerator Size Change on Stirling Engine Performance," Proceedings of the 26th IECEC, 5: 293-298 (1991).

Haselden, G.G. Cryogenic Fundamentals. London: Academic Press, 1971.

Holman, J.P. Heat Transfer (Second Edition). New York: McGraw-Hill, 1968.

Huang, F.E. Engineering Thermodynamics. New York: Macmillan Publishing Co., Inc., 1976.

Hutchinson, R.A. and Ross, B.A. "Fundamental Flow and Heat Transfer Results Relevant to Oscillating Flow Regenerators," Proceedings of the 22nd IECEC, 4: 1859 (1987).

Incropera, F.P. and Dewitt, D.P. Introduction To Heat Transfer. New York: John Wiley and Sons, 1985.

Jones, J.D. "Performance of a Stirling Engine Regenerator Having Finite Mass," Journal of Engineering for Gas Turbines and Power, 108: 669-673 (Oct 1986).

Kays, W.M. and London, A.L. Compact Heat Exchangers (3rd Ed). New York: McGraw-Hill (1984). (TJ263.K35)

Krazinski, J.L. et al. "An Analysis of Pressure Drops Under Reversing Flow Conditions," Proceedings of the 21st IECEC, 1: 519 (1986).

Kreith, F. Principles of Heat Transfer (Third Edition). New York: IEP-A Dun-Donnelly Publisher, 1973.

LABVIEW for Windows, Data Acquisition VI Reference Manual, National Instruments Corp Part No. 320536-01, Dec 1993.

Ledford, O.C. "An Overview of Spacecraft Cryocooler Development in the USA," Proceedings of the 24th International Conference on Environmental Systems and 5th European Symposium on Space Environmental Control Systems. Friedrichschafen Germany (Jun 1994). SAE Paper #941619

Liang, C.Y. and Yang, W. "Modified Single-Blow Technique for Performance Evaluation of Heat Transfer Surfaces," Transactions of the ASME - Journal of Heat Transfer: 16-21 (February 1975).

Locke, G.L. "Heat Transfer and Flow Friction Characteristics of Porous Solids," Test Report No. 10. Department of Mechanical Engineering, Stanford University, Stanford CA (1 Jun 1950).

Martini, W.R. Stirling Engine Design Manual. NASA CR-135382 (1980).

MATLAB, High Performance Numeric Computation and Visualization Software. The MATH WORKS Inc., v4.1 1993.
(Including Signal Processing TOOLBOX) (QA188.M39)

Miyabe, H. et al. "An Approach to the Design of Stirling Engine Regenerator Matrix Using Packs of Wire Gauze," Proceedings of the 17th IECEC, 4: 1839-1844, 1982.

Nagawa, M. et al. "Development of NS30A Engine," Proceedings of the 22nd IECEC, 4: 1797-1801 (1987).

Organ, A.J. "An Enquiry into the Mechanism of Pressure Drop in the Regenerator of the Stirling Cycle Machine," Proceedings of the 19th IECEC, 3: 1776-1780, 1984.

Organ, A.J. Thermodynamics and Gas Dynamics of the Stirling Cycle Machine. Cambridge U. Press, 1992. (TJ765.074)

Patankar, S.V. Numerical Heat Transfer and Fluid Flow. New York: McGraw-Hill, 1980. (QC320.P37)

Pucci, P.F. et al. "The Single Blow Transient Testing Technique for Compact Heat Exchangers Surfaces," Journal of Engineering for Power, 89: 29-40 (January 1967).

Radebaugh, R. and Louie, B. "A Simple 1st Step to Optimizing Regenerator Geometry," Proceedings of the 3rd Cryocooler Conference: 177-198, Boulder CO, 17-18 September, 1986.

Radebaugh, R. "Development of Cryocoolers in the United States," Proceedings of the 4th International Cryocooler Conference: 1-8, Hangzhou, China, May 1989.

Romm, M.J. and Smith, J.L. "Stirling Engines Losses in Dead Volume Between Components," Proceedings of the 28th IECEC, 2: 751, 1993.

Ross, R.G. "JPL Cryocooler Development and Test Program Review," Proceedings of the 7th International Cryocooler Conference: 14-23, Santa Fe, NM, Nov 1992.

Seume, J. and Simon, T.W. "Oscillating Flow in Stirling Engine Heat Exchangers," Proceedings of the 21st IECEC, 1: 533-538, 1986.

Shoup, Terry E. A Complete Guide to Computer Methods for Engineers. Englewood Cliffs, N.J: Prentice-Hall, 1979. (TA345.S56.1979)

Stang, J.H. and Bush, J.E. "The Periodic Method for Testing Compact Heat Exchanger Surfaces," Journal of Engineering for Power: 87-94 (April 1974).

Taylor, P.R. and Narayankhedkar, K.G. "Thermodynamic Analysis of the Stirling Cycle," Cryogenics, 28: 36-45 (Jan 1988).

Tanaka, M. et al. "Flow and Heat Transfer Characteristics of the Stirling Engine Regenerator in an Oscillating Flow," JSME International Journal, Series II; 33: 283-289 (May 1990).

Tew, R.C., "Overview of Heat Transfer and Fluid Flow Problem Areas Encountered in Stirling Engine Modeling," NASA Technical Memorandum 100131TM. (Feb 1988)

Thieme, L.G. and Swec, D.M. "Overview of the NASA-Lewis Component Technology Program for Stirling Power Converters," Proceedings of the 27th IECEC, 5: 283, 1992. A9326073

Thomas, P.J. "SDIO and Air Force Cryocooler Technology Developments at USAF Phillips Laboratory," Proceedings of the 7th International Cryocooler Conference: 3-13, Santa Fe NM, Nov 1992.

Urieli, I. and Berchowitz, D.M. Stirling Cycle Engine Analysis. Bristol, England: Adam Hilger Ltd., 1984.

Venkatarathnam, G. et al. "Heat Transfer and Flow Friction Correlations in Perforated Plate Matrix Heat Exchangers," Cryogenics (Supplement), 30: 313 (Sep 1990).

Walker, G. Cryocoolers, Part I: Fundamentals. New York: Plenum Press, 1983. (TP482.W34)

Walker, G. and Fauvel, R. "Ross - Stirling Engines: Variations on a Theme", Proceedings of the 21st IECEC, 1: 610, 1986.

Wiese, J.L. Experimental Analysis of Heat Transfer Characteristics and Pressure Drop through Screen Regenerative Heat Exchangers. Masters Thesis, AFIT/GAE/ENY/93D-30, School of Engineering, Air Force Institute of Technology (AU), Wright-Patterson AFB OH, December 1993.

Wiese, J.L., Capt, USAF, Phillips Lab/Thermal Sciences Kirtland AFB NM. Telephone Interview. 6 Jul 1994.

Wyche, W. and Bruning, J. "The AFSTC Cryocooler Technology Development Program Plan for Meeting SDIO Requirements," Proceedings of the 4th Interagency Meeting on Cryocoolers: 3-10, Plymouth MA, Oct 1990.

Yagi, Y. and Mochizuki, S. "Development of a Modified Single-Blow Method - An Application to Parallel-Plate Heat Transfer Surfaces," Heat Transfer - Japanese Research, 20: 646-655 (Is. 7, 1991).

Yuan, Z. et al. "Oscillating Flow and Heat Transfer in a Stirling Engine Regenerator," ASME Heat Transfer Division, Fundamentals of Heat Transfer in Porous Media, 28th Natl Heat Transfer Conference and Exhibition, 193: 73-85 (1992).

VITA

Captain Timothy J. Murphy [REDACTED]

[REDACTED] After graduating from St. Ignatius College Preparatory in San Francisco, he entered the College of Mechanical Engineering at Marquette University in Milwaukee, Wisconsin. He received a Bachelor of Science degree in mechanical engineering. After leaving Marquette he worked on projects involving a computer simulation of high-temperature fuel cells and basic heat transfer in fluidized particle beds.

Captain Murphy was commissioned from Officer Training School in July of 1986, and reported to his first duty station at the Ballistic Missile Office (BMO), Norton Air Force Base, California. His duty titles included Peacekeeper Nuclear Hardness and Survivability Project Manager and executive officer to both the Director of Engineering for Rail Garrison and the Program Manager for the Minuteman System Program Office. Captain Murphy was awarded a master's degree in systems management from USC in June 1989 and a master's degree in Astronautical Engineering from AFIT in December of 1992. After attending Squadron Officer's School, he returned to AFIT to enter the doctoral program. Captain Murphy's lovely wife is named Maria, and his beautiful daughter is named Nora.

[REDACTED]
[REDACTED]

REPORT DOCUMENTATION PAGE

Form Approved
OMB No. 0704-0188

Public reporting burden for this collection of information is estimated to average 1 hour per response, including the time for reviewing instructions, searching existing data sources, gathering and maintaining the data needed, and completing and reviewing the collection of information. Send comments regarding this burden estimate or any other aspect of this collection of information, including suggestions for reducing this burden, to Washington Headquarters Services, Directorate for Information Operations and Reports, 1215 Jefferson Davis Highway, Suite 1204, Arlington, VA 22202-4302, and to the Office of Management and Budget, Paperwork Reduction Project (0704-0188), Washington, DC 20503.

1. AGENCY USE ONLY (Leave blank)	2. REPORT DATE	3. REPORT TYPE AND DATES COVERED	
	June 1996	Doctoral Dissertation	
4. TITLE AND SUBTITLE An Investigation of the Characteristics of Regenerative Heat Exchangers			5. FUNDING NUMBERS
6. AUTHOR(S) Timothy J. Murphy, Capt, USAF			
7. PERFORMING ORGANIZATION NAME(S) AND ADDRESS(ES) Air Force Institute of Technology 2750 P Street WPAFB OH 45433-7765		8. PERFORMING ORGANIZATION REPORT NUMBER AFIT/DS/ENY/96-5	
9. SPONSORING / MONITORING AGENCY NAME(S) AND ADDRESS(ES) Air Force Phillips Laboratory/VTP Kirtland AFB NM 87117-5776		10. SPONSORING / MONITORING AGENCY REPORT NUMBER	
11. SUPPLEMENTARY NOTES			
12a. DISTRIBUTION / AVAILABILITY STATEMENT Approved for public release; Distribution unlimited.		12b. DISTRIBUTION CODE	
13. ABSTRACT (Maximum 200 words) The objective of the current research was to investigate the effects of a reduction in screen thickness on the volume and compactness factor of stacked, wire-screen regenerators. An improved transient step-change method was devised which integrates experimental data with a numerical model of the flow to determine the heat transfer coefficient. The improvements to the method are: 1) the measured inlet temperature trace is used, 2) the heat transfer coefficient is based on the sponge effect delay time, and 3) the important effect of the tube surrounding the matrix is included in the model. The data show that the heat transfer is the same for reduced thickness screens as it is for unrolled screens once the decrease in surface area caused by rolling the screens is taken into account. However, the friction increases, significantly for a 50% reduction in screen thickness. Consequently, the ratio of the Colburn factor to the friction factor, called the compactness factor, decreases as the thickness of the screen decreases. The effectiveness of the regenerator was also adversely affected by rolling the screens.			
14. SUBJECT TERMS Regenerator Heat Exchangers Heat Transfer Coefficient Regenerative Cooling Porous Materials Stirling Cycle			15. NUMBER OF PAGES 157
			16. PRICE CODE
17. SECURITY CLASSIFICATION OF REPORT Unclassified	18. SECURITY CLASSIFICATION OF THIS PAGE Unclassified	19. SECURITY CLASSIFICATION OF ABSTRACT Unclassified	20. LIMITATION OF ABSTRACT UL